CHARACTERIZATION OF HOST FACTORS AFFECTING VIRAL ENTRY

APPROVED BY SUPERVISORY COMMITTEE

John Schoggins, Ph.D., Supervising Professor

Neal Alto, Ph.D.

Julie Pfeiffer, Ph.D.

Tiffany Reese, Ph.D.

DEDICATION

I would like to thank my mentor, Dr. John Schoggins for his extreme patience, guidance, and incredible help throughout the course of my graduate career. He allowed me a great degree of freedom to explore the scientific questions of my choosing at my own pace and in my own way. I would also like to thank the members of my dissertation committee: Dr. Julie Pfeiffer, Dr. Neal Alto, and Dr. Tiffany Reese for their support and guidance. In no small way their thoughtful critiques and suggestions shaped my work for the better.

I would like to thank my family and my parents Glenn and Anita in particular for their support. From a young age, I was set on becoming a scientist. Despite many considerable barriers due to my young age, my family made my dream possible. In addition, graduate school was a major change in my life and a very difficult experience overall for me which I endured in large part via the efforts of my family. My mother Anita deserves a great deal of credit here. Her kindness and love lightened my burdens considerably.

Finally, I would like to thank God, my largely unsung savior. I can never hope to thank God enough for his impact on and guidance throughout my life. God has made what was impossible for me possible, taught me more than I could say, and shown me more love than I could have imagined. Without God, I couldn’t have performed the work presented herein. I wouldn’t have even made it to graduate school. Praise be to God now and forevermore.

CHARACTERIZATION OF HOST FACTORS AFFECTING VIRAL ENTRY

by

NICHOLAS RYAN RINKENBERGER

DISSERTATION

Presented to the Faculty of the Graduate School of Biomedical Sciences

The University of Texas Southwestern Medical Center at Dallas

In Partial Fulfillment of the Requirements

For the Degree of

DOCTOR OF PHILOSOPHY

The University of Texas Southwestern Medical Center at Dallas

Dallas, Texas

Degree Conferral May, 2019

CHARACTERIZATION OF HOST FACTORS AFFECTING VIRAL ENTRY

Nicholas Ryan Rinkenberger, Ph. D.

The University of Texas Southwestern Medical Center at Dallas, 2019

Supervising Professor: John W. Schoggins, Ph. D.

Viruses are obligate, intracellular parasites. For a virus to infect a host cell, it must gain access to the interior of the host cell by some means. In animals, this often involves the exploitation of host processes such as receptor-mediated endocytosis and vesicular trafficking. Zika virus is an emerging arbovirus with global health and economic impacts. Interestingly, while Asian lineage Zika virus causes human disease and has been associated with severe neurological complications, African lineage Zika virus has only rarely been reported to cause human disease. Large strides have been made in understanding Zika virus infection. However, the mechanism used by Zika virus to enter host cells remains somewhat obscure. In chapter 2, I delineate and compare the pathway utilized by both Asian and African lineage Zika virus to enter host cells. I

find that these viruses require clathrin-mediated endocytosis and Rab5a function in a conserved manner. Additionally, all Zika virus strains tested were sensitive to pH in the range of 6.5-6.1 and were reliant on endosomal acidification for infection. I found that Zika virus preferentially fuses with late endosomes. Comparing lineages, Zika virus enters cells in a highly conserved manner.

Just as viruses have evolved to exploit host factors to promote their entry and replication, hosts have developed mechanisms of defense against viral infection. Recognition of viral infection by vertebrate hosts results in the expression and secretion of interferon. Interferon signaling subsequently results in the induction of hundreds of interferon-stimulated genes (ISGs) which restrict pathogen infection. Some of these ISGs specifically block viral entry. Surprisingly, a small group of ISGs was previously identified which actually promote viral infection. In chapter 3, I characterize the mechanism of action of MCOLN2, one of the ISGs found to promote viral infection. I assign a role for MCOLN2 in modulating viral entry. I show that MCOLN2 specifically promotes viral vesicular trafficking and subsequent escape from endosomal compartments. This mechanism requires channel activity, occurs independently of antiviral signaling, and broadly applies to enveloped RNA viruses that require endosomal acidification for infection, including influenza A virus, yellow fever virus, and Zika virus.

TABLE OF CONTENTS

PRIOR PUBLICATIONS

Mar K, **Rinkenberger N,** Boys I, Eitson J, McDougal M, Schoggins J. LY6E mediates an evolutionarily conserved enhancement of virus infection by targeting a late entry step. 2018. Nat. Commun 9:3603.

Rinkenberger N, Schoggins J. MCOLN2 Cation Channel Increases Vesicular Trafficking Efficiency of Endocytosed Viruses. 2018. mBio 9:e02314-17.

LIST OF FIGURES

LIST OF TABLES

LIST OF APPENDICES

LIST OF DEFINITIONS

AAV2 – adeno-associated virus 2

ADP – adenosine diphosphate

Ad2 – adenovirus 2

Ad5 – adenovirus 5

AMP – adenosine monophosphate

AP-2 – adaptor protein 2

Arf6 – ADP-ribosylation factor 6

ATPase – adenosine triphosphatase

BafA – bafilomycin A1

CAR – coxsackie and adenovirus receptor

CCR5 – C-C chemokine receptor type 5

Cdc42 – cell division cycle 42

CD4 – cluster of differentiation 4

cGAS – cyclic GMP-AMP synthase

CHIKV – Chikungunya virus

CH25H – Cholesterol-25-hydroxylase

CLIC/GEEC – clathrin-independent carriers/glycosylphosphatidylinositol-anchored protein enriched endocytic compartments

CLTC – clathrin heavy chain 1

CME – clathrin-mediated endocytosis

CMV – cytomegalovirus

CpG – cytosine-guanosine

CRISPR – clustered regularly interspaced short palindromic repeats

CSF-1 – macrophage colony stimulating factor-1

CVB – coxsackievirus B

CXCR4 – C-X-C chemokine receptor type 4

DAF – decay accelerating factor

DAI – deoxyribonucleic acid-dependent activator of IFN regulatory factor

DC-SIGN – dendritic cell-specific intracellular adhesion molecule-3-grabbing non-integrin

DENV – dengue virus

DNA – deoxyribonucleic acid

DNM2 – dynamin 2

dsDNA – double stranded deoxyribonucleic acid

dsRNA – double stranded ribonucleic acid

E – envelope

EAV – equine arteritis virus

EEA1 – early endosome antigen 1

EGF – epidermal growth factor

EGFR – epidermal growth factor receptor

EIPA – 5-(N-Ethyl-N-isopropyl)amiloride

ER – endoplasmic reticulum

ERC – endosomal recycling complex

GMP – guanosine monophosphate

gp – glycoprotein

GTPase – guanosine triphosphatase

HA – hemagglutinin

HIV-1 – human immunodeficiency virus 1

HPV – human papillomavirus

IAV – influenza A virus

IFI – interferon alpha-inducible protein

IFITM3 – interferon-induced transmembrane 3

IFN – interferon

IFNAR – type I interferon α/β receptor

IFN-I – type I interferon

IFN-II – type II interferon

IL2 – interleukin-2

Irf – interferon regulatory factor

ISG – interferon stimulated gene

ISGF – IFN-stimulated gene factor

ISRE – IFN-stimulated response element

JAK – Janus kinase

JEV – Japanese encephalitis virus

LAMP1 – lysosomal-associated membrane protein 1

LPS – lipopolysaccharide

LY6E – lymphocyte antigen 6 family member E

MBCD – methyl-β-cyclodextran

MCOLN2 – mucolipin-2

MDA5 – melanoma differentiation-associated protein 5

ML-IV – mucolipidosis type IV

MVB – multivesicular body

NP - nucleoprotein

NPC1 – Niemann-Pick C1

PAMP – pathogen associated molecular pattern

PAX5 – paired box 5

PBCV-1 – paramecium bursaria chlorella virus

PDGF – platelet derived growth factor

PIKfyve - 1-phosphatidylinositol 3-phosphate 5-kinase

PI3K – phosphoinositide-3-kinase

PI(3,5)P2 - phosphatidylinositol 3,5 bis-phosphate

PKR – protein kinase R

prM – precursor membrane

PRR – pathogen recognition receptor

PS – phosphatidylserine

Rac1 – Ras-related C3 botulin toxin substrate 1

Rab – Ras-related in brain

Rluc – *Renilla* luciferase

RIG-I – retinoic acid-inducible gene 1

RLR – retinoic acid-inducible gene 1-like receptors

RNA – ribonucleic acid

RNAi – RNA interference

RSV – respiratory syncytial virus

R18 – octadecyl rhodamine B

SINV – sindbis virus

SOC – store operated channel

SOCE – store operated calcium entry

SOCS3 – suppressor of cytokine signaling 3

SV-40 – simian virus 40

ssRNA – single stranded ribonucleic acid

STAT – signal transducer and activator of transcription

TAM – Tyro3, Axl, Mer

TBEV – tick-borne encephalitis virus

TCEP – tris(2-carboxyethyl)phosphine

TFEB – transcription factor EB

TGN – trans-Golgi network

TLR – toll-like receptor

TMP – tape measure protein

TRP – transient receptor potential

TRPA – transient receptor potential ankyrin

TRPC – transient receptor potential canonical

TRPM – transient receptor potential melastatin

TRPML – transient receptor potential mucolipn

TRPP – transient receptor potential polycystin

TRPV – transient receptor potential vanilloid

UTR – untranslated region

VACV – vaccinia virus

VEEV – Venezuelan equine encephalitis virus

vRNP – viral ribonucleoprotein

VSV – vesicular stomatitis virus

V-ATPase – vacuolar-type H^+ ATPase

WNV – West Nile virus

YFV – yellow fever virus

ZAP – zinc-finger antiviral protein

ZIKV – Zika virus

ZMPSTE24 – zinc metallopeptidase STE24

25HC – 25-hydroxycholesterol

CHAPTER ONE
Review of the literature

MECHANISMS OF VIRAL INFECTION

Viruses infect hosts from all domains of life. In fact, estimates suggest that viruses outnumber host cells by an order of magnitude(1). Viruses are obligate intracellular parasites that commonly require and exploit an array of host factors for their replication. Additionally, viruses often have an extracellular phase in their life cycle during dissemination amongst organisms in a population or during cell-to-cell spread within multicellular organisms. The host cell envelope is an important physical barrier which these extracellular viruses must cross in order to gain access to the cytoplasm of the host cell. This requires viruses to possess methods of traversing these barriers in order to establish infection. Commonly, viruses produce a sophisticated structure encapsulating the viral genome both for protection against the environment and to allow the virus to effectively infect new hosts.

Viral attachment to host cells

The first step in viral infection is the attachment of the virus to the host cell. If an extracellular virus particle cannot attach to a cell, it typically cannot infect the cell. The importance of viral attachment has been appreciated since the beginning of the twentieth century. One of the first studies on the subject identified viral attachment as the critically important first step in viral infection via co-sedimentation experiments of a *Shigella* sp. with a bacteriophage. However, the bacteriophage would not co-sediment with other bacterial species. This illustrated

the importance of viral attachment in determining cell tropism for the first time(2). Near a century later, viral attachment continues to be an important field of research.

Viral attachment was first characterized in bacteriophages and generally occurs in three stages. These stages are initial contact, reversible binding, and irreversible binding. In the first stage of attachment, viruses first come into contact with host cells generally via Brownian motion, diffusion, or flow. In the second stage of attachment, the virus interacts with the surface of the host cell in a reversible manner. This interaction tends to be weak and allows the virus to transiently interact with or roll across the surface of the host cell. This may help the virus to bind to its receptor on the cell surface if different from the attachment factors utilized above for transient cell binding(3). For example, the L-shaped fibers of phage T5 reversibly interact with lipopolysaccharide (LPS) on the cell surface of *E. coli* before phage tail protein pb5 irreversibly binds to the outer membrane protein FhuA(4, 5). In the third stage of attachment, the virus binds to its receptor. This commonly induces irreversible conformational changes in one or more structural proteins of the virus, resulting in translocation of the viral genome into the host cell cytoplasm(3).

Different organisms and cell types present different cell envelopes and challenges for viral infection. Thus, viruses have adapted to utilize an incredible variety of attachment factors and receptors in order to infect their hosts. The receptors and attachment factors utilized by plant and archaeal viruses are not well characterized. Animal cells are enclosed by a single, flexible lipid bilayer. Animal viruses tend to use host proteins, cell surface associated sugar moieties, and lipids as attachment factors and receptors(6). For example, influenza A virus (IAV) attaches to sialic acid moieties on cell surface glycoproteins, human immunodeficiency virus 1 (HIV-1)

utilizes cluster of differentiation 4 (CD4) as a cell receptor, and coxsackie and adenovirus receptor (CAR) serves as a receptor as its name suggests(7-10). In contrast, in Gram-positive bacteria, the cell membrane is surrounded by a thick cell wall consisting of peptidoglycan. Additionally in Gram-negative bacteria, a second membrane containing LPS is present outside of the cell wall. Thus, viruses infecting bacteria have evolved to use cell envelope components such as lipopolysaccharide, peptidoglycan moieties, and teichoic acid in addition to membrane proteins, and pillin proteins as receptors(3). Currently, our knowledge of host factors utilized by archaeal and plant viruses for attachment is lacking(11). Plant viruses are not known to actively penetrate the plant cell wall. Instead, plant viruses tend to be spread via vectors and mechanical injuries or are vertically transmitted through seeds(11, 12). That said, interaction of tobacco mosaic virus with intracellular plasmodesmata-associated factors has been found to be important for intercellular spread(13).

Some viruses interact with more than one receptor, or coreceptor, during attachment. For example, HIV-1 initially interacts with CD4 on the surface of lymphocytes. This leads to conformational changes allowing the virus to subsequently interact with the coreceptors C-C chemokine receptor type 5 (CCR5) or C-X-C chemokine receptor type 4 (CXCR4). This receptor complex formation triggers conformational changes in HIV-1 glycoprotein (gp) gp160 resulting in gp41-mediated viral entry(14). Coxsackievirus B (CVB) similarly interacts with multiple receptors during attachment. CVB infects polarized epithelium where its receptor, CAR, is localized to tight junctions such that the virus cannot interact with it(9). To circumvent this, many CVB isolates interact with decay accelerating factor (DAF) which induces a cell signaling

cascade resulting in actin rearrangement and relocalization of CVB to tight junctions where it can subsequently bind to CAR(15).

Viral entry into host cells

Following attachment of a virus to a host cell, the virus must transfer its genome and any viral factors necessary for infection into the cytoplasm of the host cell. The mechanisms involved in viral entry depend upon the physical barriers presented by the host. Despite this, there are also significant similarities between the mechanisms of viral entry. As such, the entry of many viruses can be grouped into the following general entry mechanisms: genome injection through an icosahedral capsid vertex, coat dissociation at the cell envelope, and internalization of virus particles.

Host barriers which impact viral entry

The plasma membrane is the basic barrier which all viruses must traverse. While all hosts have some variety of cell membrane, many organisms also possess a rigid cell wall. Most bacteria, excluding members of the *Chlamydiaceae* and *Mycoplasmataceae* families, possess a rigid layer of peptidoglycan ranging between 2.5-7.5 nm thick for Gram-negatives and up to around 25 nm thick in Gram positives(16). This layer of peptidoglycan prevents the passage of globular proteins of approximately 50 kDa or greater(17). As such, viruses cannot diffuse through the peptidoglycan layer. Additionally, Gram-negative bacteria possess a second lipid bilayer as previously mentioned. This outer membrane is generally permeable to small

metabolites due to pores. However, the passage of large protein complexes as well as viruses is prevented(18). Bacteria can also have capsules or slime layers which further prevent viral infection(19). A variety of cell walls have been described in archaea. However, the effects of these cell walls on viral infection is not well characterized. In fungi, the cell wall is commonly made of chitin. In plants, the primary component of the cell wall is cellulose and prevents the diffusion of proteins of approximately 60 kDa or particles of about 5 nm in size or greater(12).

Genome injection through an icosahedral capsid vertex

Due to the above described host barriers to viral infection, many nonenveloped viruses puncture or perforate the cell envelope and inject their genome into the host cell cytoplasm, leaving the bulky viral capsid behind on the cell surface. This mechanism of entry is commonly observed amongst viruses such as bacteriophages which infect hosts protected by a cell wall. Injection of the genome is often accomplished by packaging of the genome at high pressure relative to the intracellular environment. Intracellular pressure in bacteria has been estimated at 2-5 atmospheres while capsid pressures of up to 60 atmospheres have been documented in certain bacteriophages(16, 20, 21). This method of entry is utilized by tailed bacteriophages such as phage T4 wherein an icosahedral capsid storing the viral genome is connected on one of its vertices to a long tail filament, forming a tube through which the viral genome is injected into the host cell cytoplasm(22). Bacteriophage-like archaeal viruses such as ψM1 and the algal virus paramecium bursaria chlorella virus (PBCV-1) probably enter cells through a similar mechanism(23, 24).

While many viruses utilize this general approach to enter cells, the specific mechanism for genome injection into the host cell differs between viruses. Of the viruses utilizing this method of entry, bacteriophages are some of the best studied. For bacteriophages with long, contractile tails such as myophages including phage T4, the tail is surrounded by a layer of sheath proteins. Upon receptor engagement, a conformational change in the icosahedral capsid of T4 results in a contraction of the sheath causing an extension of the tail into and through the bacterial outer membrane(22). The spike proteins, including gp5, at the end of the tail are suggested to be released and whereupon gp5 locally cleaves peptidoglycan(25). This allows further sheath contraction and extension of the tail through the peptidoglycan layer. From here, it has been hypothesized that either the tail further forms a pore through the inner bacterial membrane or associates with a host derived inner membrane pore, allowing passage of the viral genome into the cytoplasm(26). Long, noncontractile tailed phages including siphophages such as T5 and HK97 as well as tailless phages are thought to enter cells through a similar mechanism. However, rather than utilizing a contractile sheath to puncture the cell envelope, these viruses are thought to puncture the bacterial outer membrane with phage tail proteins and inject a tape measure protein (TMP) into the periplasmic space(27). It has been suggested that after TMP injection into the periplasmic space the TMPs undergo a conformational change which may be assisted by host chaperones, forming a tube through which the viral genome is injected into the cell(28-30). The entry mechanisms of bacteriophages infecting Gram-positive bacteria are not as well understood. That said, bacteriophage ϕ29 is one of the best studied. After cell attachment, it is suggested that the peptidoglycan layer is degraded by the phage tail protein gp13(31). Conformational changes in the phage tail result in the exposure of six hydrophobic

loops thought to insert into the bacterial membrane and form a pore. This subsequently allows injection of the viral genome through the tail and into the host cell cytoplasm(32).

Coat dissociation at the cell envelope

A common strategy for enveloped virus entry is direct membrane fusion with the plasma membrane of the host cell. This results in the immediate dissociation of the viral envelope from the viral genome after which capsid uncoating quickly follows. An example of this is bacteriophage φ6 which fuses its envelope with the outer membrane of the Gram-negative bacterium *P. syringae* during cell entry(33). This strategy is more common with bacterial viruses than animal viruses which tend to utilize host endocytic machinery for entry as will be discussed. However, paramyxoviruses are thought to enter animal cells by this mechanism but direct evidence of plasma membrane fusion is lacking(34). Similarly, HIV-1 was thought for a long time to use this entry mechanism. However, mounting evidence suggests that this virus is instead endocytosed before fusion(35). Noneveloped viruses such as filamentous bacteriophages including fd may also utilize this entry mechanism. In bacteriophage fd, the major capsid protein contains a central hydrophobic domain. Following receptor binding, it has been hypothesized that the entire capsid of fd inserts into the plasma membrane of the host cell, uncoating and releasing the viral genome into the cytoplasm(36).

Internalization of virus particles

Another common mechanism of viral entry is endocytosis into the host cell followed by penetration of an internal cellular membrane. This is commonly observed among viral infections

in animals in which cells lack a cell wall and have the ability to engulf relatively large volumes of extracellular material via endocytosis. Plants and bacteria, on the other hand, generally lack the ability to endocytose virus-sized particles(24). In animal cells, endocytosed material is quickly transported to mildly acidic early endosomes. Early endosomes in turn serve as a hub for cargo transport and sorting(37). Many animal viruses such as IAV, lentiviruses, flaviviruses, and members of the *Herpesviridae* family are endocytosed during viral entry and replicate in the nucleus or on the endoplasmic reticulum (ER) membrane(38-40). The viscosity of the cytoplasm effectively prevents passive diffusion of virus-sized particles(24, 41). Thus, it may be advantageous for such viruses to exploit the vesicular trafficking machinery of the host in order to efficiently gain access to the perinuclear region of the cell.

Animal cells possess a multitude of endocytic pathways which viruses are known to exploit. The most studied of these pathways are macropinocytosis, clathrin-mediated endocytosis (CME), caveolar endocytosis, and phagocytosis. However, other pathways exist as well including the clathrin-independent carriers/glycosylphosphatidylinositol-anchored protein enriched endocytic compartments (CLIC/GEEC), clathrin independent-ADP-ribosylation factor 6 (Arf6), interleukin-2 (IL2), and flotillin pathways.

Clathrin-mediated endocytosis (CME) it utilized by the cell to endocytose a wide range of cargo including transferrin and transferrin receptor. CME is initiated when cargo such as ligand-bound receptors on the cell surface bind to cytoplasmic adaptor proteins such as adaptor protein 2 (AP-2). These adaptor proteins subsequently recruit coat and scaffolding proteins from the cytoplasm including clathrin for which the pathway is named. As more proteins are recruited, including additional cargo, a clathrin coated pit is formed due to coat mediated membrane

curvature. Finally, membrane scission occurs through the action of the large guanosine triphosphatase (GTPase) dynamin-2 (DNM2) which forms a constricting ring around the neck of the clathrin coated pit(42). CME is one of the most common pathways utilized by viruses for entry. Viruses utilizing CME include IAV, dengue virus (DENV), vesicular stomatitis virus (VSV), Sindbis virus (SINV), and adenovirus 5 (Ad5)(43-48). Three general scenarios have been identified for CME involving virus particles. Either the particles are recruited to preformed clathrin-coated pits as reported for DENV, remain relatively stationary and induce clathrin assembly at the site of receptor binding as reported for IAV, or exhibit both behaviors as reported for VSV(49-51).

Caveolar endocytosis is not as well characterized as CME nor have many viruses been identified to require it. It is much more difficult to ascertain if viruses are endocytosed through this pathway as this pathway does not possess easily definable characteristics which discriminate it from similar pathways(38). Membrane invaginations referred to as caveolae are formed in cholesterol rich lipid rafts on the plasma membrane. Caveolae formation is dependent on the scaffolding protein caveolin-1. While caveolae are not normally involved in endocytosis, interaction with certain ligands can induce rapid internalization of caveolae via DNM2-mediated membrane scission(52). It is well known that Simian virus 40 (SV40) is endocytosed via caveolar endocytosis(53).

Macropinocytosis is characterized by large scale, nonspecific fluid uptake which is induced in response to specific signals. These signals are generally growth factors such as epidermal growth factor (EGF), macrophage colony stimulating factor-1 (CSF-1), and platelet-derived growth factor (PDGF). Recognition of membranes containing phosphatidylserine (PS)

also induces macropinocytosis. In response to these signals, the small rho-family GTPases Ras-related C3 botulin toxin substrate 1 (Rac1) and to a lesser extent cell division cycle 42 (Cdc42) induce actin-mediated membrane ruffling and subsequently endocytosis of fluid in a nonspecific manner(54). Vaccinia virus (VACV) is known to induce and be endocytosed by macropinocytosis. This is proposed to be due to exposure of PS on its envelope(55). IAV, respiratory syncytial virus (RSV) and Ebola virus have also been found to enter cells through macropinocytosis(56-60). Some viruses induce macropinocytosis such as adenovirus 2 (Ad2)(61). However, the role of macropinocytosis in the infection of such viruses is poorly understood. Viruses dependent on macropinocytosis tend to be inhibited by loss of Rac1 function as well as drugs such as methyl-β-cyclodextran (MBCD), Na^+/K^+ exchange inhibitors such as amilorides, and the actin depolymerizing agent cytochalasin D(38, 57, 62).

In addition to the pathways above, viruses infrequently exploit other cellular endocytic pathways. For example, the amoeba pathogen Mimivirus enters host cells via phagocytosis(63). The CLIC/GEEC pathway is utilized by adeno-associated virus 2 (AAV2) for endocytosis(64).

Penetration of internalized virus particles

Once a virus particle has been endocytosed, it must still penetrate the vesicle membrane encompassing it in order to gain access to the cytoplasm of the host cell. To this end, viruses have been reported to preferentially penetrate specific internal cellular compartments(65). Often this specificity in the site of penetration is determined by pH. For example, IAV undergoes conformational changes in its capsid proteins resulting in exposure of a membrane fusion peptide in an environment where the pH is less than 5.5, such as that found in late endosomes(43).

However, other factors including lysosomal cathepsins, lipids, and cholesterol can also be involved in promoting viral penetration(66-68). As an example, the cysteine protease cathepsin W has been found to be important for IAV entry(67). In contrast, during Ebola virus entry, cathepsin B and L-mediated proteolysis in endosomes exposes a receptor binding site for Niemann-Pick C1 (NPC1) on the viral capsid which is crucial for viral entry(69-71). The intracellular compartments that endocytosed viruses penetrate are described below in greater detail.

Endocytosed vesicles are quickly sorted to the Ras-related in brain 5- (Rab5)-dependent early endosome compartment and acidify via the action of the vacuolar-type H^+ ATPase (V-ATPase) to a pH of 6.8-6.2. Early endosomes in turn serve as a hub for cargo transport and sorting(37). After reaching early endosomes, much of the endocytosed membrane as well as some cargo is quickly recycled back to the cell surface via Rab4- and Rab35-dependent recycling endosomes. Alternatively, cargo is more slowly recycled back to the cell surface through the perinuclear endosomal recycling compartment (ERC) in a Rab11-dependent manner(72). Cargo can also be transported to the TGN and ER. Finally, cargo can be sorted into the degradative pathway, in which endosomes mature into multivesicular bodies (MVBs)/late endosomes and subsequently lysosomes. During this process, a Rab5 to Rab7 switch takes place in which Rab5 is replaced with Rab7 on the endosomal membrane. These endosomes are transported along microtubules in a dynein-dependent manner. MVBs/late endosomes acidify further to a pH of 6.2-5.0. In a Rab7-dependent manner, MVBs/late endosomes fuse with lysosomes which contain a variety of proteases, lipases, amylases, and nucleases. These endosomes eventually mature into lysosomes themselves, acidifying further to a pH of 5.0-4.5. Importantly, Rab7 is necessary for

late endosome maturation, homotypic fusion, lysosomal function and lysosomal fusion with late endosomes(37, 73-75). However, Rab7 is not required for initial MVB/late endosome formation(76).

Endocytosed viruses commonly penetrate early endosomes (RSV, reoviruses) and MVBs/late endosomes (VSV, IAV, DENV2, tick-borne encephalitis virus)(43, 57, 77-80). Other viruses have been found to penetrate recycling endosomes (VACV) in addition to the trans-Golgi network and the ER (SV40, papillomaviruses) (81-83). Membrane penetration commonly occurs in one of three ways. For enveloped viruses such as IAV, tick-borne encephalitis virus (TBEV), and DENV2, receptor binding coupled with environmental signals such as low pH induce pH-dependent or -independent fusion peptide exposure. This fusion peptide subsequently inserts into adjacent host membranes, resulting in membrane fusion and release of the viral capsid into the cytoplasm(43, 79, 84-86).

For nonenveloped viruses such as poliovirus, a hydrophobic domain is suggested to be exposed on the viral capsid following endocytosis. This inserts into the host membrane, forming a pore and allowing injection of the poliovirus genome into the host cell(87-89). Alternatively, endocytosed nonenveloped viruses can disrupt the host membrane encompassing them to gain access to the cytoplasm. For example, adenoviruses partially uncoat in the lumen of early endosomes in a pH-dependent manner. This releases the viral protein pIV from the capsid which is suggested to cause catastrophic disruption of the endosomal membrane by inducing severe positive membrane curvature stress(90, 91).

Strain-specific differences in viral entry

A common assumption is that different strains of the same viral species enter cells in an identical manner. However, it is important to note that this is not always the case. A number of studies have identified strain-specific differences in the entry animal viruses into their hosts. For example, while yellow fever virus (YFV) and Chikungunya virus (CHIKV) are thought to be endocytosed via clathrin-mediated endocytosis, certain strains of these viruses have been found to enter cells in a clathrin-independent manner(92-96). Furthermore, the dependence of Rab7 for CHIKV infection differs between viral strains(94, 96). As mentioned above, the IAV coat proteins undergo conformational changes in response to acidic endosomal pH which are important for membrane fusion. The hemagglutinin (HA) protein of IAV is thought to undergo an irreversible conformational change during this process, exposing a fusion peptide which quickly embeds into the adjacent endosomal membrane(43, 97). However, a comparison of multiple IAV strains found that the extent and rate of the reversibility of this process was highly variable among the strains tested(97). Similarly, the pH required for efficient membrane fusion of SINV varies widely by strain from pH 5.6-6.5(66, 98-100). In summary, it is important to compare the entry of multiple strains of a virus in order to properly understand the entry pathway(s) utilized by the overarching viral species.

THE CELL-INTRINSIC IMMUNE RESPONSE DURING VIRAL INFECTION AND ITS IMPACTS ON VIRAL ENTRY

Just as viruses have evolved to infect their hosts, hosts have developed mechanisms to defend against viral infection. In vertebrates, expression of intrinsic antiviral restriction factors

and the IFN response are crucial for cell-intrinsic immunity during viral infection. Detection of pathogen associated molecular patterns (PAMPs) by host expressed pattern recognition receptors (PRRs) during infection commonly results in the expression of type I interferons (IFN-I). Many PRRs are important for recognition of viral infection by the host.

Detection of viral infection by the host

The main PAMPs recognized during viral infection by the host are the viral genome as well as replication intermediates produced during infection such as double stranded ribonucleic acid (dsRNA). The main PRRs responsible for recognition of virus-associated PAMPs are thus toll-like receptors (TLRs), retinoic acid-inducible gene 1-like receptors (RLRs) and cytosolic double stranded deoxyribonucleic acid (dsDNA) sensors. The endosomal TLRs -3,-7, and -8 recognize RNA. TLR3 specifically recognizes dsRNA while TLR7 and -8 recognize single stranded ribonucleic acid (ssRNA). In contrast, TLR9 recognizes unmethylated DNA containing cytosine-guanosine (CpG) repeats in endosomes. Retinoic acid-inducible gene 1 (RIG-I) recognizes cytosolic RNAs with 5’-triphosphate ends, such as genomic RNA from IAV(101). Additionally, the RLRs RIG-I and melanoma differentiation-associated protein 5 (MDA5) preferentially recognize short - less than 19 bp - or long dsRNA regions respectively(102, 103). Cytosolic sensors such as cyclic GMP-AMP synthase (cGAS), interferon-inducible protein 16 (IFI16), and deoxyribonucleic acid-dependent activator of IFN regulatory factor (DAI) recognize cytosolic dsDNA(104-106). Receptor activation results in divergent signal transduction cascades which converge on the induction of IFN-I expression.

Following expression, IFN-Is are secreted and signal in an autocrine or paracrine manner through the type I interferon α/β receptor (IFNAR) on the cell surface. This activates Janus kinase 1 (JAK1) which phosphorylates cytoplasmic signal transducer and activator of transcription 1 (STAT1) and STAT2. STAT1 and STAT2 subsequently heterodimerize, translocate to the nucleus, and bind to IFN-regulatory factor 9 (IRF9), forming the complex known as IFN-stimulated gene factor 3 (ISGF3). ISGF3 binds to DNA elements known as IFN-stimulated response elements (ISREs) upstream of promoters for IFN-stimulated genes (ISGs) and directly promotes the transcription of these ISGs. ISGs form a complex defense network against invading pathogens(107-109).

Discovery of host restriction factors affecting viral entry

Host defense against viral infection is dependent on basally expressed antiviral restriction factors in addition to ISGs expressed in response to viral infection(110). In the last two decades, there have been major advances in the approaches available for high-throughput screening. These approaches include RNA interference (RNAi) based screening, clustered regularly interspaced short palindromic repeats (CRISPR)-mediated genome editing based screening, and ectopic overexpression based screening. Due in large part to these advances, a number antiviral restriction factors have been identified.

Antiviral restrictions factors have been identified targeting every general viral life cycle stage including entry (IFITM3, CH25H, ZMPSTE24), replication (IFI6, ZAP, PKR), assembly (ISG15), and egress (tetherin)(110, 111). However, I will focus specifically on those found to

target viral entry. Interferon-induced transmembrane 3 (IFITM3) was first identified as an antiviral ISG in an RNAi screen for restriction factors affecting IAV infection(112). However, IFITM3 has since been found to be an important restriction factor for IAV, West Nile virus (WNV), cytomegalovirus (CMV), and CHIKV *in vivo*(113). Further mechanistic work has shown that IFITM3 localizes to endosomes and prevents IAV fusion with late endosomes during viral entry(114). This is suggested to either occur via an IFITM3-mediated reduction in membrane fluidity or IFITM3-mediated alteration of membrane curvature(110). Recently, zinc metallopeptidase STE24 (ZMPSTE24) was identified via co-immunoprecipitation experiments as a cofactor necessary for IFITM3 mediated inhibition of viral infection(115).

Cholesterol-25-hydroxylase (CH25H) was first identified as an antiviral ISG targeting VSV via an ectopic expression screen involving an ISG library(116). Subsequent work showed that CH25H converts cholesterol to the soluble antiviral factor 25-hydroxycholesterol (25HC) which inhibits infection of a diverse array of enveloped viruses. It is suggested that 25HC integration into host membranes alters the properties of these membranes, preventing viral membrane fusion similarly to IFITM3(117).

In a similar ISG library based ectopic expression screen, another group identified stannin as an antiviral ISG targeting human papillomavirus infection (HPV). This group found that stannin prevented retrograde transport of HPV from late endosomes to the TGN during viral entry which is important for subsequent release of HPV into the cytoplasm(118).

While ISGs are thought to prevent infection, some ISGs have been shown to promote viral infection. One example is suppressor of cytokine signaling 3 (SOCS3) which serves as a negative regulator of the IFN response. Expression of SOCS3 in response to IFN-II indirectly

promotes viral infection by inhibiting IFN signaling and ISG induction(119). However, ISGs have also been found to promote viral infection directly. In 2014, Schoggins et al. published the results of an ectopic expression screen for an IFN-I ISG library which was challenged against a panel of 14 viruses representing 7 viral families and 11 genera. A number of novel antiviral ISGs were identified by this screen, including IFI6 which was later characterized in detail to be an antiviral ISG affecting the replication of certain flaviviruses(111). Interestingly, a handful of ISGs including mucolipin-2 (MCOLN2) and lymphocyte antigen 6 family member E (LY6E) were identified which enhanced viral infection for a diverse group of viruses including certain flaviviruses and IAV(120). Subsequent mechanistic characterization of MCOLN2 and LY6E revealed that these ISGs both directly promote viral entry. LY6E was found to promote the uncoating of IAV during cell entry(121). In contrast, I demonstrated that MCOLN2 promotes trafficking of IAV to late endosomes during viral entry which is necessary for efficient pH-dependent penetration of the endosomal membrane by IAV(122). The previous literature and experimentation leading to the identification of MCOLN2 as an ISG promoting IAV entry will be discussed in more detail in chapter 3.

CHAPTER TWO
Comparative analysis of viral entry for Asian and African lineage Zika virus strains

INTRODUCTION

Zika virus is an emerging arboviral pathogen

Zika virus (ZIKV) is an emerging arbovirus of the *Flaviviridae* family which has caused recent outbreaks in the Yap Islands (2007), Pacific Islands (2013-2015), and the Americas (2015-2017). Zika virus infection has been associated with chorioretinal scarring in addition to severe neurological complications including microcephaly in newborns as well as Guillan Barre syndrome in adults(123, 124). ZIKV was first identified in a sentinel rhesus monkey in Uganda in 1947(125). However, ZIKV has been known to circulate in both Africa and Asia since the 1960s(126). Sequencing and phylogenetic analysis of ZIKV isolates from recent outbreaks identified these strains as originating from Asian lineage ZIKV(127-131). Intriguingly, only very rare cases of infection have been associated with African lineage ZIKV. Therefore, studying the striking difference in neurovirulence observed between the two lineages of ZIKV may help to elucidate important elements of ZIKV infection in humans and associated neurological disorders.

Phylogenetic analysis of ZIKV strains has identified a number of amino acid substitutions. One such study identified 75 amino acid substitutions comparing African vs Asian lineage ZIKV, 24 comparing pre- vs post-epidemic Asian lineage ZIKV, and reported 5 substitutions conserved among all epidemic Asian lineage ZIKV strains included in the analysis. In the MR 766/Uganda/1947 ZIKV strain, the precursor membrane (prM) and envelope (E)

proteins important for viral attachment, entry, and antigenic profile make up ~20% of the viral polyprotein. However, ~25% of African vs Asian lineage amino acid substitutions were present in the prM and E proteins, ~33% in the pre- vs post-epidemic Asian lineage ZIKV comparison, and 60% of the reported amino acid substitutions conserved amongst epidemic ZIKV strains were present in these proteins(127). Similar phylogenetic analyses have also identified high variability in the prM protein comparing African and Asian lineage ZIKV(132, 133).

This enrichment of mutations in structural proteins predominantly in epidemic strains of ZIKV suggests that alterations in the function or antigenic profile of the structural proteins may be important for virulence/pathogenicity. In agreement with this, a recent study reported a mutation present in the prM protein of an epidemic ZIKV strain causing significantly increased neurovirulence in neonatal mice(134). Additionally, significant differences in viral infection rates, apoptosis induction, and host response to infection have been observed between African and Asian lineage ZIKV *in vivo* and *in vitro(135-138).* A recent study suggests that this *in vitro* phenotype is due in part to differences in the structural proteins of African and Asian lineage ZIKV strains(139).

Zika virus host cell attachment and entry

Flaviviruses are enveloped viruses with (+)sense, ssRNA genomes that replicate in the cytoplasm. Clinically relevant flaviviruses include YFV, DENV, WNV, TBEV, and ZIKV. Commonly during flaviviral infection, initial attachment to the host cell surface is accomplished through interaction of the viral E protein with glycosaminoclygans such as heparan-sulfate

proteoglycans. Subsequently, the E protein interacts with host receptors such as C-type lectin receptors, DC-SIGN, TIM receptors and TAM receptors (Tyro3, Axl, Mer) which results in receptor-mediated endocytosis of the virus(140). Flaviviruses are commonly endocytosed via clathrin-mediated endocytosis(78, 141). However, flaviviruses exploit other endocytic pathways as well(142). For example, Japanese encephalitis virus (JEV) enters neuronal cells via a clathrin-independent endocytic pathway(143). In contrast, opsonized DENV particles have been suggested to be endocytosed by macrophages, monocytes, and dendritic cells via phagocytosis(142, 144, 145). However, direct experimental support for this hypothesis is currently lacking. Following endocytosis, flaviviruses generally fuse with endosomes in a pH-dependent manner(78, 84, 85, 141, 146, 147). Viral fusion with endosomes is also dependent on cholesterol for DENV and WNV(148).

Similarly to other flaviviruses, Axl has been suggested to be a cell receptor for ZIKV. However, the necessity of Axl in ZIKV infection both *in vitro* and *in vivo* is disputed(149-158). Currently, findings suggest that while Axl may be a cell receptor for ZIKV, other receptors may exist which have not yet been identified. Previous work with individual ZIKV strains has shown that infection is dependent on clathrin and Rab5 function, but not Rab7(149, 152). Additionally, African lineage ZIKV strains have been shown to be dependent on endosomal pH as determined with lysosomotropic agents and experiments with liposomes(150, 159). However, the endosomal population with which ZIKV fuses has not been determined. The African lineage ZIKV strain MR 766 has been frequently used to study ZIKV entry and infection(150, 152, 160). It is important to note that MR 766 has been passaged extensively in tissue culture. In this study, I characterized general features of ZIKV entry and compared African and Asian strains. I included

MR 766 in this comparison to determine if extensive passage in tissue culture has altered its mode of cell entry relative to other ZIKV strains. All strains of ZIKV tested required endosomal acidification, clathrin-mediated endocytosis, and Rab5 for infection. Using viruses with fluorophore-labeled envelopes, I provide the first direct identification of the endosomal populations with which ZIKV fuses.

RESULTS

African and Asian lineage Zika virus strains enter cells in a pH-dependent manner

Enveloped viruses either fuse directly with the plasma membrane or are endocytosed and fuse with an endosomal compartment to enter the cytoplasm. Flaviviruses are generally endocytosed through clathrin-mediated endocytosis and are subsequently released into the cytoplasm from an endosomal compartment(142). Previous studies with the African lineage ZIKV strain MR 766 have suggested a similar entry pathway for African lineage ZIKV(149, 150, 152, 159). To confirm that ZIKV is endocytosed before release into the cytoplasm, I utilized the fluorophore octadecyl rhodamine B (R18) to identify the location of viral membrane fusion. R18 is a lipophilic, self-quenching fluorophore which can be inserted into viral envelopes at a high enough concentration to quench R18 fluorescence. Upon fusion of the labelled viral envelope with another membrane, lipid mixing causes dilution of R18, resulting in fluorescence dequenching. I labelled Asian lineage ZIKV strain PRVABC59 with R18 and infected the human hepatoma cell line Huh7.5 with labelled virus for 15 minutes to allow viral entry. I subsequently

observed the location of R18 fluorescence relative to the plasma membrane marker wheat germ agglutinin (WGA) with confocal microscopy. As a control, I imaged the colocalization of the plasma membrane marker PM-GFP with WGA. R18 fluorescence was observed predominantly just underneath the plasma membrane (Figure 1A-B, Figure 2A). While plasma membrane localized GFP colocalized with WGA, there was little to no colocalization of R18 fluorescence with WGA (Figure 1B, Figure 2B). These data indicate that ZIKV is released from an internal cell compartment into the cytoplasm.

Certain endocytosed viruses require an acidic environment for efficient fusion with host membranes. African lineage ZIKV strains are sensitive to environmental pH as well as perturbation of endosomal pH by lysosomotropic agents such as Bafilomycin A1 (BafA1), chloroquine, and ammonium chloride (NH_4Cl)(150, 159, 160). To determine if Asian and African lineage ZIKV have differential sensitivity to endosomal pH, I infected Huh7.5 cells with two Asian lineage ZIKV strains (PRVABC59, PB-81) and two African lineage ZIKV strains (MR 766, DAKAR 41519) in the presence of NH_4Cl and BafA1. Cells were treated with relatively low concentrations of NH_4Cl since higher concentrations resulted in significant cell death (data not shown). All ZIKV strains tested responded similarly to both treatments (Figure 1C). ZIKV infection trended towards a reduction with NH_4Cl treatment and was highly impaired by BafA1 treatment. Since this result suggested that dependence on endosomal acidification is conserved between ZIKV lineages, I further wanted to characterize the pH sensitivity of ZIKV. The exposed surface proteins of certain endocytosed viruses, including flaviviruses, undergo pH-dependent conformational changes resulting in fusion peptide exposure and burial in eukaryotic cell membranes(65, 161-164). This process is often irreversible(97, 147, 161, 165). Thus,

exposure of virions to low pH in the absence of a target cell membrane results in loss of infectivity due to premature conformational changes in the virion and fusion peptide exposure. To determine the pH sensitivity of ZIKV in more detail, I incubated African and Asian lineage ZIKV strains in buffers ranging from pH 7.0-4.4 in increments of 0.2 pH units and assessed ZIKV infectivity. As a control, the acidic pH was neutralized with HEPES buffer before incubation with virus. Both Asian lineage ZIKV strains were affected equally by pH treatment, with half-maximal inactivation of PRVABC59 at pH 6.29 ± 0.064 and PB-81 at pH 6.29 ± 0.065 (Figure 1D, Figure 3A). The African lineage ZIKV strain DAKAR 41519 was similarly affected, with half-maximal loss of infectivity at pH 6.15 ± 0.14. However, half-maximal inactivation for MR 766 was significantly different when compared to DAKAR 41519, occurring at pH 6.58 ± 0.22. For all ZIKV strains except MR 766, I noticed that infection was primed by mild viral pre-acidification as has been previously observed with influenza A virus(166). A similar phenotype has also been reported for MR 766 when incubated in a mildly basic solution prior to infection(160). Only MR 766 infection was reduced by incubation in solutions with higher concentrations of HEPES buffer (Figure 3B). Furthermore, HEPES buffer concentration only impacted MR 766 infection at concentrations present well after the observed point of pH-induced virus inactivation.

African and Asian lineage Zika virus strains require clathrin-mediated endocytosis and Rab5 function for infection

Next, I compared the dependence of African and Asian lineage ZIKV strains on viral entry-associated host factors and processes known to be important for MR 766 infection. I characterized the effect of siRNA-mediated knockdown of clathrin heavy chain 1 (CLTC), Ras-related C3 botulinum toxin substrate 1 (Rac1), and caveolin-1 (CAV1) on African and Asian lineage ZIKV infection in HeLa cells (Figure 4A, D, G)(150, 152). These host factors are important for clathrin-mediated endocytosis, macropinocytosis, and caveolar endocytosis respectively. I found that infection by all strains of ZIKV was unaffected by Rac1 and CAV1 knockdown. However, CLTC knockdown resulted in a significant reduction in infection irrespective of ZIKV lineage. To validate that gene knockdown impaired endocytic function, I confirmed that clathrin-mediated endocytosis of transferrin was reduced after CLTC knockdown, and that uptake of 70 kDa dextran by macropinocytosis was similarly reduced by Rac1 knockdown (Figure 4B, E). Reduction in protein expression was confirmed by western blot (Figure 4C, F, H).

Following endocytosis, enveloped viruses fuse with a specific internal cellular compartment. The most commonly reported site of endocytosed virus fusion is endosomes(65). Rab5 is important for early endosome function and homotypic fusion(37). Rab7 is important for endosomal maturation and lysosomal function as well as late endosomal and lysosomal fusion(75). It was previously shown that expression of a dominant negative mutant variant of Rab5a reduced infection of one ZIKV strain while a dominant negative mutant variant of Rab7a did not (149). To compare the dependency of African and Asian lineage ZIKV infection on Rab5 and Rab7, I expressed the commonly used dominant negative constructs Rab5a S34N and Rab7a N125I in Huh7.5 cells (Figure 5A). Compared to the control vector, expression of Rab5a S34N

but not Rab7a N125I resulted in significantly reduced infection by all ZIKV strains tested. To corroborate these findings, I targeted all *RAB5* and *RAB7* isoforms with CRISPR/Cas9 mediated gene editing. Ablation of Rab5 expression resulted in a similar reduction in infection by all strains of ZIKV tested (Figure 5B-C). Reduction in Rab7 expression resulted in a significant impairment of Asian lineage ZIKV infection, but only a modest impairment of African lineage ZIKV infection. The observed difference in phenotype between Rab7 dominant negative expression and knockout is likely due to a greater loss in Rab7 function with CRISPR/Cas9 mediated gene editing. Microtubules have also been found to be important for cell entry of MR 766(167). I found that treatment of Huh7.5 cells with nocodazole efficiently induced microtubule depolymerization, which resulted in a modest reduction of infection by both ZIKV lineages (Figure 5D, Figure 6).

Zika virus preferentially fuses with late endosomes

Our findings indicate that ZIKV is endocytosed and subsequently released into the cytoplasm from an internal cell compartment. I sought to identify the host compartment(s) from which ZIKV is released into the cytoplasm. Considering the above findings suggesting that ZIKV entry is generally conserved between lineages, I only focused on characterizing the entry of the Asian lineage ZIKV strain PRVABC59 in greater detail. Many endocytosed viruses are released into the cytoplasm after penetration or fusion with early endosomes or with multivesicular bodies (MVBs)/late endosomes. To determine if ZIKV is released from early or MVBs/late endosomes, I created stable Huh7.5 cell lines expressing doxycycline-inducible

EGFP-Rab5a or EGFP-Rab7a to fluorescently label early endosomes or MVBs/late endosomes respectively. Doxycycline-induced expression of EGFP-Rab5a or EGFP-Rab7a did not significantly impact EGFR degradation kinetics suggesting that vesicular trafficking kinetics and lysosome function were unaffected by EGFP-Rab expresssion (Figure 7A-B). I then infected these cells with R18-labelled PRVABC59. Colocalization of lipid mixing events with endosomal markers was observed via R18 fluorescence both in real time by confocal microscopy as well as in fixed cells 15 minutes after infection (Movie 1-2, Figure 8A, Figure 9). Interestingly, in both data sets I found that the majority of lipid mixing events colocalized with EGFP-Rab7a and a minority of lipid mixing events were colocalized with EGFP-Rab5a (Figure 8B-C). Our data indicates that ZIKV is capable of fusing with both early and late endosomes but is biased towards late endosomes. This may suggest that ZIKV escapes from endosomes as they are maturing from early to MVBs/late endosomes. The GFP-Rab experiments corroborate our dominant negative and knockout data that indicate that Rab5 is necessary for optimal ZIKV infection while Rab7 perturbation has a milder impact on ZIKV infection (Figure 5). Additionally, the pH range of early endosomes is 6.8-6.2. This decreases to pH 6.2-5.0 in MVBs/late endosomes during endosomal maturation(37, 73, 74). Our findings indicate that all tested ZIKV strains except for MR766 are highly sensitive to pH 6.3-6.1. This further suggests that ZIKV fuses with endosomes as they are maturing into MVBs/late endosomes.

METHODS

Cell lines and viruses

Huh7.5 human hepatoma, HeLa human adenocarcinoma, and human embryonic kidney-derived 293T cells were grown in DMEM supplemented with 10% FBS and 0.1 mM nonessential amino acids. To induce Rab expression, pTRIPZ.GFP-Rab stably expressing Huh7.5 cells were seeded at 4 x 10^5 cells/well in 24 well plates in normal growth media supplemented with 1.5 µg/mL doxycycline. Cells were replated for experiments 3 days later in doxycycline free media.

ZIKV strain PRVABC59 was obtained from the CDC (GenBank Accession #KU501215). The virus had been passaged three times in Vero cells prior to our acquisition. ZIKV strains DAKAR 41519 and PB-81 were kindly provided by Dr. Kenneth Plante, director of the World Reference Center for Emerging Viruses and Arboviruses. ZIKV strain MR 766 was purchased from ATCC. Virus was propagated no more than 6 total passages for PRVABC59, 3 total passages for PB-81, and 3 total passages for DAKAR 41519. MR 766 has been passaged over 100 times in tissue culture. Viral stocks were prepared by infecting Vero-E6 cells with 0.01-0.05 MOI ZIKV. Cell supernatant was collected 4 days post-infection for MR 766 and 6 days post-infection for all other viruses. Cell supernatant was clarified by centrifugation at 2,000 x *g* for 20 min to remove cellular debris. Virus stocks were stored at -80 °C until use.

Plasmids and cloning

The lentiviral vector pTRIP.EGFP-PM (gift from C. Rice) expresses EGFP with a 20 amino acid plasma membrane-targeting farnesylation signal from HRAS fused the C terminus(168). The pSCRPSY control construct was prepared as previously described(169). A

plasmid containing the WT Rab5a open reading frame was kindly provided by Dr. Neal Alto. The Rab5a S34N mutant was generated from WT Rab5a by overlap extension PCR using primer sets listed in Appendix B. A DNA fragment containing the Rab7a N125I open reading frame was synthesized. Genes were amplified by PCR and cloned into pDONR.221 using BP Clonase (Invitrogen) according to manufacturer's protocol. Genes were cloned using LR Clonase II (Invitrogen) into the previously described lentiviral vector, SCRPSY-DEST, which is puromycin selectable and co-expressed TagRFP (Evrogen) with a gene of interest (170).. For CRISPR/Cas9 experiments, pLentiCRISPRv2 plasmid (a gift from Feng Zhang, Addgene plasmid # 52961) containing Rab targeting guides were kindly provided by Dr. Neal Alto (see Appendix B). The N-terminally linked GFP-Rab5a open reading frame was PCR amplified with indicated primers (Appendix B). A DNA fragment containing the N-terminally linked GFP-Rab7a open reading frame was synthesized. The doxycycline-inducible pTRIPZ.GFP-Rab constructs were produced by digesting pTRIPZ (Dharmacon) and above GFP-Rab inserts with AgeI and MluI (NEB) followed by ligation with T4 DNA ligase (NEB).

Lentivirus production and transduction

SCRPSY lentiviruses were produced as previously described(170). For lentiCRISPRv2 and TRIPZ.Rab lentivirus production, 293T cells were seeded at 4 x 10^5 cells per well into 6-well plates. The next day, cells were transfected with 1 µg lentiCRISPRv2, 0.2 µg plasmid expressing VSVg, and 0.8 µg plasmid expressing HIV-1 gag-pol using X-tremeGENE 9 (Roche). Media was changed 6 hours later and lentivirus-containing culture supernatants were

collected at 48 and 72 hr post-transfection. Pooled supernatants were clarified by centrifugation at 800 x *g* for 5 min. HEPES was added to a final concentration of 25 mM. Lentivirus was stored at -80 °C until use.

Cells were seeded at 7 x 10^4 cells per well in 24 well plates. Media was changed to DMEM supplemented with 4 µg/mL polybrene, 3% FBS, and 25 mM HEPES the next day. Cells were transduced by spinoculation at 800 x *g*, 45 min, 37°C. Media was changed 6 hours later to 10% FBS DMEM supplemented with 0.1 mM nonessential amino acids. For Rab dominant negative experiments, cells were replated at 48 hours post-transduction for subsequent experimentation. For Rab CRISPR/Cas9 targeting and TRIPZ.Rab stable cell line generation, cells were selected in 4 µg/mL puromycin for 10-12 days before subsequent experimentation.

Viral infections

Cells were seeded at 1 x 10^5 in 24 well plates 24 hours prior to infection. Cells were infected at a MOI of 2.5 with virus diluted in 200 µl (total volume) DMEM containing 1% FBS for 1 hr at 37 °C. Afterwards, 500 µl normal growth medium was added to each well. After 24 hours, cells were dislodged with Accumax, centrifuged at 800 x *g* for 2 min at 4°C, fixed in 1% PFA for 10 min, and resuspended in PBS with 3% FBS for antibody staining and flow cytometry analysis.

pH inactivation experiments

Huh7.5 cells were seeded at 1 x 10^5 in 24 well plates 24 hours prior to infection. Phosphate-acetate buffer solutions consisted of 0.9 mM $CaCl_2$, 2.6 mM KCl, 0.5 mM $MgCl_2$, 10 mM K_2HPO_4, and 50 mM acetic acid. Buffer solutions were titrated in 0.2 pH unit increments between pH 4.4 and 7.0 with 5 M NaOH. NaCl was added to each solution to bring the final NaCl concentration to 73.5 mM. The pH of 900 µl of each of the above buffers was or was not changed to pH 7 by addition of 1 M, pH 8.2 HEPES buffer. 1% FBS was added to all solutions. ZIKV strains, diluted to 100 µl in DMEM, were added to each buffer or neutralized control for 40 min at 37 °C. Solution pH after addition of 100 µl DMEM was determined and the adjusted pH was used for the analysis of the experiment. ZIKV containing solutions were adjusted to pH 7 by addition of 1 M, pH 8.2 HEPES buffer. Huh7.5 cells above were infected with 500 µl of the above solutions for 2 hr at 37 °C. Media was subsequently changed to 500 µl normal growth media. Infection was quantitated 24 hr later by flow cytometry. The best-fit asymmetric 5 parameter curve and corresponding $logEC_{50}$ value was determined for each data set using Prism 7.

Drug treatments

Cells were treated with 2.5 µM nocodazole, 200 nM Bafilomycin A1, 10 mM NH_4Cl, or 0.1% DMSO in DMEM containing 1% FBS at 37 °C for 1 hr before cell infection. Respective drugs were added to infection media as well as the normal growth media added to each well after infection.

Zika virus R18 labelling and infection

PRVABC59 was concentrated with ultracentrifugation through a 20% sucrose cushion in an SW-28 rotor at 110,000 x *g* for 90 min. PRVABC59 was diluted to 100 µg/mL viral protein. 6 µL of a 1 mM octadecyl rhodamine B (R18) stock in EtOH was added per mL of ZIKV for 2 hr at room temperature. The labelling reaction was filtered through a 0.22 µm filter to remove excess R18. For infections, Huh7.5 cells were seeded at 1 x 10^5 cells/well in 8 well chamber slides or 35 mm glass bottom dishes (MatTek) the day before infection for fixed or live cell experiments respectively. For the fixed cell data sets, cells were chilled to 4 °C for 30 min. Labelled PRVABC59 was bound to cells at a MOI of 1 in 200 µL DMEM containing 1% FBS for 1 hr at 4 °C. Media was subsequently changed to 300 µL DMEM containing 1% FBS warmed to 37 °C. After 15 min, 100 µL 4% PFA was added. For WGA colocalization experiments, cells were then stained with 2 µg/mL Alexa Fluor 488 conjugated WGA (ThermoFisher) for 10 min. Cells were washed twice with PBS containing Ca^{2+}/Mg^{2+} and fixed again with 1% PFA. Alternatively, uninfected Huh7.5 cells stably expressing TRIP.PM-GFP were stained with Alexa Fluor 647 conjugated WGA (ThermoFisher) as above. Slides were mounted with Prolong Gold Antifade Mountant. Rab-R18 colocalization images for fixed cells were taken on a Zeiss LSM 780 confocal microscope. WGA-R18 colocalization z-stacks were taken on an FV10i confocal microscope. After image acquisition, colocalization of R18 dequenching events and PM-GFP with WGA was quantitated with CellSense Dimension Software. Acquired z-stacks were deconvoluted using 50 iterations of the constrained iterative approach. The average Pearson correlation coefficient for all images in deconvoluted z-stacks was determined. Due to the limited amount of R18 signal present in acquired images, Pearson

correlation coefficients were determined only for image regions with high R18 signal. For the live cell data set, cells and virus were equilibrated to room temperature (23° C) for 30 min. Labelled PRVABC59 was added to cells at a MOI of 1 in 500 µL DMEM containing 1% FBS. Due to timing constraints, images were taken on an FV10i confocal microscope starting at 10 min post-infection every 26s with the 5X confocal aperture setting. After image acquisition, R18 dequenching events and their colocalization with Rab markers was quantitated manually.

Western blot

Samples were run on a 10% polyacrylamide SDS-PAGE gel, transferred onto nitrocellulose membrane, and blocked for 30 min with 5% milk in TBS containing 0.1% Tween-20 (TBS-T). Membranes were probed with one of the following primary antibodies: 1:1000 anti-CLTC (Sigma, C1860), 1:1000 anti-CAV1 (Sigma, C4490) 1:1000 anti-Rac1 (ThermoFisher, PA1-091), 1:3000 anti-actin (abcam, ab6226), or 1:1000 anti-EGFR (Cell Signaling Tech, 4267). For standard experiments, membranes were washed with TBS-T, probed with goat anti-rabbit or goat anti-mouse HRP conjugated antibodies (Pierce), incubated with ECL substrate (Pierce) according to manufacturer's instructions, and exposed to film. For quantitative experiments, membranes were probed with goat anti-mouse or donkey anti-goat IR Dye conjugated antibodies (Licor). Membranes were washed with TBS and signal was detected using a Licor Odyssey system.

EGFR degradation assay

Huh7.5 cells were plated in 24-well plates at 1 x 10^5 cells per well with standard growth media the day before. Cells were washed 2 times with PBS and media was changed to DMEM without serum for 4 hours. Media was changed to DMEM containing 100 nM cycloheximide with or without 200 ng/mL EGF. At 0, 1, 2, 3, or 4 hours later, cells were washed with PBS and lysed in RIPA buffer containing a 1X protease inhibitor (Roche). EGFR levels relative to actin were quantitated by western blot as described above.

Antibody staining and flow cytometry

For quantitation of ZIKV infections, infected cells were harvested, permeabilized and stained with 1:2500 anti-Flavivirus Group Antigen Antibody (D1-4G2-4-15) using the Cytofix/Cytoperm kit according to the manufacturer's instructions (BD Bioscience). Samples were subsequently stained with Alexa Fluor 488 conjugated goat anti-mouse antibody (Invitrogen) and cell fluorescence quantified by flow cytometry. An S1000 flow cytometer (Stratedigm) was used and data were analyzed using FlowJo (Treestar). On average a minimum of 10,000 cells were counted per condition. For the virus pH inactivation experiments specifically, a minimum of 4,000 cells were counted per condition due to cell loss.

Immunofluorescence

Wash buffer (WB) consisted of 1% BSA, 0.1% Tween-20 in PBS with Ca^{2+}/Mg^{2+}. Samples were permeabilized for 10 min with 0.2% Triton X-100 in WB and blocked overnight in WB. Samples were incubated with 1:1000 anti-α-tubulin (Sigma, T6074) in WB for 1 hr, washed 2 times in WB for 1 min each, and probed with 1:1000 goat anti-mouse Alexa Fluor 488 conjugated antibody (Life Technologies) in WB for 1 hr. Samples were washed twice with WB. Samples were mounted with Prolong Gold Antifade Mountant (ThermoFisher). Immunofluorescence samples were imaged with epifluorescence microscopy on a Nikon ECLIPSE Ti.

siRNA mediated knockdown

HeLa cells were seeded at 5 x 10^4 cells/well in 24 well plates 24 hours before siRNA transfection in 500 µL normal growth media. 0.2 µL of 20 µM SMARTpool siRNAs (Dharmacon) targeting *CLTC* (L-004001-01-0005), *RAC1* (L-003560-00-0005), *CAV1* (L-003467-00-0005), or nontargeting control (D-001206-14-05) were diluted in 100 µL DMEM. Subsequently, 3 µL HiPerfect transfection reagent was added. After 10 min, transfection complexes were added to the above cells. 2 days later, cells were replated for experimentation.

Endocytic marker uptake

HeLa cells were seeded at 2 x 10^4 cells/well in 8-well chamber slides in normal growth media. The next day, cells were washed once and incubated in serum free DMEM for 1 or 24 hours for transferrin or dextran uptake assays respectively. For transferrin uptake, cells were incubated with 25 µg/mL Alexa Fluor 488 conjugated transferrin (ThermoFisher) in DMEM for 20 min. For dextran uptake, cells were incubated with 2 mg/mL FITC conjugated 70 kDa dextran (ThermoFisher) for 30 min. Cells were washed once with DMEM and fixed with 4% PFA for 10 min. Slides were mounted with Prolong Gold Antifade Mountant and imaged with an FV10i confocal microscope.

Statistical analysis

For normalized data sets, a ratio paired T test was used to determine statistical significance. For the EGFR degradation experiments, a two-way ANOVA was used. For analysis of $\log EC_{50}$ values generated from the pH inactivation experiment, a one-way analysis of variance (ANOVA) with Sidak's post-test was used. For all other data sets, statistical significance was determined using a Student's T test with Welch's correction.

FIGURES AND TABLES

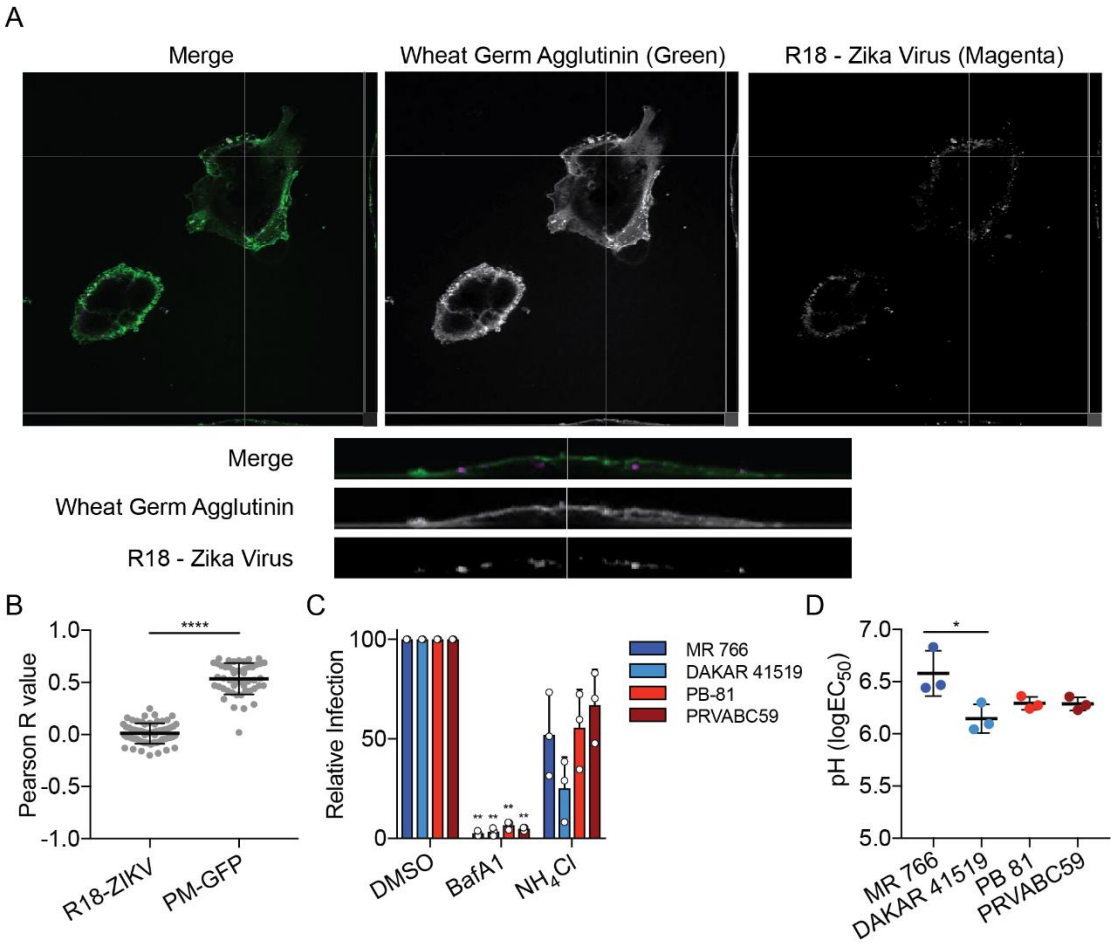

Figure 1: Zika Virus is endocytosed during cell entry and enters in a conserved, pH dependent manner. (A, Top) Huh7.5 cells were infected with R18 labeled PRVABC59 for 15 min, fixed, stained with WGA-AF488, and z-stacks acquired on a confocal microscope. (Bottom) Enlarged z-stack cross sections in the X-Z direction. (B) Pearson correlation coefficients for R18-ZIKV (N=68) and PM-GFP control (N=50) colocalization with WGA. (C) Huh7.5 cells pretreated with indicated drugs were infected with the ZIKV strains shown. (D) Indicated ZIKV strains were incubated in buffers between pH 4.4-7.0 for 40 minutes. The pH of virus-containing buffers was adjusted to pH 7.0 with 1 M pH 8 HEPES and virus inactivation was assessed by infection of Huh7.5 cells. Calculated $\log EC_{50}$ values are shown. Infections were quantitated 24 hours post-infection by 4G2 staining and flow cytometry. In A, representative images from one of three independent experiments are shown. In B, data was collected from three independent experiments. In C, data represents means of three independent experiments performed in technical triplicate. In D data represents means of three independent experiments performed in technical singlet or duplicate. Error bars represent SD. (* $P \leq 0.05$, ** $P \leq 0.01$, **** $P \leq 0.0001$).

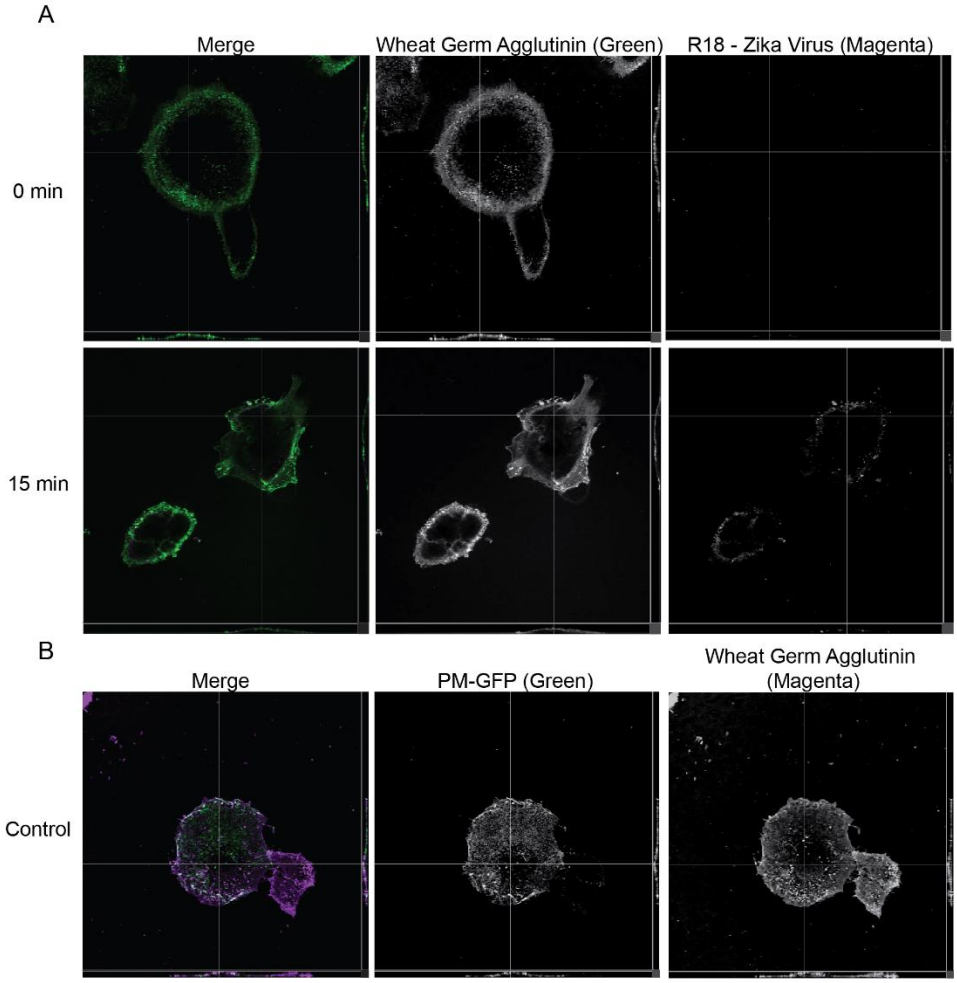

Figure 2. Zika virus fuses with the membrane of an internal cellular compartment. (A) Huh7.5 cells were infected with R18 labeled PRVABC59 for 0 or 15 minutes, fixed, stained with WGA-AF488, and z-stacks acquired on a confocal microscope. (B) Huh7.5 cells stably expressing PM-GFP were fixed, stained with WGA-AF647, and z-stacks acquired on a confocal microscope. Representative images from three independent experiments are shown.

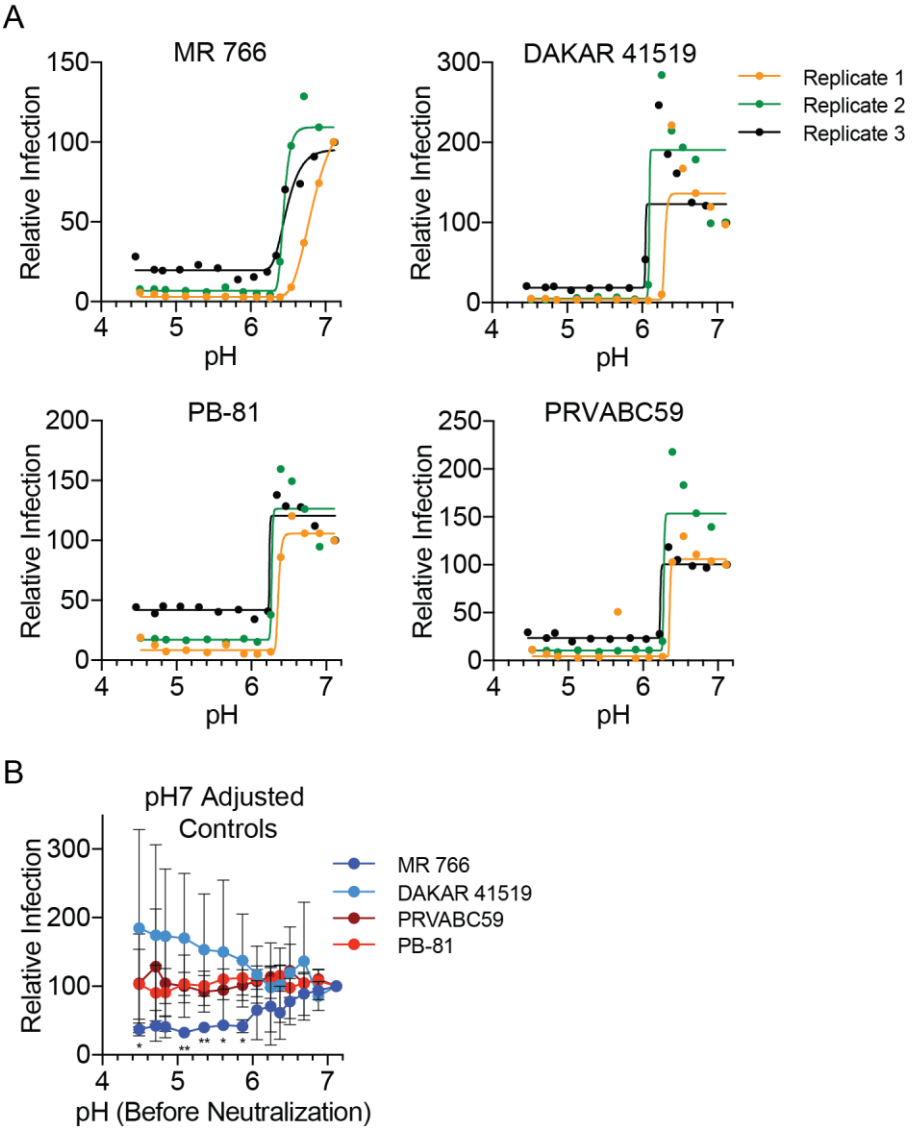

Figure 3. Determining the pH sensitivity of Zika virus. (A) Indicated ZIKV strains were incubated in buffers between pH 4.4-7.0 for 40 min. The pH of virus-containing buffers was adjusted to pH 7.0 with 1 M pH 8 HEPES and virus inactivation was assessed by infecting Huh7.5 cells. Data for each replicate were fit to an asymmetric 5 parameter logistic curve. (B) As in A, except buffer pH was adjusted back to pH 7.0 with 1M pH 8 HEPES buffer before incubation with viruses. Infections were quantitated 24 hours post-infection by 4G2 staining and flow cytometry. Data represents means of three independent experiments performed in technical singlet or duplicate. Error bars represent SD. (* $P \leq 0.05$, ** $P \leq 0.01$).

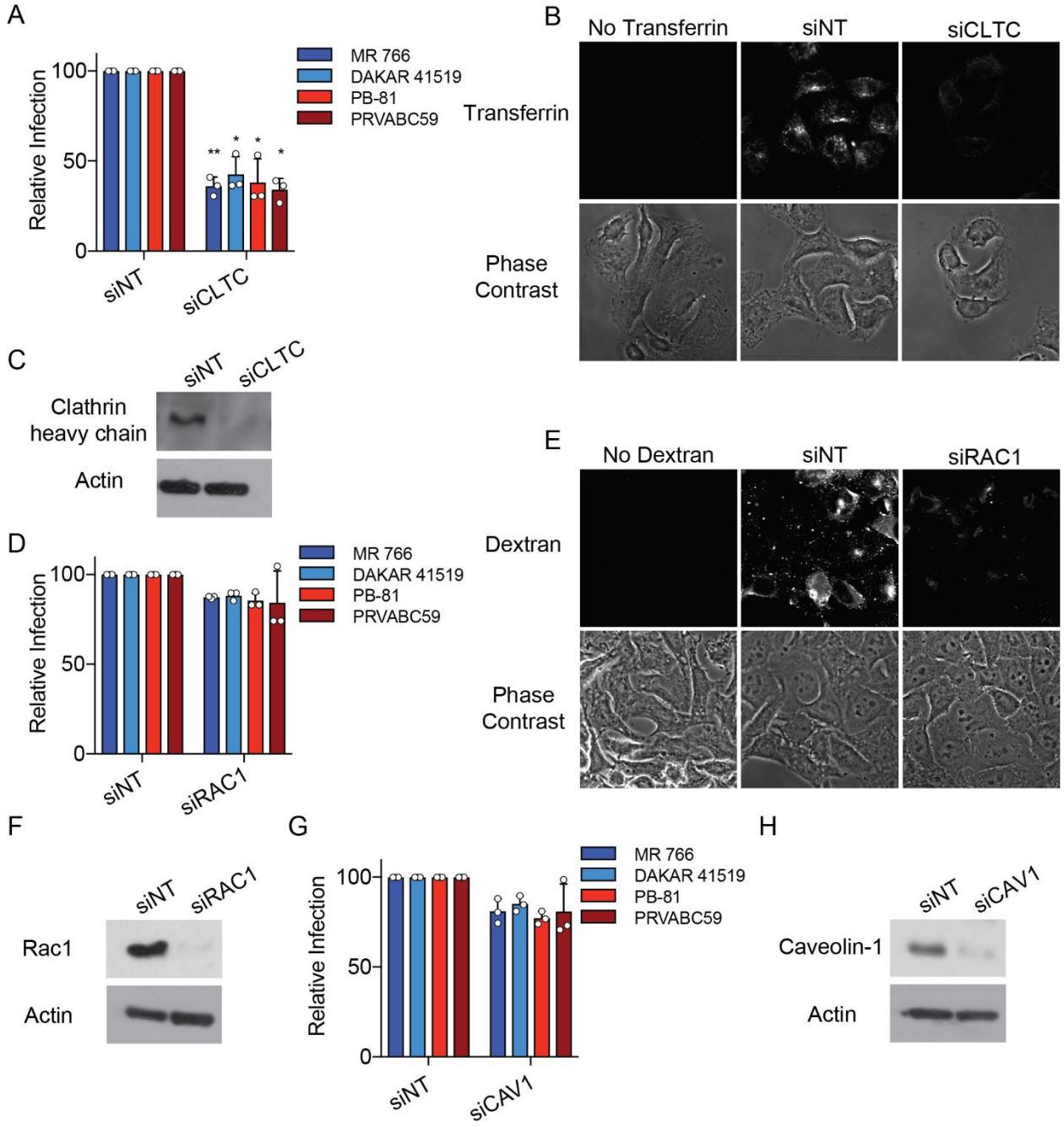
A
Relative Infection
100
50
0
siNT
siCLTC
MR 766
DAKAR 41519
PB-81
PRVABC59
B
No Transferrin
siNT
siCLTC
Transferrin
Phase Contrast
C
siNT
siCLTC
Clathrin heavy chain
Actin
D
Relative Infection
siNT
siRAC1
MR 766
DAKAR 41519
PB-81
PRVABC59
E
No Dextran
siNT
siRAC1
Dextran
Phase Contrast
F
siNT
siRAC1
Rac1
Actin
G
Relative Infection
siNT
siCAV1
MR 766
DAKAR 41519
PB-81
PRVABC59
H
siNT
siCAV1
Caveolin-1
Actin

Figure 4: Asian and African lineage Zika virus require clathrin for infection. HeLa cells were transfected with a pool of 3 siRNAs targeting *CLTC* (A-C), *RAC1* (D-F), *CAV1* (G-H), or nontargeting control. (A,D,G) Transfected cells were infected with indicated ZIKV strains. Infection was quantitated 24 hours post-infection by 4G2 staining and flow cytometry. (B) Representative confocal images from siRNA transfected Huh7.5 cells serum starved for 1 hour and subsequently incubated with or without 2.5 µg/mL transferrin-AF488 for 20 minutes. (C) CLTC protein expression levels with indicated siRNA treatment. (E) Representative confocal images from siRNA-transfected Huh7.5 cells that were serum starved for 24 hours and subsequently incubated with or without 2 mg/mL 70 kDa FITC-conjugated dextran for 30 min. (F) Rac1 protein expression levels with indicated siRNA treatment. (H) CAV1 protein expression levels with indicated siRNA treatment. In A, D, and G, data represents means of three independent experiments performed in technical triplicate. In all other panels, representative images from at least three independent experiments are shown. Error bars represent SD. (* $P \leq 0.05$, ** $P \leq 0.01$).

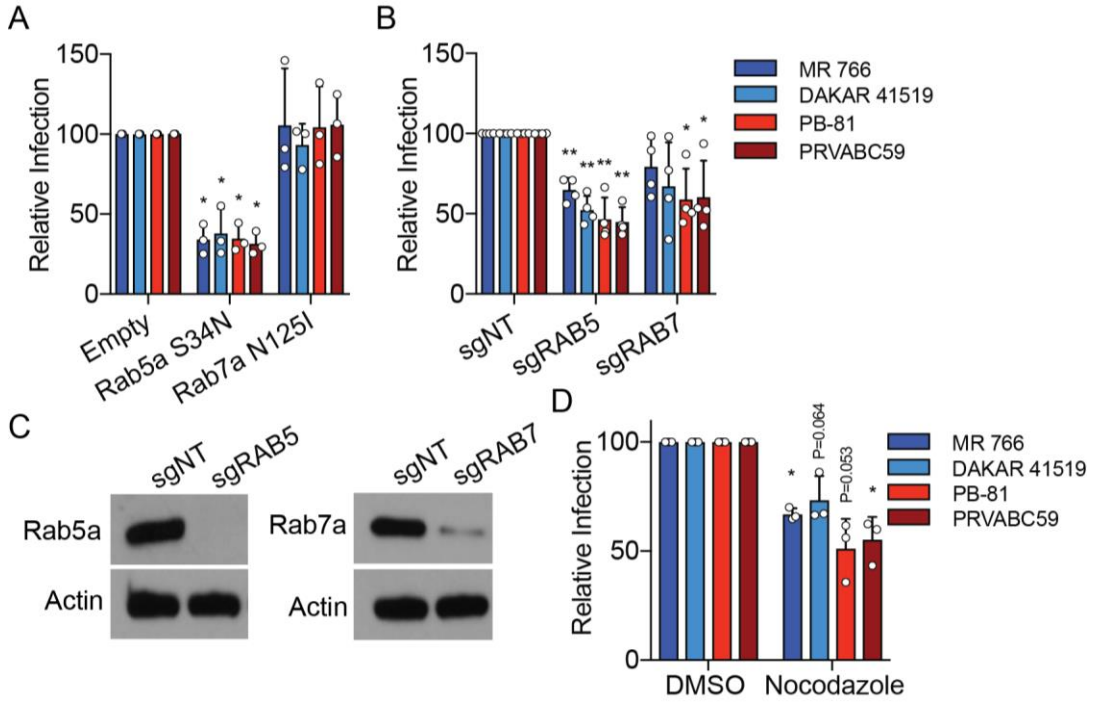

Figure 5: Asian and African lineage Zika virus require Rab5 for infection. (A) Huh7.5 cells expressing indicated constructs were infected with the ZIKV strains shown. (B) *RAB5* and *RAB7* loci were targeted with the CRISPR/Cas9 gene editing system in Huh7.5 cells. Cells were subsequently infected with the ZIKV strains shown. (C) Rab5 or Rab7 protein expression after indicated CRISPR/Cas9 mediated gene editing. (D) Huh7.5 cells pretreated with indicated drugs were infected with the ZIKV strains shown. Infections were quantitated 24 hours post-infection by 4G2 staining and flow cytometry. In A, B, and D, data represents means of three or four independent experiments performed in technical triplicate. In C, representative images from at least three independent experiments are shown. Error bars represent SD. (* $P \leq 0.05$, ** $P \leq 0.01$).

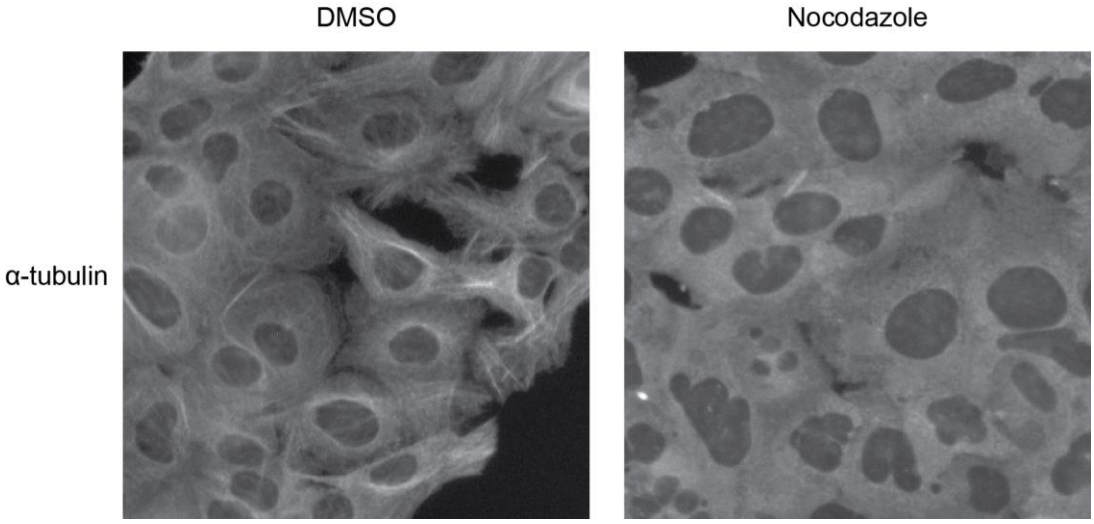

Figure 6. Nocodazole treatment depolymerizes microtubules in Huh7.5 cells. Huh7.5 cells were treated with 2.5 µM nocodazole or 0.1% DMSO for 24 hours. Cells were subsequently fixed and stained with anti-α-tubulin. Cells were imaged with epifluorescence microscopy. Representative images from three independent experiments are shown.

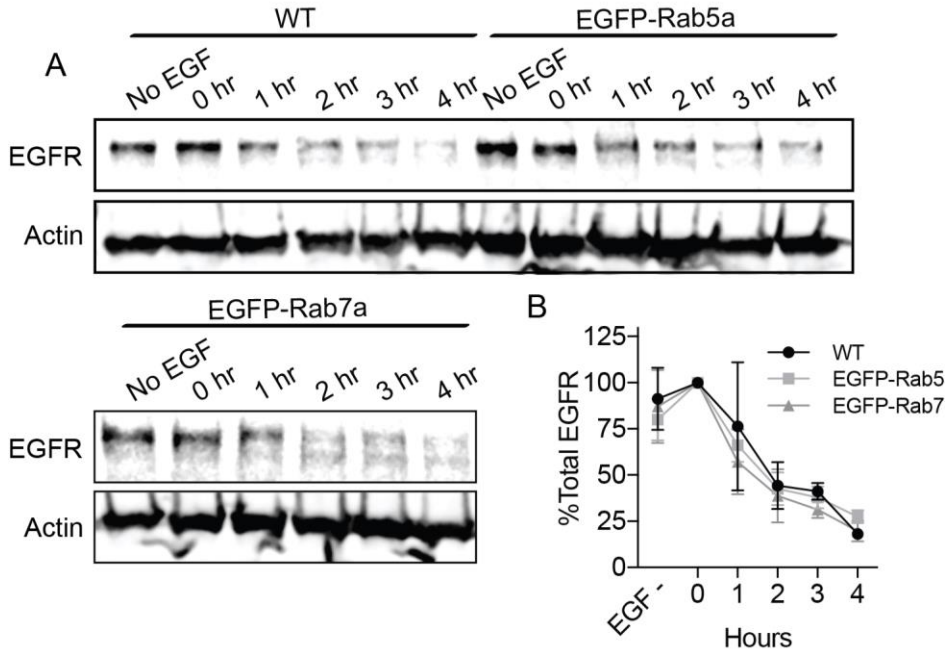

Figure 7. Doxycycline-induced expression of EGFP-Rab constructs does not affect vesicular trafficking or lysosomal degradative capacity. WT Huh7.5 cells or cells expressing doxycycline-inducible EGFP-Rab5a or EGFP-Rab7a were serum starved for 4 hours. Cells were treated with 200 ng/mL hEGF and 100 nM cycloheximide containing media and lysed at the time points indicated after the start of hEGF treatment. (A) EGFR protein levels were visualized over time (B) and quantified. In A, representative images from three independent experiments are shown. In B, data represents means of three independent experiments. Error bars represent SD.

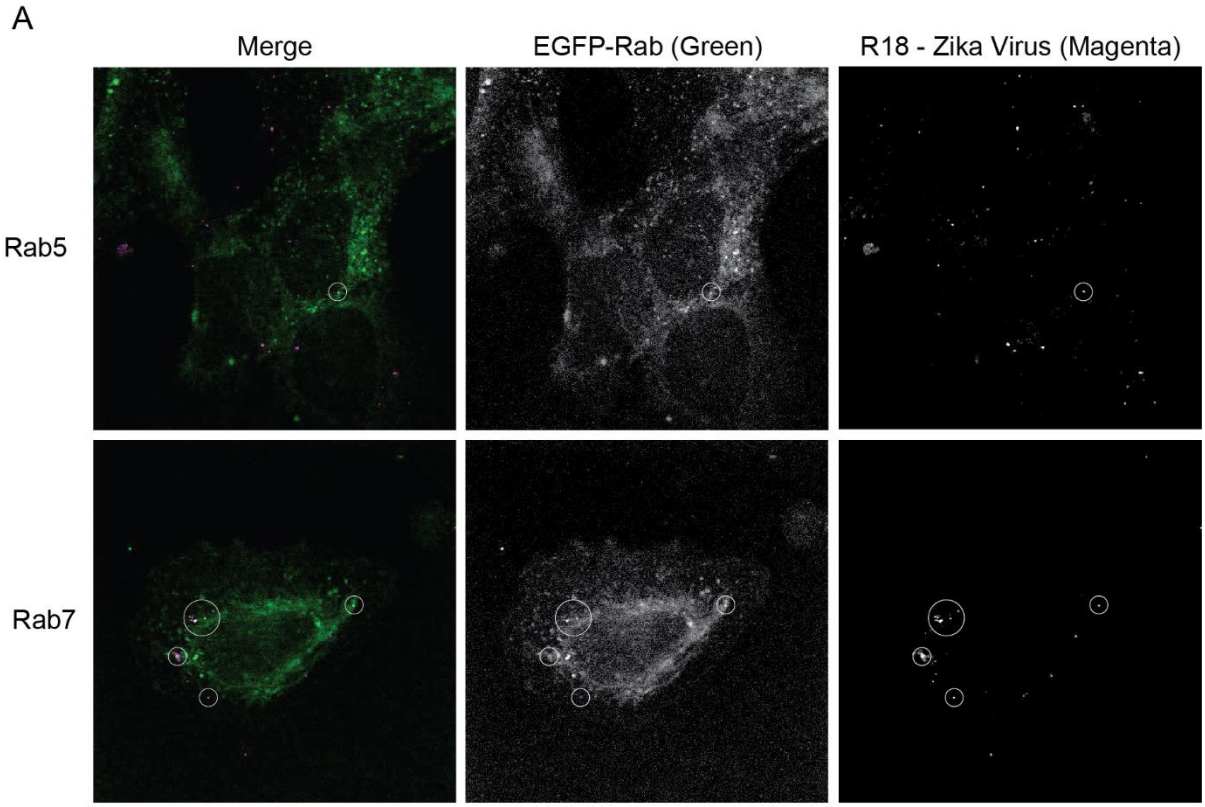
A
Merge
EGFP-Rab (Green)
R18 - Zika Virus (Magenta)
Rab5
Rab7

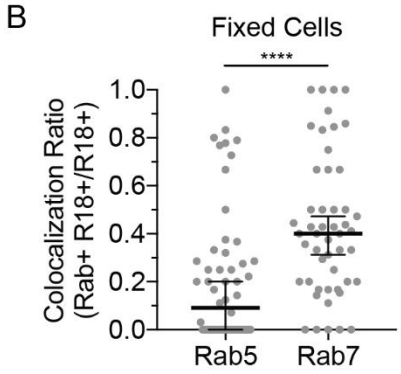
B
Fixed Cells
****
Colocalization Ratio
(Rab+ R18+/R18+)
1.0
0.8
0.6
0.4
0.2
0.0
Rab5
Rab7

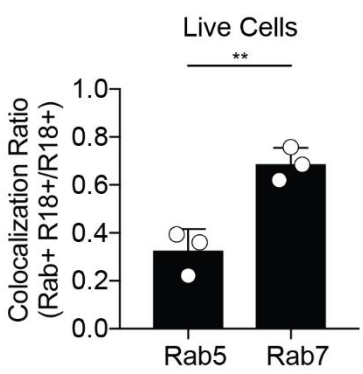
C
Live Cells
**
Colocalization Ratio
(Rab+ R18+/R18+)
1.0
0.8
0.6
0.4
0.2
0.0
Rab5
Rab7

Figure 8: Zika Virus fuses preferentially with late endosomes. (A-B) Huh7.5 cells expressing doxycycline-inducible EGFP-Rab5a or EGFP-Rab7a were infected with R18-labelled PRVABC59 for 15 minutes. (A) Cells were fixed and imaged with confocal microscopy. (B) The ratio of colocalizing R18/EGFP-Rab puncta to the total number of R18 puncta per cell was quantitated for Rab5 (N=56) and Rab7 (N=50). (C) Huh7.5 cells expressing doxycycline-inducible EGFP-Rab5a or EGFP-Rab7a were infected with R18-labelled PRVABC59 and imaged in real time with confocal microscopy. The ratio of colocalizing R18/EGFP-Rab puncta to the total number of R18 puncta per experiment was quantitated for Rab5 and Rab7. In A, representative images from three independent experiments are shown. In B, data was collected from three independent experiments. In C, data points represent three independent experiments with $N \leq 25$ for each data point. Error bars represent SD. (** $P \leq 0.01$, **** $P \leq 0.0001$).

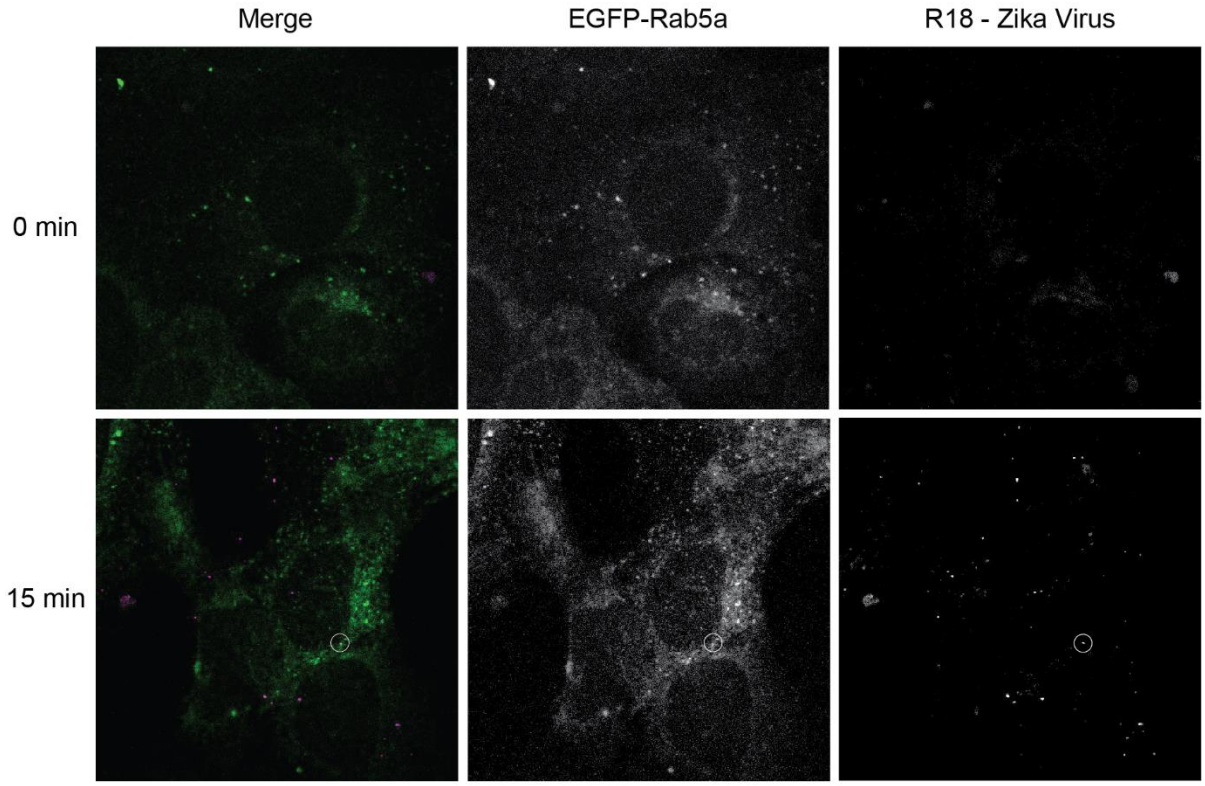
Merge
EGFP-Rab5a
R18 - Zika Virus
0 min
15 min

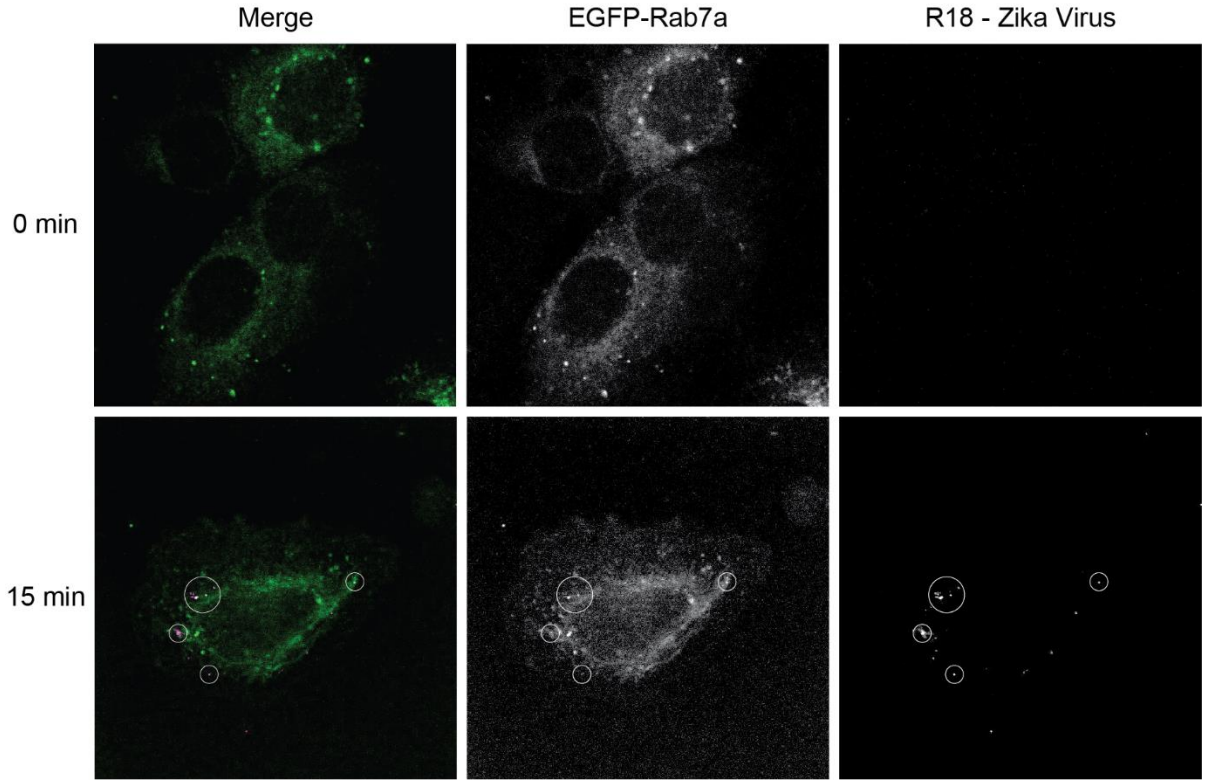
Merge
EGFP-Rab7a
R18 - Zika Virus
0 min
15 min

Figure 9. Colocalization of early and late endosomes with Zika virus fusion events. Huh7.5 cells expressing doxycycline-inducible EGFP-Rab5a or EGFP-Rab7a were infected with R18-labelled PRVABC59 for 0 or 15 minutes. (A) Cells were fixed and imaged with confocal microscopy. Representative images from three independent experiments are shown.

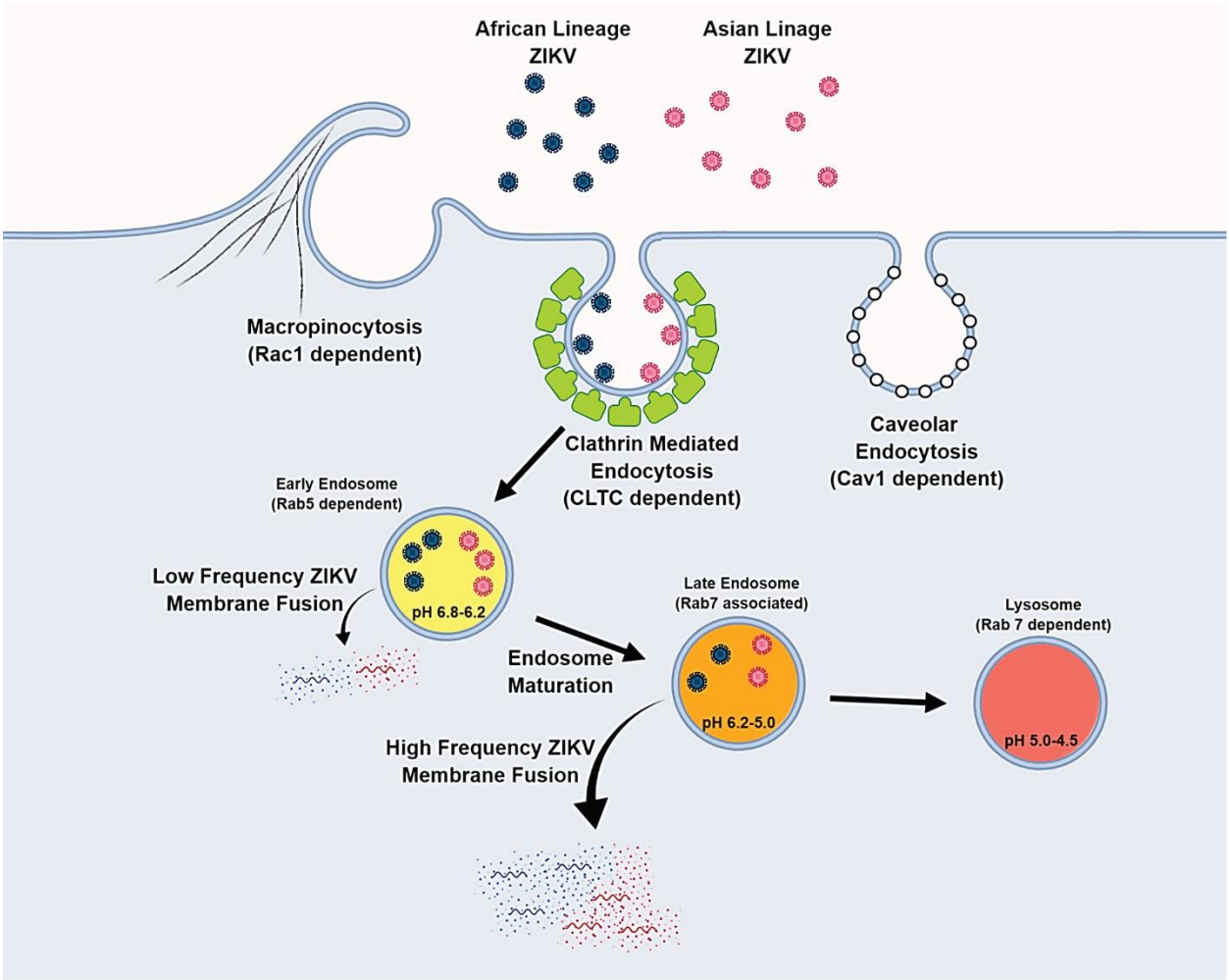

Figure 10: Model of Zika virus entry: ZIKV entry is highly conserved between African and Asian lineages. Following cell surface attachment, ZIKV enters cells through clathrin-mediated endocytosis. Endocytic vesicles containing ZIKV are targeted to the mildly acidic early endosome compartment where the viral envelope fuses with the endosomal membrane at a lower frequency. For the majority of entry events, ZIKV-containing endosomes mature to moderately acidic MVBs and late endosomes, where the viral envelope fuses with the endosomal membrane at a higher frequency.

CHAPTER THREE
Mucolipin-2 cation channel increases trafficking of endocytosed viruses

INTRODUCTION

Animal viruses enter host cells by direct penetration at the plasma membrane or by endocytosis. Endocytic viruses rely on diverse uptake mechanisms, including but not limited to clathrin-mediated endocytosis, macropinocytosis, and caveolin/lipid raft-mediated uptake. A growing number of host factors have been found to be involved in these diverse viral uptake pathways, including coat proteins (clathrin, caveolin), scission factors (DNM2) as well as regulatory and trafficking factors (Ras, Rac1, Cdc42, PI3Ks, Rab GTPases, etc.)(38). Identifying new factors that regulate these viral entry processes is critical for understanding the complexities of the viral life cycle and for identifying key vulnerabilities in the infection process.

In recent screening efforts for IFN-inducible factors that modulate viral infection, Schoggins et al. found that MCOLN2 enhanced the infectivity of diverse viruses, including yellow fever virus, dengue virus, influenza A virus, and equine arteritis virus(120, 169). MCOLN2 belongs to the transient receptor potential (TRP) protein superfamily, which consists of gated, tetrameric cation channels with diverse physiological functions, particularly in sensory signaling.

The transient receptor potential superfamily

The first transient receptor potential (TRP) family member was identified in a *Drosophila* mutant which had impaired light sensitivity. This mutant only had a transient, rather than

sustained, response to light(171). The gene responsible was so named *trp* and later identified in 1989(171). Since then, 28 functional TRP channels have been identified in mammals. These proteins have been further grouped into the subfamilies: TRPC (canonical), TRPM (melastatin), TRPV (vanilloid), TRPA (ankyrin), TRPP (polycystin), and TRPML (mucolipin).

Properties of TRP family proteins

TRP family members are all integral membrane proteins which homo- or heterotetramerize to form gated, cation permeable channels. TRP channels are typically permeable to divalent cations including Ca^{2+} which is thought to play a key role in TRP channel-mediated signaling. In fact, TRPV1-4 are weakly Ca^{2+} selective. Notably however, TRPM4b and TRPM5 have been shown to only be permeable to monovalent cations(172).

These proteins share a conserved structure of 6 transmembrane helices with varying cytoplasmic oriented N- and C-terminal domains. The channel is formed by transmembrane domains 5 and 6 as well as a pore loop in between these two transmembrane domains. In the canonical structure of TRP family proteins, such as that observed with the TRPC subfamily, the N-terminus contains 3-4 ankyrin repeats, a putative coiled-coil region, and a putative caveolin binding region. After the transmembrane domain region, the C-terminus contains the so called TRP motif (EWKFAR), a proline rich motif, a calmodulin / IP_3 receptor binding region, and another coiled coil region. However, while the transmembrane domain region of TRP family members is conserved, the N- and C-termini of TRP family members differ considerably. For example, members of the TRPA subfamily possess 14-17 ankyrin repeats in the N-terminus and lack the C-terminal TRP motif. TRPM6 and 7 have a functional, C-terminal atypical alpha

protein kinase domain. In contrast, TRPML subfamily members have much shorter N- and C-termini, lacking both ankyrin repeats and the TRP motif(172-174).

TRP family members have been shown to be expressed in a diverse array of tissues. Many TRPs have divergent expression patterns. Some are only expressed in a subset of tissues while others are ubiquitously expressed. However, at the cellular level, the majority of TRP channels seem to either localize to the plasma membrane or only have activity if relocalized to plasma membrane from internal compartments. In contrast, the members of the TRPML subfamily are localized to and active in endosomal compartments(172-176).

Functions of TRP Family Proteins

TRP family members are generally recognized as cell sensors or receptors. Beyond this, TRP channels have been found to have diverse functions. TRPC1 was originally identified as a putative store operated channel (SOC) in store operated calcium entry (SOCE)(177). SOCE is a method of Ca^{2+} signal amplification and intracellular Ca^{2+} store replenishment. In response to induced release of Ca^{2+} from the ER, SOCs on the cell surface open. This results in further calcium diffusion into the cytoplasm, amplifying Ca^{2+} signaling and the increasing cytosolic Ca^{2+} concentrations to replenish intracellular calcium stores(178). While TRP channels have not been directly identified as the channels responsible for SOCE, members of the TRPC subfamily have been found to be important for SOCE(177). For example, TRPC1 may be important for SOCE-mediated fluid and electrolyte secretion from salivary gland cells(179). Additionally, $TRPC1^{-/-}$ mice are reported to display impaired vasorelaxation of the aortic rings which has been suggested to be due to a defect in SOCE(180). SOCE is also important for fertilization of mammalian eggs

by sperm. While TRPC2 was not found to be important for fertility in mice, the TRPC related protein TRP-3 was found to be important for fertility in *C. elegans*(181, 182).

TRPM6 deficiency has been found to result in hypomagnesemia and, to a lesser extent, hypocalcemia(183, 184). TRPM6 is predominantly expressed in the small intestine as well as the kidneys and is known to be permeable to Mg^{2+}(185). This has led to the suggestion that TRPM6 is important for calcium and magnesium absorption. Additionally, TRPV1 has been shown to be important for bladder function in mice(186).

The most common function attributed to TRP channels is sensory perception. Certain TRP channels are expressed on sensory neurons and play important roles in mechanosensation, thermosensation, chemosensation, and hearing(173). For example, TRP channels have been identified which are sensitive temperatures greater than 40 °C (TRPV1-4, TRPM2-5) or less than 20 °C (TRPM8) as well as capsaicin (TRPV1) and menthol (TRPM8)(174). Mechanosensitive TRP channels have also been identified. For example, $TRPV4^{-/-}$ mice have been shown to be less sensitive to hyposmolarity(187). In contrast, constitutive activity of TRPML3 has been associated with early onset hearing loss in mice(188).

The transient receptor potential mucolipin subfamily

The TRPML subfamily contains three proteins, MCOLN1, MCOLN2, and MCOLN3. Most TRP proteins are localized to or only functional at the plasma membrane(189, 190). However, the TRPML subfamily of proteins are localized predominantly to endosomes, where they form gated cation channels with strong, inwardly rectifying currents. All of these channels

have been found to be permeable to Na^+, K^+ and Ca^{2+}(175, 191). However, only MCOLN1 and MCOLN2 are suggested to be permeable to Fe^{2+}(192). MCOLN channels have roles in vesicular trafficking, autophagy, and membrane fusion(175, 176, 191). Additionally, perturbation of the function of certain MCOLN subfamily members is known to cause disease in humans and mice.

Expression patterns and sub-cellular localization of MCOLN channels

MCOLN channels have divergent expression patterns. MCOLN1 is ubiquitously expressed(193). In contrast, MCOLN2 is predominantly expressed in lymphoid tissues and kidneys(194). Unlike other MCOLNs, MCOLN2 expression is induced in mouse macrophages in response to LPS(195) as well as in chimpanzee peripheral blood mononuclear cells in response to type I IFN(196). MCOLN3 has been detected at high levels in cochlear hair cells and skin melanocytes using MCOLN3-specific antibodies(197, 198). MCOLN3 is also expressed in endocrine tissues(193).

MCOLN channels are localized predominantly to endosomal compartments. MCOLN1 localizes to late endosomes/lysosomes and MCOLN3 localizes to early endosomes as well as late endosomes/lysosomes(199-202). MCOLN2 was originally thought to localize to recycling endosomes, late endosomes, and lysosomes based on the localization of ectopically expressed recombinant MCOLN2(199, 203). Later, endogenously expressed MCOLN2 was found to localize to recycling endosomes in primary macrophages isolated from mice(195). Further evidence suggesting that MCOLN channels function predominantly in endosomes came from the finding that all MCOLN subfamily members are activated by phosphatidylinositol 3,5 bis-phosphate(204). PI(3,5)P2 is generated by 1-phosphatidylinositol 3-phosphate 5-kinase

(PIKfyve), a kinase localized to endolysosomal compartments(205, 206). However, expression of a dominant negative DNM2 results in the accumulation of MCOLN proteins at the cell surface(199, 202). This suggests that MCOLN protein localization may be dynamic, cycling between endocytic compartments and the cell surface.

While MCOLN proteins are known to form homotetrameric cation channels, multiple studies have reported that ectopically coexpressed MCOLN channels can also form functional heterotetrameric channels(207, 208). Additionally, expression of MCOLN2 appears to be dependent on MCOLN1 expression in mice(194). However, due to the divergent expression patterns of MCOLN subfamily members, the functional relevance of heterotetramerization *in vivo* is questionable.

Disease associated with abnormal function of MCOLNs

Loss of function mutations in MCOLN1 cause the human autosomal recessive disorder mucolipidosis type IV (ML-IV)(209, 210). This disorder is characterized by severe mental and psychomotor retardation, retinal degeneration, and hypotonia(211-213). At the cellular level, ML-IV is characterized by a lysosomal storage disease in which enlarged late endosomes/lysosomes form with an unusual retention of gangliosides, phospholipids, and mucopolysaccharides. Irregular retention of metabolites and lipids in the lysosomal compartment is due to a defect in trafficking of lysosomal cargo to the plasma membrane and the Golgi(213). While humans possess three MCOLN subfamily members, *Drosophila* and *C. elegans* both have only a single MCOLN isoform named *trpml* and *cup-5* respectively. Perturbation of MCOLN isoforms in *Drosophila* or *C. elegans* results in a similar enlargement of late

endosomes/lysosomes as is seen with ML-IV in humans(214-216). Additionally, *trpml*$^{-/-}$ *Drosophila* have been found to exhibit similar characteristics to ML-IV including severe motor defects, neurodegeneration, and eye defects(216).

While not associated with any disease phenotype in humans, a mutation causing constitutive activity of MCOLN3 results in early onset hearing loss and vestibular impairment, a phenotype in mice known as the varitint-waddler phenotype(188, 198). Hearing loss and vestibular impairment are suggested to result from the loss of hair cells expressing constitutively active MCOLN3. Hair cell loss is suggested to be caused by the MCOLN3-mediated sustained release of calcium into the cytoplasm at toxic levels(197). MCOLN2 perturbation is not associated with any disease phenotype. However, expression of a constitutively active MCOLN2 channel in fibroblasts *in vitro* is cytotoxic in a similar manner to MCOLN3 mutant expression(217).

Function of MCOLN proteins

MCOLNs have been found to be involved in a number of host processes. One such process is iron uptake. Release of iron from endosomes is important for iron metabolism. Patch clamping experiments have shown that the MCOLN1 channel is permeable to Fe^{2+} and that MCOLN2 may be permeable as well. Additionally, a retention of Fe^{2+} in lysosomes is observed in MCOLN1 deficient fibroblasts, suggesting that MCOLN1 is important for iron uptake(192, 218). MCOLNs may also play a role in endosomal acidification. However, this claim has been disputed(175). Conflicting reports describe lysosomal pH as significantly increased or decreased in ML-IV cells(216, 219, 220). Additionally, MCOLN2 and MCOLN3 have been shown to be

impermeable to H^+. The permeability of the MCOLN1 channel to H^+ is disputed(175, 191). Additionally, while MCOLN1 channel-derived currents are increased at low pH, MCOLN2- and MCOLN3-derived currents are reduced even at a mildy acidic pH(198, 221, 222). For MCOLN3, the pH EC_{50} is approximately pH 6.4 which implies that MCOLN3 current is reduced even in early endosomes where only mild endosome acidification has occurred(73, 75, 221).

MCOLN subfamily proteins play a role in many vesicular trafficking events and autophagy(175, 216). MCOLN1 is important for lysosomal fission(204). In turn, the impact of MCOLN1 on lysosomal fission impacts the efficiency of lysosomal trafficking and fusion events. These include lysosomal exocytosis as well as fusion of lysosomes with autophagosomes and late endosomes(200, 223-229). In addition to impacting autophagosome-lysosome fusion, MCOLN1 and MCOLN3 expression promotes autophagosome formation(202, 230). In response to sensing of reactive oxygen species and under conditions of nutrient starvation, MCOLN1 activates transcription factor EB (TFEB) which induces the expression of genes important for lysosome biogenesis and autophagy proliferation(231-234). Overexpression of MCOLN3 promotes EGF degradation and delays autophagosome clearance(201, 235). Additionally, a role for MCOLN3 in the expulsion of bacteria from bladder epithelium via a lysosomal expulsion pathway was recently identified(236). In contrast, MCOLN2 plays a role in the Arf6-associated recycling pathway(203).

Compared to MCOLN1 and MCOLN3, the function of MCOLN2 was poorly understood until recently. Recent findings implicate a role for MCOLN2 in immunity. Unlike other MCOLNs, MCOLN2 expression is induced in mouse macrophages in response to LPS(195) as well as in chimpanzee peripheral blood mononuclear cells in response to type I IFN(196). The B

cell transcription factor paired box 5 (PAX5) promotes MCOLN2 expression(237). In a mouse model, *Mcoln2* knockout resulted in impaired chemokine secretion and reduced peripheral macrophage recruitment after bacterial challenge(195, 238). Together, these findings implicate a role for MCOLN2 in immunity. Interestingly, a recent screen identified MCOLN2 as an ISG which promoted the infection of a diverse group of viruses(120). However, the mechanism by which MCOLN2 affects viral infection is unknown.

Here, I characterize the mechanism by which MCOLN2 enhances viral infection. I found that MCOLN2 enhances viral entry. Specifically, MCOLN2 promotes trafficking of viruses from early to late endosomes resulting in increased pH dependent release to the cytosol. This process is dependent on the channel activity of MCOLN2 and does not involve regulation of IFN signaling. Intriguingly, a rare genetic variant of *MCOLN2* fails to enhance viral infection in our cell culture model. Overall, our findings reveal a role for MCOLN2 as an endosomal host factor that modulates entry of a diverse group of endocytosed viruses.

RESULTS

MCOLN2 enhances infection of diverse RNA viruses

To confirm that MCOLN2 is IFN inducible, I treated THP-1 monocytes with IFN-α or poly(I·C) and assessed MCOLN2 expression by Western blotting 24 h later (Figure 11A)(196). As previously reported, MCOLN2 is induced in response to type I IFN treatment. In previous screening efforts, Schoggins et al. showed that MCOLN2 enhances infection of viruses from

multiple families, including yellow fever virus (YFV, *Flaviviridae*), IAV (*Orthomyxoviridae*), and equine arteritis virus (EAV, *Arteriviridae*). However, MCOLN2 had no effect on Venezuelan equine encephalitis virus (VEEV, *Togaviridae*), RSV (*Rhabdoviridae*), or VSV (*Paramyxoviridae*)(120, 169). To confirm these results and extend our findings to Zika virus (*Flaviviridae*), immortalized *STAT1*$^{-/-}$ human skin-derived fibroblasts stably expressing MCOLN2 or a control vector were generated using a lentiviral expression cassette co-expressing TagRFP. Cell lines were infected at a low MOI with recombinant GFP-expressing reporter viruses (YFV, EAV, VEEV, SINV, VSV) or non-reporter strains of IAV (WSN) and ZIKV (PRVABC59). After approximately 1 viral replication cycle, infectivity was assessed by quantitating the percentage of GFP-positive cells using flow cytometry. Alternatively, for IAV and ZIKV, I used virus-specific antibodies to quantify infectivity. Ectopically expressed MCOLN2 had similar effects on each of the previously studied viruses, as expected (Figure 11B). I also found that MCOLN2 enhanced ZIKV infection by approximately 75% over control cells. Similarly, cells ectopically expressing MCOLN2 released nearly twice as much infectious virus when infected with a non-reporter YFV (Figure 11C). To test whether the enhancing effect of MCOLN2 extends to other cellular backgrounds, I stably expressed MCOLN2 or an empty vector in human A549 lung adenocarcinoma cells and challenged cells with IAV. MCOLN2 expression enhanced both IAV infectivity (Figure 11D) and infectious virus production (Figure 11E).

To determine if loss of MCOLN2 expression affects viral infection, MCOLN2 was knocked out of U-2 OS and A549 cells using the CRISPR/Cas9 system. Loss of expression in U-2 OS cells was confirmed by western blot (Figure 11F). In both cell types, loss of MCOLN2

expression caused a significant reduction in viral infection (Figure 11G,H). Together, these data indicate that endogenous MCOLN2 is required for optimal infection in diverse cell types, and that infection can be enhanced by ectopic MCOLN2 expression.

MCOLN2 mediated enhancement is not dependent on the IFN response

Since the MCOLN2 enhancing effects occurred in *STAT1*$^{-/-}$ cells, I suspected that its effects were direct and not linked to negative regulation of antiviral signaling. However, MCOLN1 has been shown to modulate viral PAMP recognition during TLR signaling(223). I therefore tested whether MCOLN2 modulates antiviral signaling in IFN-responsive A549 cells. Cells ectopically expressing MCOLN2 or control cells were treated with IFNα and assessed for antiviral ISG induction by RT-PCR. At various doses of IFN, I found no differences in *MX1*, *IFITM3*, or *IFI27* induction between the two cell types (Figure 12A). I next monitored *IFNB1* and ISG induction in MCOLN2-expressing or control cells infected with either IAV or Sindbis virus (Figure 12A,B). IAV infection is enhanced by MCOLN2 (Figure 11B) but blocks IFN signaling by multiple mechanisms(239). SINV infection is similarly affected by MCOLN2 (Figure 11B). MCOLN2 promoted ISG but not *IFNB1* expression in response to SINV, despite having a net positive effect on viral infection. Induction of *IFNB1* and ISGs in response to IAV were not affected by ectopic MCOLN2 expression (Figure 12). Combined with our original discovery of a MCOLN2 phenotype in a *STAT1*$^{-/-}$ background(120), these data suggest that MCOLN2-mediated enhancement of viral infection is not linked to impairment of IFN or ISG induction.

MCOLN2 channel activity is necessary for enhancement of viral infection

To determine if MCOLN2 channel activity is important for its viral enhancing effect, I tested the infection phenotype of a well characterized dominant negative mutant, referred herein as MCOLN2-DD/KK, in which two conserved aspartates D463 and D464 are mutated to lysine. Homologous mutations in all MCOLN subfamily members perturb the selectivity pore of the channel and have been found to prevent cation flow through these channels(200, 203, 217, 240). When stably expressed in A549 cells, the MCOLN2-DD/KK mutant was unable to enhance IAV infection (Figure 13A), suggesting that channel activity is required for the viral phenotype. Since all members of the TRPML subfamily localize to endosomal compartments, I tested whether any other members of this subfamily enhanced viral infection (Figure 13B). MCOLN3, but not MCOLN1, enhanced IAV infection when ectopically expressed.

MCOLN2 enhances early, but not late stages of the viral life cycle

I next sought to determine which steps of the viral replication cycle were affected by MCOLN2. To examine viral entry, I first focused on IAV. IAV virions enter cells through endocytosis, and the viral genome escapes into the cytosol after pH-dependent fusion of the viral envelope with the endosome. Viral ribonucleoprotein (vRNP) complexes, which are comprised of viral RNA, nucleoprotein (NP) and the viral polymerase, translocate into the nucleus via the NP nuclear localization signal. Once in the nucleus, IAV genomes are replicated. Thus, NP

staining can be used as a surrogate to directly monitor cytosolic-to-nuclear trafficking of incoming IAV particles, prior to the onset or replication. To determine if MCOLN2 affects entry of IAV, A549 cells ectopically expressing MCOLN2 or an empty vector were infected with IAV in the presence of cycloheximide to inhibit *de novo* protein synthesis, thereby restricting NP detection to incoming virus only. NP localization was monitored over a 3 hr time course by immunofluorescence and confocal microscopy (Figure 14A). Compared to control cells, I found that a greater number of MCOLN2-expressing cells contained NP in their nuclei at all time points (Figure 14B,C). As a control, I also showed that bafilomycin A1 (BafA), an ATPase inhibitor that prevents endosome acidification, blocked NP translocation to the nucleus. To confirm these results, a similar experiment was conducted using nuclear-cytoplasmic fractionation (Figure 14A). Western blotting revealed that the nuclear fractions of MCOLN2-expressing cells contained significantly more viral NP than control cells (Figure 14D,E). Together, these experiments show that MCOLN2 enhances an early step in viral infection prior to replication.

To determine if MCOLN2 affects later stages of the viral life cycle, I first used a YFV subgenomic reporter replicon that lacks structural proteins essential for virus production and contains a *Renilla* luciferase (Rluc) transgene under the control of the viral 5' untranslated region (UTR) (YFRP-Rluc)(241). This replicon RNA can be used to uncouple viral entry from genome translation and replication by monitoring Rluc levels. YFRP-Rluc RNA synthesized *in vitro* was transfected into *STAT1*$^{-/-}$ fibroblasts stably expressing the antiviral transcription factor IRF1 or MCOLN2. Rluc levels were quantified at early (2-6 hr) and late time points (24-72 hr) by

luciferase assay to measure viral protein translation and RNA replication, respectively (Figure 14F). While the antiviral ISG IRF1 significantly inhibited replicon activity, MCOLN2 had no effect at any time point. To confirm this finding, an acid bypass experiment was conducted. A549 cells ectopically expressing MCOLN2 were infected with IAV in the presence of a low pH buffer. This results in direct fusion of IAV with the plasma membrane, bypassing the normal entry process. Under these conditions, MCOLN2 no longer enhanced viral infection (Figure 14G). Together, these data suggest that MCOLN2 does not affect post-entry stages in the viral life cycle.

MCOLN2 enhances vesicular trafficking of viruses

I next sought to identify which step of viral entry is affected by MCOLN2. To determine if MCOLN2 modulates attachment of IAV to cells, I bound IAV to control or MCOLN2-expressing A549 cells at 4° C and quantified the amount of cell bound viral genomic RNA by qRT-PCR. At 4° C, IAV can bind to the cell surface but is not efficiently endocytosed into cells. As a control, I shifted a subset of cells to 37° C and quantified infection by flow cytometry. Similar experiments were also conducted with YFV. While MCOLN2 still enhanced infection under the temperature shift conditions, there was no significant difference in the number of viral genomes bound at 4° C to MCOLN2-expressing cells compared to control cells (Figure 15A,B and Figure 16A). However, expression of TIM1, a protein known to enhance YFV surface attachment, increased YFV binding to the cells. This indicates that MCOLN2 does not affect attachment of virus to the cell surface.

To determine if MCOLN2 affects the rate or total amount of virus endocytosed into cells, I tagged IAV with a sulfo-NHS-SS-biotin tag, as previously described(242). The biotin tag allows viral particle detection using streptavidin conjugated fluorophores. The disulfide bridge linker can be reduced by the cell impermeable reducing agent tris(2-carboxyethyl)phosphine (TCEP), allowing efficient tag removal from cell surface bound IAV, but not from internalized virus. Thus, this assay measures the accumulation of a TCEP-resistant (endocytosed) population of biotin-tagged virus within infected cells over time (Figure 15C). Biotin accumulation was quantified indirectly by streptavidin-Alexa Fluor 488 staining and subsequent fluorescence detection by flow cytometry.

The method used to tag the virus did not significantly affect the infectivity of the virus *(t* test: P = 0.61) (Figure 16B). Additionally, MCOLN2 expression still enhanced infection by the labeled virus (Figure 16C). However, neither the rate nor amount of virus endocytosed into MCOLN2 expressing cells was significantly different from control cells. By contrast, treating cells with a combination of 5-(N-Ethyl-N-isopropyl)amiloride (EIPA) and Dynasore blocked IAV endocytosis as previously described (Figure 15D, Figure 16D)(56). These data suggest that MCOLN2 does not affect endocytosis of viral particles.

Certain viruses, including IAV and flaviviruses such as DENV and YFV, efficiently fuse with endosomal membranes under acidic conditions(78, 243-245). These viruses require transport from early endosomes to MVBs or late endosomes for efficient endosomal escape to occur. To determine if MCOLN2 promotes the rate or efficiency of this process, I used confocal microscopy to assess IAV NP colocalization with the early endosome marker early endosome antigen 1 (EEA1) or the late endosome/lysosome marker lysosomal-associated membrane

protein 1 (LAMP1) at various time points (Figure 17A, Figure 18A). After image acquisition, data files were randomized and blinded with a computational algorithm, and endosome-NP colocalization was quantified manually. The number of EEA1 and LAMP1 staining puncta were not significantly different between MCOLN2 or control expressing cells. However, I noted a difference in the number of IAV/EEA1 colocalizing puncta at early time points during entry ($P = 0.05$) (Figure 17B, Figure 18B). On average, more virus was present in early endosomes of control cells at early time points when compared to MCOLN2 expressing cells. This is intriguing considering that similar amounts of IAV are endocytosed (Figure 15D). By contrast, more virus was present in late endosomes of MCOLN2-expressing cells at later time points ($P = 0.04$) (Figure 17C, Figure 19). These data suggest that MCOLN2 promotes the efficiency of IAV trafficking to late endosomes or prevents virion degradation in this compartment, resulting in increased endosomal escape.

To assess the effect of MCOLN2 on the degradative capacity of late endosomes/lysosomes, I qualitatively measured late endosomal/lysosomal pH and the ability of MCOLN2-expressing cells to degrade endosomal cargo. To measure endosomal pH, I stained cells with the cell-permeable, pH-sensitive dye acridine orange. No significant difference in staining intensity was observed between control cells and MCOLN2-expressing cells. For a control, I confirmed that the dye was sensitive to ammonium chloride treatment. These data suggest that MCOLN2 does not have a significant effect on the pH of late endosomes or lysosomes (Figure 20A). To determine the effect of MCOLN2 on the degradative capacity of late endosomes/lysosomes, I quantitated the rate of epidermal growth factor receptor (EGFR) degradation after the addition of its ligand epidermal growth factor, which is endocytosed and

transported to late endosomes/lysosomes where it is degraded by endosomal proteases. MCOLN2-expressing cells degraded EGFR more rapidly than control cells did after EGF addition (Figure 20B,C), suggesting that MCOLN2 either promotes the transport of EGFR to late endosomes/lysosomes or increases the degradative activity of this compartment. In either case, MCOLN2 does not attenuate the degradative capacity of late endosomes/lysosomes. Together, these experiments further support a model in which MCOLN2 promotes IAV infection by increasing the efficiency of IAV trafficking to late endosomes.

If MCOLN2 enhances viral infection by increasing the efficiency of vesicular trafficking, then I hypothesized that more virus should fuse with and escape from endosomes in cells ectopically expressing MCOLN2. To test this, I took advantage of octadecyl rhodamine B (R18)-labelled IAV. R18 is a lipophilic, self-quenching dye commonly used in the study of enveloped virus fusion kinetics. R18 can be incorporated into the viral envelope at high concentration, resulting in self-quenching of its fluorescence. Fusion of the labelled virus with a host membrane results in dilution of R18 into the host membrane and dequenching of its fluorescent signal, which can be monitored by flow cytometry (Figure 17D). A549 cells ectopically expressing MCOLN2 or a control vector were infected with R18-labeled IAV. After infection, there was a significant increase in dequenched R18 signal in MCOLN2 expressing cells, indicating that ectopic MCOLN2 expression promotes fusion of IAV (Figure 17E).

I next wanted to determine if the role of MCOLN2 in vesicular trafficking could explain why certain seemingly unrelated viruses are affected by MCOLN2. To this end, I re-evaluated our previously published screen of 14 viruses and present results here to group viruses based on their MCOLN2 phenotype(120). Viruses were grouped based on membrane fusion/release point:

plasma membrane, early endosomes, or MVBs/late endosomes. Viruses with understudied, disputed, or poorly characterized strain-specific entry mechanisms were left out of this analysis. I then compared these three groups to infection data in MCOLN2-expressing cells (Table I). I found that only viruses that require transport to MVBs/late endosomes are affected by MCOLN2, supporting our finding that MCOLN2 modulates viral trafficking through the endosomal system.

A rare genetic variant of human MCOLN2 fails to enhance viral infection

Loss of function mutations in *MCOLN1* cause mucolipidosis type IV disorder(209, 210), while mutations in murine *Mcoln3* cause the Varitint-Wadler phenotype. To date, genetic variation in *MCOLN2* has not been associated with any known disease state. I searched the Phase 3 1000 Genomes database for rare *MCOLN2* nonsynonymous mutations that are predicted to be damaging to the encoded protein(246). I found a G/T single nucleotide polymorphism (SNP) *rs6704203* at chr1:85405238, which encodes a lysine to glutamine change at amino acid 370 of MCOLN2. Across 2504 individuals representing 26 populations worldwide, the genotype frequencies are: TT (94.4%, 2364 individuals), GT (5.3%, 133 individuals), and GG (7 individuals, 0.3%) (Figure 21A)(247). While the *rs6704203* G allele occurs at a frequency of only 2.9% across all individuals in the 1000 Genomes database, this frequency is enriched to an average of 11% in various African sub-populations. Similar results were obtained from the Exome Aggregation Consortium (EXAC), which contains sequencing data from more than 60,000 individuals(248). Of 121,350 *rs6704203* alleles annotated in the EXAC database, the G allele occurs at a general frequency of 0.77%, with an enrichment to 8.5% in African

populations. Only 42 individuals in the EXAC are homozygous for the *rs6704203* GG genotype, confirming the rareness of this variant. To test whether MCOLN2-K370Q affects the viral enhancing phenotype in our heterologous system, I first expressed the mutant and monitored expression levels by Western blot. Both wild type and MCOLN2-K370Q were expressed at similar levels, indicating the mutation does not disrupt expression (Figure 21B). A549 cells ectopically expressing MCOLN2-K370Q showed a near complete loss of viral enhancement when compared to wild type (Figure 21B). These data indicate K370Q disrupts the ability of MCOLN2 to enhance viral infection, raising the intriguing possibility that humans bearing one or two G alleles at *rs6704203* may have altered susceptibility to certain viral infections.

METHODS

Cell lines and viruses

A549 lung cancer, U-2 OS osteosarcoma, and human embryonic kidney-derived 293T cells were grown in DMEM supplemented with 10% FBS and 0.1 mM nonessential amino acids. *STAT1*$^{-/-}$ fibroblasts were grown in RPMI supplemented with 10% FBS and 0.1 mM nonessential amino acids. Stable cell lines transduced with SCRPSY lentiviral vectors(170) were selected for 3 days in media supplemented with 4 µg/mL puromycin and maintained in normal media.

The construction, characterization and generation of viral stocks for the following viruses have been previously described: EAV-GFP (derived from infectious clone pEAV211-GFP2aT)[26,] SINV-A-GFP(derived from infectious clones pS300-GFP)[27] , VEEV-GFP (derived from

infectious clone pTC83-GFP)[4]. YFV-17D-Venus was produced by electroporation of *STAT1*$^{-/-}$ fibroblasts with *in vitro* transcribed RNA as previously described(169). Influenza A virus (IAV, strain A/WSN/33) was propagated in MDCKs as previously described(249). For entry assays, IAV was concentrated by pelleting through a 30% sucrose cushion in PBS with Ca^{2+}/Mg^{2+} using ultracentrifugation in an SW-28 rotor at 110,000 g for 1 hr.

Plasmids and cloning

MCOLN2, IRF1 and control constructs were prepared as previously described(169). Plasmids containing MCOLN1 or MCOLN3 open reading frames were kindly provided by Neal Alto. TIM-1 (also known as HAVCR1) was obtained from DNASU. pENTR.MCOLN2 was used as a starting point for all mutagenesis. MCOLN2 D463D/KK and K370Q mutants were generated from WT MCOLN2 by overlap extension PCR using primer sets listed in Appendix A. All genes were amplified out of their respective plasmids by PCR and cloned into pDONR.221 using BP Clonase (Invitrogen) according to manufacturer's protocol. Genes were cloned into the previously described lentiviral, puromycin selectable, RFP coexpressing, SCRPSY-DEST vector(170) using LR Clonase II (Invitrogen) as per manufacturer's protocols. For CRISPR/Cas9 experiments, MCOLN2 and control targeting guides were cloned into plentiCRISPRv2 (a gift from Feng Zhang, Addgene plasmid #52961) (see Appendix A)(250).

Lentivirus production and viral infections

SCRPSY lentiviruses were produced as previously described(170). For lentiCRISPRv2 production, 293T cells were seeded at 4 x 10^5 cells per well into 6-well plates. The next day, cells were transfected with 1 µg lentiCRISPRv2, 0.2 µg plasmid expressing VSVg, and 0.8 µg plasmid expressing HIV-1 gag-pol using X-tremeGENE 9 (Roche) . Media was changed 6 hours later and lentivirus containing culture supernatants were collected at 48 and 72 hr post-transfection. Pooled supernatants were clarified by centrifugation at 800 x *g* for 5 min. Polybrene and HEPES were added to a final concentration of 4 µg/mL and 25 mM respectively. Lentivirus was stored at -80° C until use.

For lentivirus transductions, cells were seeded at 7 x 10^4 cells per well in 24 well plates. The next day, media was changed to DMEM supplemented with 4 µg/mL polybrene, 3% FBS, and 25 mM HEPES. Cells were transduced by spinoculation at 800 x *g*, 45 min, 37°C. Media was changed 6 hours later to 10% FBS DMEM supplemented with 0.1 mM nonessential amino acids, and cells were replated at 48 hours post transduction for subsequent experimentation.

Cells were seeded at 1 x 10^5 in 24 well plates 24 hours prior to infection. For IAV infections, cells were infected with virus diluted in DMEM containing 0.1% FBS, 0.3% BSA for 1 hr at 37 °C. For IAV infections involving ML-SI3 (U-18666A), cells were preincubated in DMEM containing 0.1% FBS and 0.3% BSA with 12.5-100 µM ML-SI3 (Sigma) or 5% DMSO for 30 min prior to infection. ML-SI3 and DMSO were also present for the first hour during infection. For all other infections, cells were infected with virus diluted in 200 µl DMEM containing 1% FBS for 1 hr at 37 °C. The virus inoculum was removed and replaced with 1 mL normal growth medium. At the designated time, cells were dislodged with Accumax, centrifuged

at 800 x *g* for 2 min at 4°C, fixed in 1% PFA for 10 min, and resuspended in 1X PBS with 3% FBS for flow cytometry analysis.

Viral binding assay

A549 cells were seeded at 1 x 10^5 cells per well in 24 well plates one day prior to infection. Cells were chilled at 4° C for 30 min, followed by virus binding at 4° C in DMEM containing 0.1% FBS, 0.3% BSA for 1 hr. Cells were washed twice with chilled 1X PBS. Cells were either lysed in RLT buffer and RNA isolated using an RNeasy mini kit (Qiagen) or shifted to 37° C in DMEM containing 10% FBS for 8 hr and harvested for infection quantitation by flow cytometry. Viral RNA in isolated RNA samples was quantified by RT-qPCR using primers listed in Appendix A.

Acid bypass

A549 cells were seeded at 1 x 10^5 cells in 24 well plates. The next day, cells were chilled at 4° C for 30 min. IAV (MOI 10) was bound to cells at 4° C in DMEM containing 0.1% FBS, 0.3% BSA for 1 hr. Media was then changed to DMEM (pH 5, 50 mM acetic acid) pre-warmed to 37° C for 5 min. Afterwards, the media was changed to DMEM (pH 7, 0.1% FBS, 0.3% BSA, 2 µg/mL TPCK (Sigma)) for 8 hr. Cells were dislodged with Accumax, fixed, and stained for infection quantitation by flow cytometry as described above.

Nuclear NP localization

For image based analysis, A549 cells were seeded at 2 x 10^4 cells in 8 well chamber slides. The next day, cells were pre-chilled on ice for 30 min and incubated with IAV (MOI 10) for 1 hr at 4° C in 150 µl DMEM containing 0.1% FBS, 0.3% BSA. 300 µl pre-warmed DMEM (10% FBS, 0.15 mM cycloheximide) with or without 15 nM Bafilomycin A1 was added and slides were incubated at 37° C. At indicated time points, wells were incubated in 4% PFA PBS with Ca^{2+}/Mg^{2+} for 10 min at indicated time points and left in PBS with Ca^{2+}/Mg^{2+} overnight before immunofluorescence. Samples were imaged using a Zeiss LSM 780 confocal microscope. Images were quantified using ImageJ software.

For cell fractionation based analysis, A549 cells were seeded at 1 x 10^7 cells in p150 dishes. The next day, cells were chilled to 4° C for 30 min and infected with IAV (MOI 10) for 1 hr at 4° C in 2 mL DMEM containing 0.1% FBS, 0.3% BSA. Media was changed to 10 mL pre-warmed DMEM (10% FBS, 0.15 mM cycloheximide) with or without 15 nM Bafilomycin A1 warmed. Cells were scraped from plates in 5 mL cold PBS with Ca^{2+}/Mg^{2+} at indicated time points. Cells were washed three times in chilled PBS with Ca^{2+}/Mg^{2+} and centrifuged at 200 x *g* for 3 min. Cells pellets were resuspended in 500 µL cold ddH_2O for 10 min and lysed with 10-20 strokes of a type B dounce homogenizer. Lysis efficiency was checked by phase contrast microscopy. Nuclei were pelleted at 200 x *g* for 10 min and stored at -80°C. The cytoplasmic-containing supernatant fraction was centrifuged at 1,500 x *g* for 10 min to remove remaining nuclei and stored at -80°C.

Immunofluorescence

Wash buffer (WB) consisted of 1% BSA, 0.1% Tween-20 in PBS with Ca^{2+}/Mg^{2+}. Samples were permeabilized for 10 min with 0.2% Triton X-100 in WB and blocked for 1 hr in WB. Samples were incubated with: 1:1000 anti-NP antibody (Sigma), 1:500 anti-EEA1 (abcam), 1:500 anti-LAMP1 (abcam), and/or 1:500 streptavidin-AF488 (abcam) in WB for 2 hr, washed 3 times in WB for 1 min each, and probed with 1:1000 goat anti-mouse Alexa Fluor 488 (Life Technoligies) or 1:200 goat anti-rabbit BV421 (BD Bio.) in WB for 1 hr. Samples were washed twice with WB and nuclei were stained for 5 min with Hoechst 33342 (Life Technologies) in WB, and samples mounted with Prolong Gold Antifade reagent (ThermoFisher).

Plaque assays

STAT1$^{-/-}$ fibroblasts and A549 cells were seeded at 7 x 10^4 cells per well in 24 well plates for YFV-17D and IAV infections, respectively. Cells were infected and supernatants harvested at 8 hours (IAV) or 24 hours (YFV). For YFV, supernatants were serially diluted and used to infect BHK-21J cells. Plates were overlaid with DMEM supplemented with 0.1% $NaHCO_3$, 10 mM HEPES, 4% FBS, 1.2% Avicel supplemented DMEM. 4 days later, plates were fixed with 3.7% formaldehyde and plaques visualized with crystal violet staining. For IAV, collected supernatant was serially diluted and used to infect MDCK cells seeded at 1 x 10^6 in 6 well plates the prior day. Plates were overlaid with DMEM supplemented with 0.1% $NaHCO_3$, 0.2% BSA, 1.2%

Avicel, 10 µg/mL TPCK. Two days later, plates were fixed with 3.7% formaldehyde and plaques visualized with crystal violet staining.

Internalization assay

Concentrated IAV stocks were diluted to 1 mg/mL viral protein and labeled with sulfo-NHS-SS-biotin (Thermofisher) at 65 nM for 2 hr at room temperature. The reaction was quenched by adding pH 7 glycine to 0.1M. Labelled virus was purified by ultracentrifugation through a 30% sucrose cushion in a SW-28 rotor at 110,000 g for 1 hr. Labelling efficiency was determined using Pierce Biotin Quantitation Kit as per manufacturer's instructions. A549 cells were washed in PBS, treated with 0.05% trypsin, centrifuged at 200 x *g* for 2 min, and resuspended in 200 µL DMEM containing 0.1% FBS, 0.3% BSA at 50,000 cells per well in a 96 well plate. Control samples were incubated in media containing 400 µM EIPA and 80 µM dynasore or 5% DMSO for 30 min at 37° C. Cells were pelleted by centrifugation at 200 x *g* for 2 min and IAV (MOI 20) was bound to cells at 4° C in 50 µL chilled DMEM containing 0.1% FBS, 0.3% BSA for 1 hr. Cells were centrifuged at 200 x *g* for 2 min, resuspended in 50 µL DMEM containing 0.1% FBS, 0.3% BSA, 400 µM EIPA and 80 µM dynasore or 5% DMSO pre-warmed to 37° C. At indicated time points, 150 µL chilled 15 mM TCEP was added for 5 min, cells were centrifuged at 200 x *g* for 2 min, and cell pellets resuspended in chilled 4% PFA. Cells were permeabilized with 0.5% saponin, stained for 30 min with 1 µg/mL streptavidin conjugated Alexa Fluor 488 and fluorescence intensity quantified by flow cytometry.

Vesicular trafficking assay

IAV was biotinylated as described above. A549 cells were plated at 1 x 10^4 in 8 well chamber slides. The next day, slides were chilled for 30 min on ice. Virus was bound to cells at an MOI of 10 in 150 µl DMEM containing 0.1% FBS, 0.3% BSA at 4° C for 1 hr. Media was changed to pre-warmed DMEM containing 0.1% FBS, 0.3% BSA, 0.15 mM cycloheximide and incubated at 37° C. At indicated time points, cells were treated with 15 mM TCEP for 5 min, fixed in 4% PFA for 10 min, permeabilized with 0.2% Triton X-100, and co-stained with streptavidin conjugated Alexa Fluor 488 and either anti-EEA1 or anti-LAMP-1 (abcam) antibodies as described above. Images were taken on a Zeiss LSM 780 confocal microscope. After image acquisition, data files were randomized and blinded with a computational algorithm. Streptavidin – endosomal marker colocalization was manually counted for at least 10 cells per condition.

Endosomal escape assay

IAV was labelled similarly to the protocol previously described(251). Briefly, concentrated IAV was diluted to 100 µg/mL viral protein. 6 µL 1.2 mM rhodamine B in EtOH was added per mL of IAV for 1 hr at room temperature. The labelling reaction was filtered through a 0.22 µm filter and virus was purified on a 30-50% sucrose gradient in an SW-40 rotor at 220,000 x *g* for 90 min. A549 cells were washed in PBS, treated with 0.05% trypsin, centrifuged at 200 x *g* for 2 min, and cell pellets were resuspended in 200 µL DMEM containing

0.1% FBS, 0.3% BSA at 50,000 cells per well in a 96 well plate. Cells were chilled to 4° C for 30 min. Labelled IAV was bound to cells at an MOI of 1 in 200 µL DMEM containing 0.1%, FBS 0.3% BSA for 1 hr at 4° C. Cells were centrifuged at 200 x g for 2 min and cell pellets were resuspended in 150 µL DMEM containing 0.1% FBS, 0.3% BSA warmed to 37° C. At indicated time points, 50 µL 4% PFA was added. Cells were resuspended in 3% FBS containing PBS and fluorescence intensity quantified by flow cytometry.

Western blot

Samples were run on a 10% polyacrylamide SDS-PAGE gel, transferred onto nitrocellulose membrane, and blocked for 30 min with 5% milk in 0.1% Tween-20 TBS-T. Membranes were probed with one of the following primary antibodies: 1:3000 α-actin (abcam), 1:1000 α-NP (Millipore), 1:1000 α-Lamin-B (Santa Cruz), or 1:200 α-MCOLN2 (Origene). For standard experiments, membranes were washed with 0.1% Tween-20 TBS-T and probed with goat α-rabbit or goat α-mouse HRP conjugated antibodies (Pierce). Membranes were washed with 0.1% Tween-20 TBS-T, incubated with ECL substrate (Pierce) according to manufacturer's instructions, and exposed to film. For quantitative experiments, membranes were probed with goat α-mouse or donkey α-goat IR Dye conjugated antibodies (Licor). Membranes were washed with TBS and signal detected using a Licor Odyssey system.

Antibody staining and flow cytometry

For quantitation of IAV infections, infected cells were permeabilized and stained with 1:1000 α-NP HT103 using the Cytofix / Cytoperm kit according to the manufacturer's instructions (BD Bioscience). HT103 was kindly provided by Thomas Moran. Samples were subsequently stained with goat α-mouse AF488 (Invitrogen) and cell fluorescence quantified by flow cytometry. An S1000 flow cytometer (Stratedigm) was used and data quantified using FlowJo. On average, 20,000 cells were counted per condition. A minimum of 10,000 cells were counted per condition. For the internalization assay specifically, a minimum of 2,000 cells were counted per condition due to cell loss.

RT-qPCR

RNA was isolated using an RNeasy Mini kit (Qiagen) according to manufacturer's instructions. For RT-qPCR, the Quantifast SYBR Green PCR kit (Qiagen) was used according to manufacturer's instructions. RNA concentration was determined by nanodrop and 40 ng total RNA was added to each reaction along with one of the following Quantitect primer sets (Qiagen): MCOLN2 (QT00090895), Mx1 (QT00090895), IFN-β (QT000203763), Arf6 (QT00236824), CCL2 (QT00212730), IFIT2 (QT02289294), IFI27 (QT00099274), or RPS11 (QT00061516). Reactions were analyzed in a 7500 Fast Real-Time PCR thermal cycler (A&B Biosystems). For analysis, expression of the housekeeping gene RPS11 was used for sample normalization.

Statistical analysis

Statistical significance for most data sets was determined using a Student's T test. For normalized data sets, a ratio paired T test was used. A single outlier from each data set, if present, was identified using Dixon's Q test and removed.

FIGURES AND TABLES

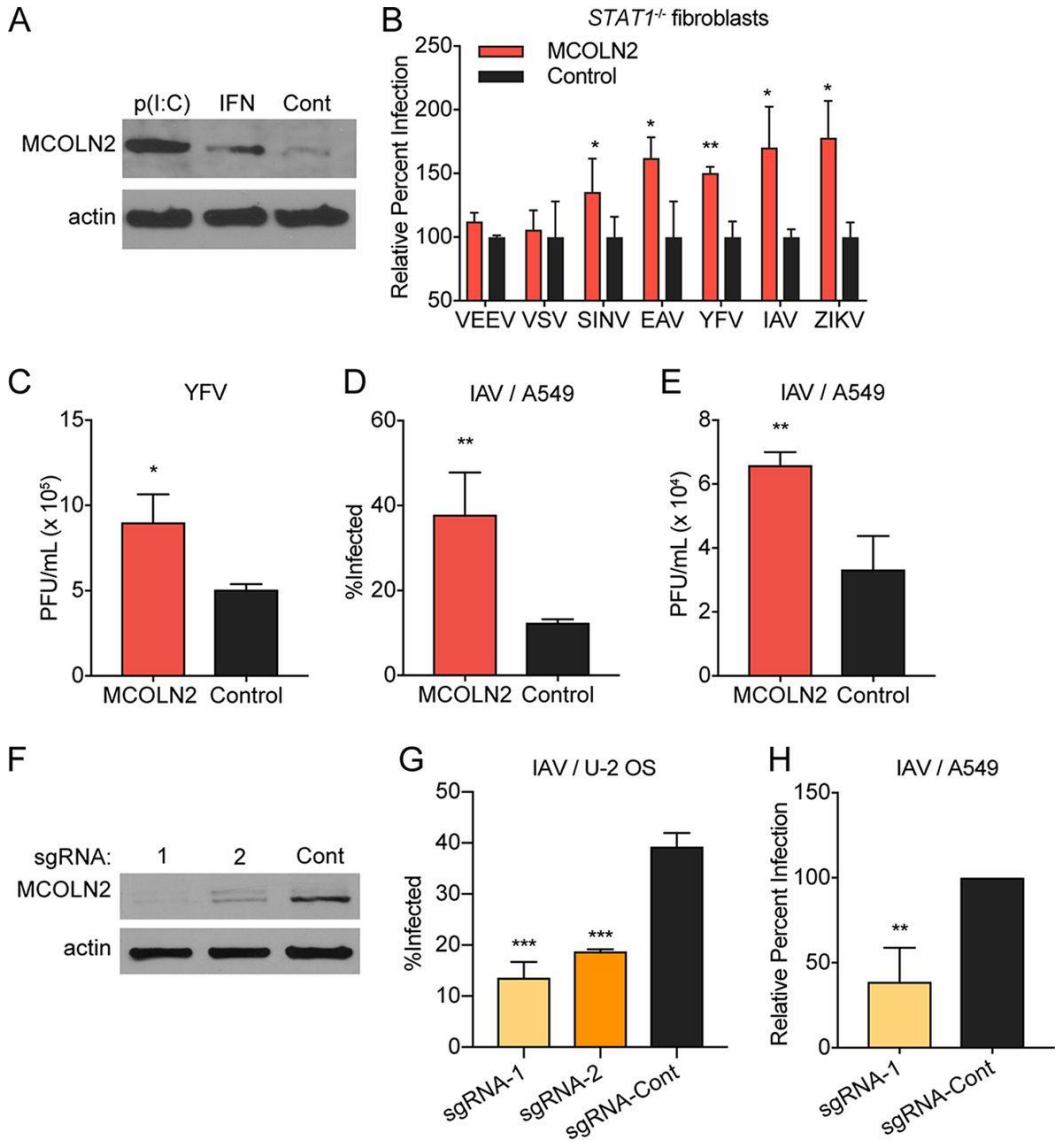

Figure 11. MCOLN2 enhances viral infection. (A) Western blot of lysates from THP-1 cells treated with 1,000 U IFN-α, 1 µg/ml poly(I·C), or PBS (negative control [Cont]) for 24 h. (B) *STAT1*$^{-/-}$ fibroblasts were infected with the indicated viruses, and infectivity was quantified by flow cytometry. (C) Viral titers in supernatants of *STAT1*$^{-/-}$ fibroblasts infected with YFV (MOI of 1) were determined by plaque assay in BHK-21J cells. (D and E) A549 cells were infected with IAV for 8 h, and infection was quantified by flow cytometry (D), or viral titers in supernatants were determined by plaque assay in MDCK cells (E). (F) MCOLN2 protein expression levels in U-2 OS cells targeted with the indicated CRISPR/Cas9 guides shown. sgRNA, single guide RNA. (G and H) CRISPR/Cas9-targeted U-2 OS (G) or A549 (H) cells infected with IAV at an MOI of 0.5 for 8 h. Infections were quantified by staining cells with anti-NP antibody and subsequent flow cytometry-based analysis. Values are means plus standard deviations (SD) (error bars) from three independent experiments performed in technical duplicate or triplicate. Values that are significantly different are indicated by asterisks as follows: *, $P \leq 0.1$; **, $P \leq 0.01$; ***, $P \leq 0.001$.

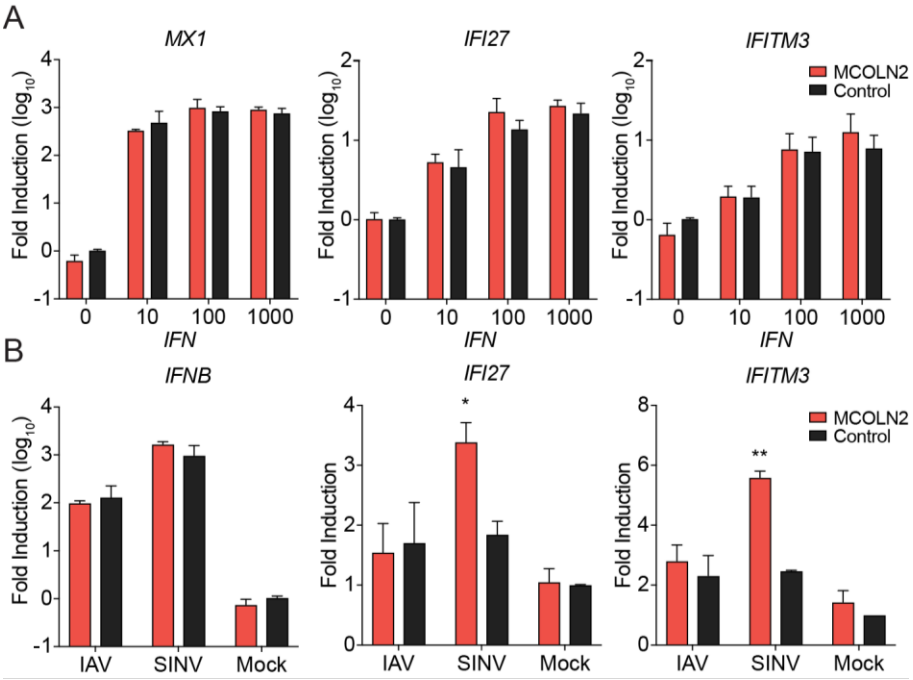

Figure 12. MCOLN2-mediated enhancement of viral infection is not dependent on the IFN response. (A and B) A549 cells were treated with the indicated doses of IFN-α for 24 h (A) or infected with IAV or SINV-GFP at an MOI of 1 for 8 h (B). ISG induction was quantified by RT-qPCR. Values are means plus SD (error bars) from three independent experiments performed in technical duplicate or triplicate. Values that are significantly different are indicated by asterisks as follows: *, $P \leq 0.1$; **, $P \leq 0.01$.

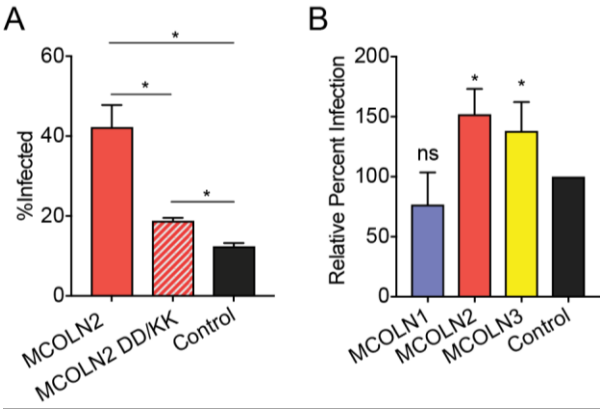

Figure 13. MCOLN2 enhancement of viral infection is channel dependent. (A and B) A549 cells were infected with IAV at an MOI of 0.2 for 8 h. Infections were quantified by staining cells with anti-NP antibody and subsequent flow cytometry-based analysis. Values are means plus SD (error bars) from three independent experiments performed in technical triplicate. Values that are significantly different ($P \leq 0.1$) are indicated by a bar and asterisk. ns, not significantly different.

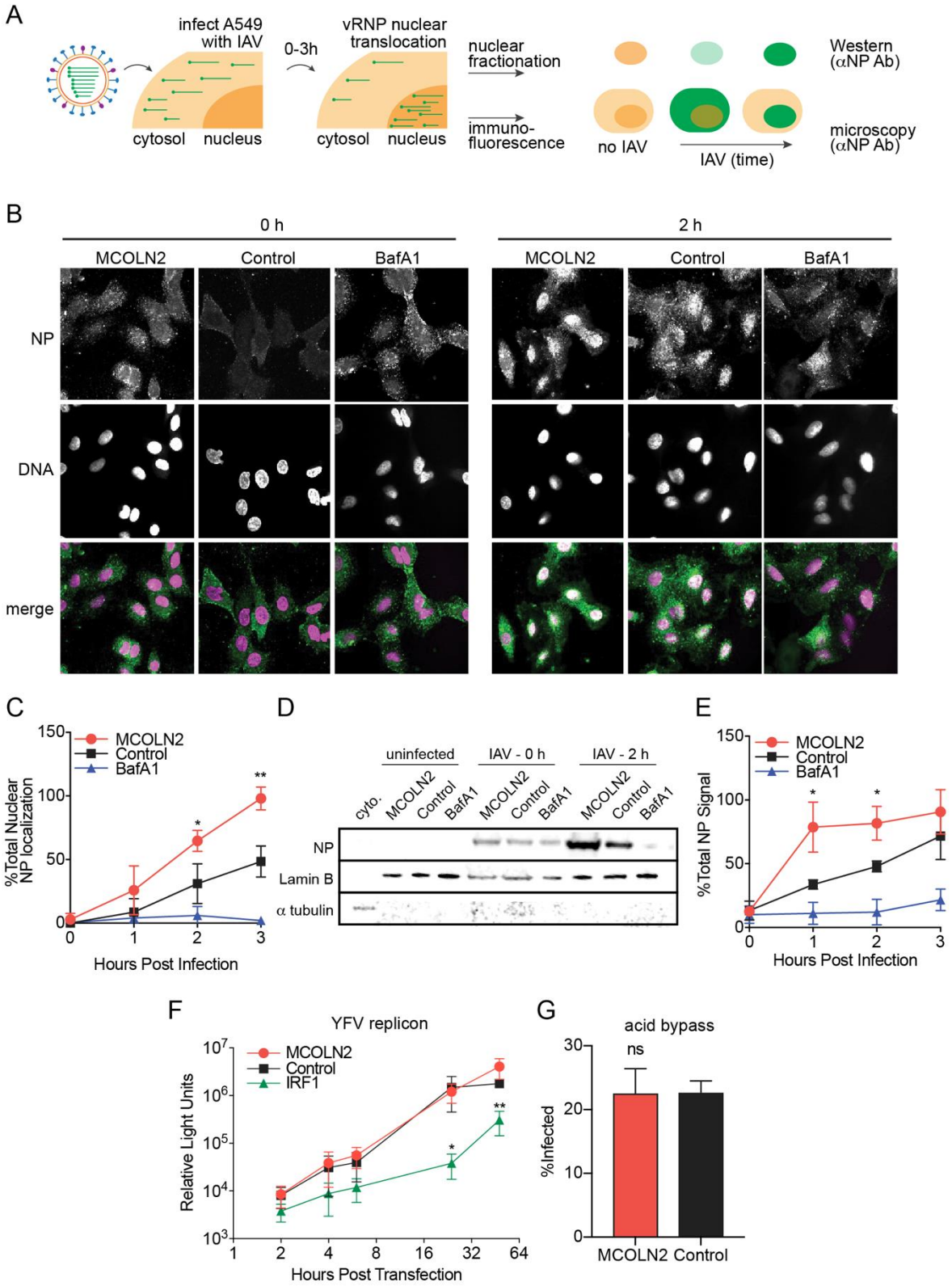
A
infect A549 with IAV
0-3h
vRNP nuclear translocation
cytosol
nucleus
nuclear fractionation
immuno-fluorescence
Western (αNP Ab)
microscopy (αNP Ab)
no IAV
IAV (time)
B
0 h
2 h
MCOLN2
Control
BafA1
NP
DNA
merge
C
MCOLN2
Control
BafA1
%Total Nuclear NP localization
Hours Post Infection
D
uninfected
IAV - 0 h
IAV - 2 h
cyto.
NP
Lamin B
α tubulin
E
%Total NP Signal
Hours Post Infection
F
YFV replicon
MCOLN2
Control
IRF1
Relative Light Units
Hours Post Transfection
G
acid bypass
ns
%Infected
MCOLN2
Control

Figure 14. MCOLN2 specifically enhances viral entry. (A) Schematic diagram of experiments shown in panels B to E. (B to E) IAV (MOI of 20) was bound to A549 cells for 1 h at 4°C. The cells were rapidly shifted to 37°C in the presence or absence of 15 nM bafilomycin A1 (BafA1) for the indicated times. The cells were fixed and stained with anti-NP antibody (αNP Ab) (green), and nuclei were stained with Hoechst 33342 (blue). NP nuclear localization was assessed by confocal microscopy (B). NP nuclear localization was quantified with ImageJ (C). (D and E) Nuclear-cytoplasmic fractionation was conducted on infected cells (D). Nuclear viral NP content was determined by quantitative Western blotting (E). (F) Luciferase assay of lysates from *STAT1*$^{-/-}$ fibroblast cell lines at the indicated time points after transfection with YFRP-Rluc subgenomic replicon RNA. (G) IAV (MOI of 10) was bound to A549 cells for 1 h at 4°C. The cells were rapidly shifted to 37°C in 50 mM acetic acid buffer (pH 5) for 5 min. The infection was continued for 8 h in pH 7 medium before harvest, staining with anti-NP antibody, and flow cytometry-based infection quantitation. Values are means ± SD (error bars) from three independent experiments. Values that are significantly different are indicated by asterisks as follows: *, $P \leq 0.1$; **, $P \leq 0.01$. ns, not significantly different.

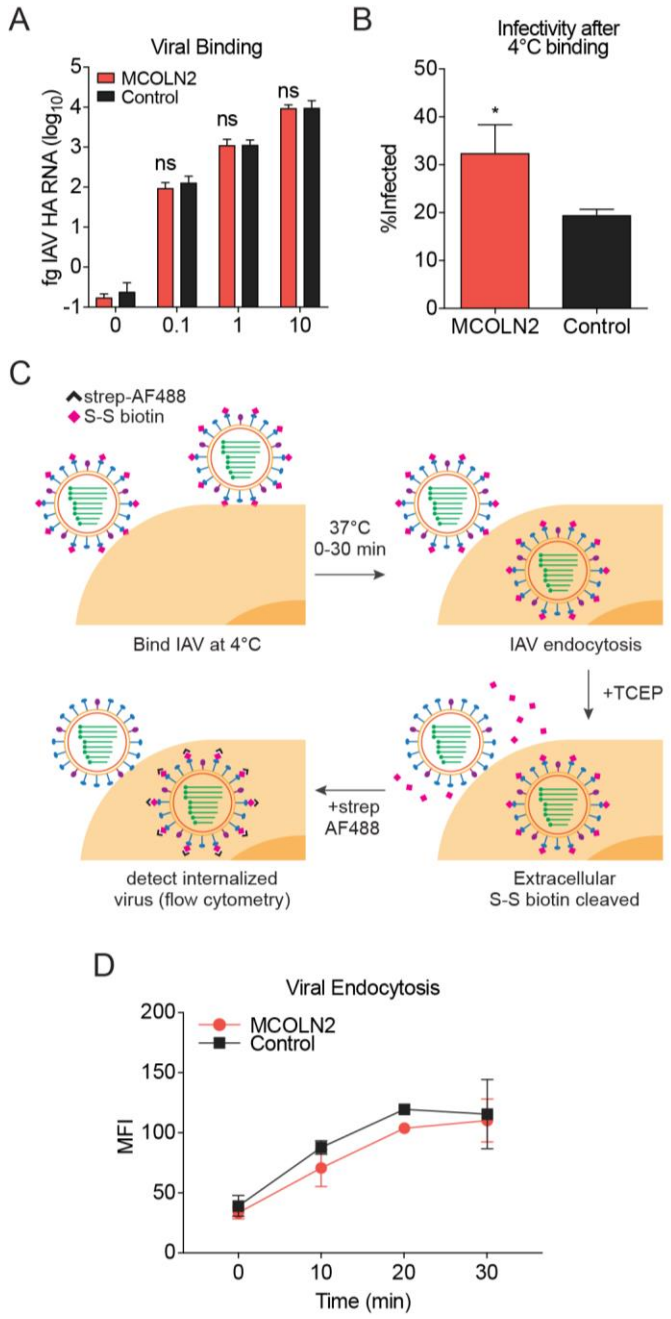
A
Viral Binding
MCOLN2
Control
fg IAV HA RNA (log10)
ns
ns
ns
0
0.1
1
10
B
Infectivity after 4°C binding
%Infected
*
MCOLN2
Control
C
strep-AF488
S-S biotin
Bind IAV at 4°C
37°C
0-30 min
IAV endocytosis
+TCEP
Extracellular S-S biotin cleaved
+strep AF488
detect internalized virus (flow cytometry)
D
Viral Endocytosis
MCOLN2
Control
MFI
Time (min)

Figure 15. MCOLN2 does not affect cell surface binding or endocytosis of IAV. (A and B) IAV was bound to A549 cells at the indicated MOIs for 1 h at 4°C. The cells were washed and either lysed and cell-bound viral RNA was detected by RT-qPCR analysis (A) or the cells were infected for 8 h at 37°C and subsequently analyzed by staining cells with anti-NP antibody and subsequent flow cytometry-based analysis (B). HA, hemagglutinin. (C) Schematic diagram of the experiment conducted in panel D. (D) Biotinylated IAV (MOI of 10) was bound to A549 cells for 1 h at 4°C. The cells were warmed to 37°C. At the time points shown, cells were treated with 15 mM TCEP, fixed, permeabilized, and stained with streptavidin-AF488. Fluorescence was quantified by flow cytometry. MFI, mean fluorescent intensity. In panels A and B, values are means plus SD from three independent experiments performed in technical triplicate. In panel D, the values are means ± SD (error bars) from two independent experiments performed in technical duplicate. Values that are significantly different ($P \leq 0.1$) are indicated by an asterisk. Values that are not significantly different (ns) are also indicated.

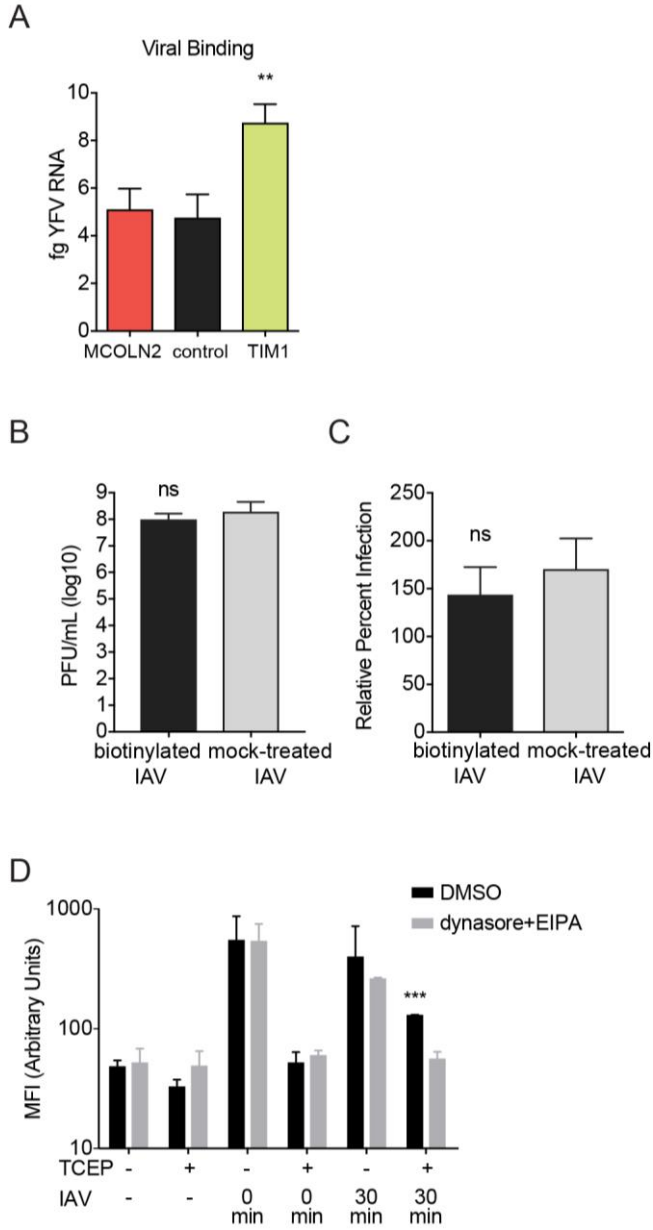
A
Viral Binding
fg YFV RNA
10
8
6
4
2
0
**
MCOLN2
control
TIM1
B
PFU/mL (log10)
9
8
7
6
5
4
3
2
1
0
ns
biotinylated IAV
mock-treated IAV
C
Relative Percent Infection
250
200
150
100
50
0
ns
biotinylated IAV
mock-treated IAV
D
MFI (Arbitrary Units)
1000
100
10
DMSO
dynasore+EIPA
***
TCEP - + - + - +
IAV - - 0 min 0 min 30 min 30 min

Figure 16. Neither cold binding of IAV to the cell surface nor biotinylation of IAV impact MCOLN2-mediated enhancement of IAV infection. (A) YFV-17D Venus was bound to the indicated cell lines at an MOI of 1 for 1 h at 4°C. Cell-bound YFV genomic RNA was quantified by RT-qPCR. (B and C) IAV was labeled with sulfo-NHS-SS-biotin as described in Materials and Methods. (B) Biotinylated or mock-treated IAV titer was determined by plaque assay on MDCK cells. (C) A549 stable cells were infected with biotinylated or mock-treated IAV at an MOI of 0.25 for 8 h. Infection was quantified by staining cells with anti-NP antibody and subsequent flow cytometry-based analysis. Data are presented as the relative infectivity of MCOLN2-expressing cells compared to control cells. (D) Biotinylated IAV was bound to A549 cells at an MOI of 10 for 1 h at 4°C in the presence of EIPA/dynasore or DMSO. Cells were shifted to 37°C. At the indicated time points, cells were treated with 15 mM TCEP or PBS, fixed with 1% PFA, and stained with streptavidin-AF488. Cell fluorescence was quantified by flow cytometry. In panels A to C, data represent means plus SD (error bars) from three independent experiments performed in technical triplicate. In panel D, data represent means plus SD (error bars) from two independent experiments performed in technical duplicate. Values that are significantly different are indicated by asterisks as follows: **, $P \leq 0.01$; ***, $P \leq 0.001$. ns, not significantly different.

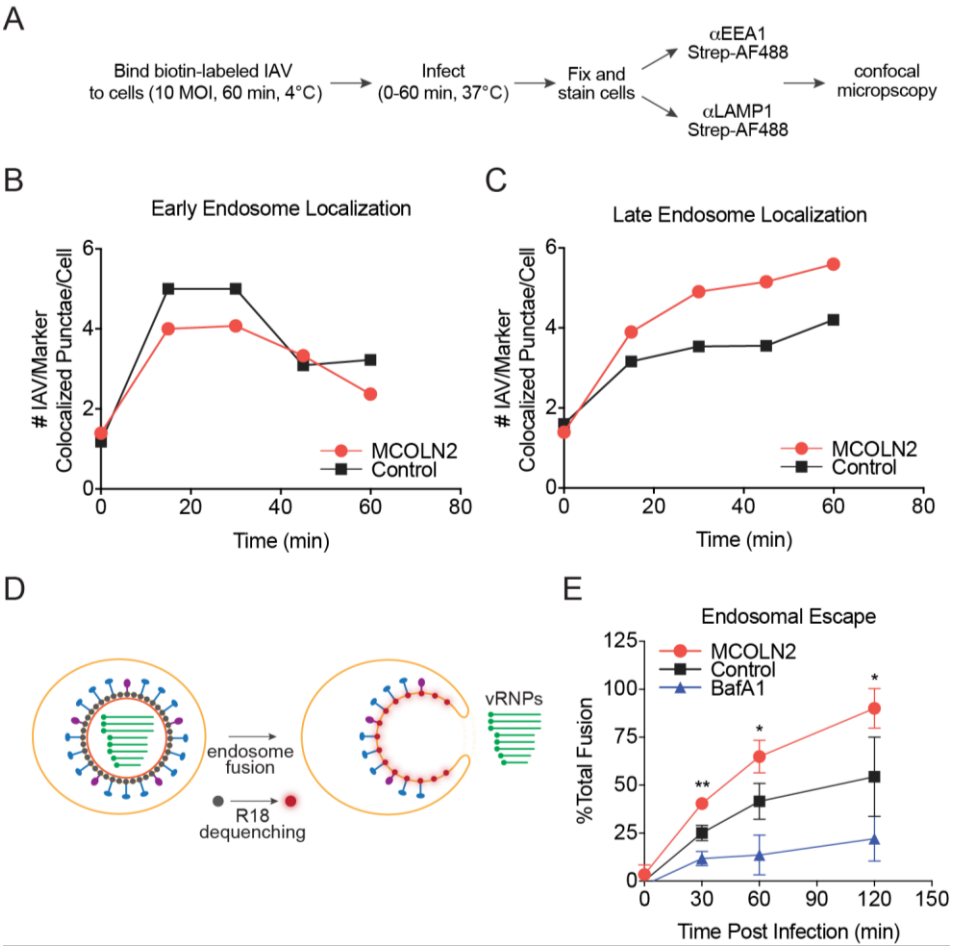

Figure 17. MCOLN2 promotes trafficking of IAV. (A) Schematic diagram of the experiments conducted in panels B and C. (B and C) Biotinylated IAV (MOI of 10) was bound to A549 cells for 1 h at 4°C. The cells were warmed to 37°C for the indicated times. The cells were fixed, treated with 15 mM TCEP, and permeabilized with Triton X-100. The cells were stained with streptavidin-AF488 and anti-EEA1 (B) or anti-LAMP-1 (C) antibodies. IAV-endosome colocalization was determined by confocal microscopy. (D) Illustration of the experiment performed in panel E. (E) R18-labeled IAV (MOI of 10) was bound to A549 cells for 1 h at 4°C. The cells were warmed to 37°C for the indicated times. The cells were fixed, and R18 fluorescence was quantified by flow cytometry. In panels B and C, the results of one representative replicate of three independent experiments are shown. In panel E, values are means ± SD (error bars) from three independent experiments performed in technical duplicate. Values that are significantly different are indicated by asterisks as follows: *, $P \leq 0.1$; **, $P \leq 0.01$.

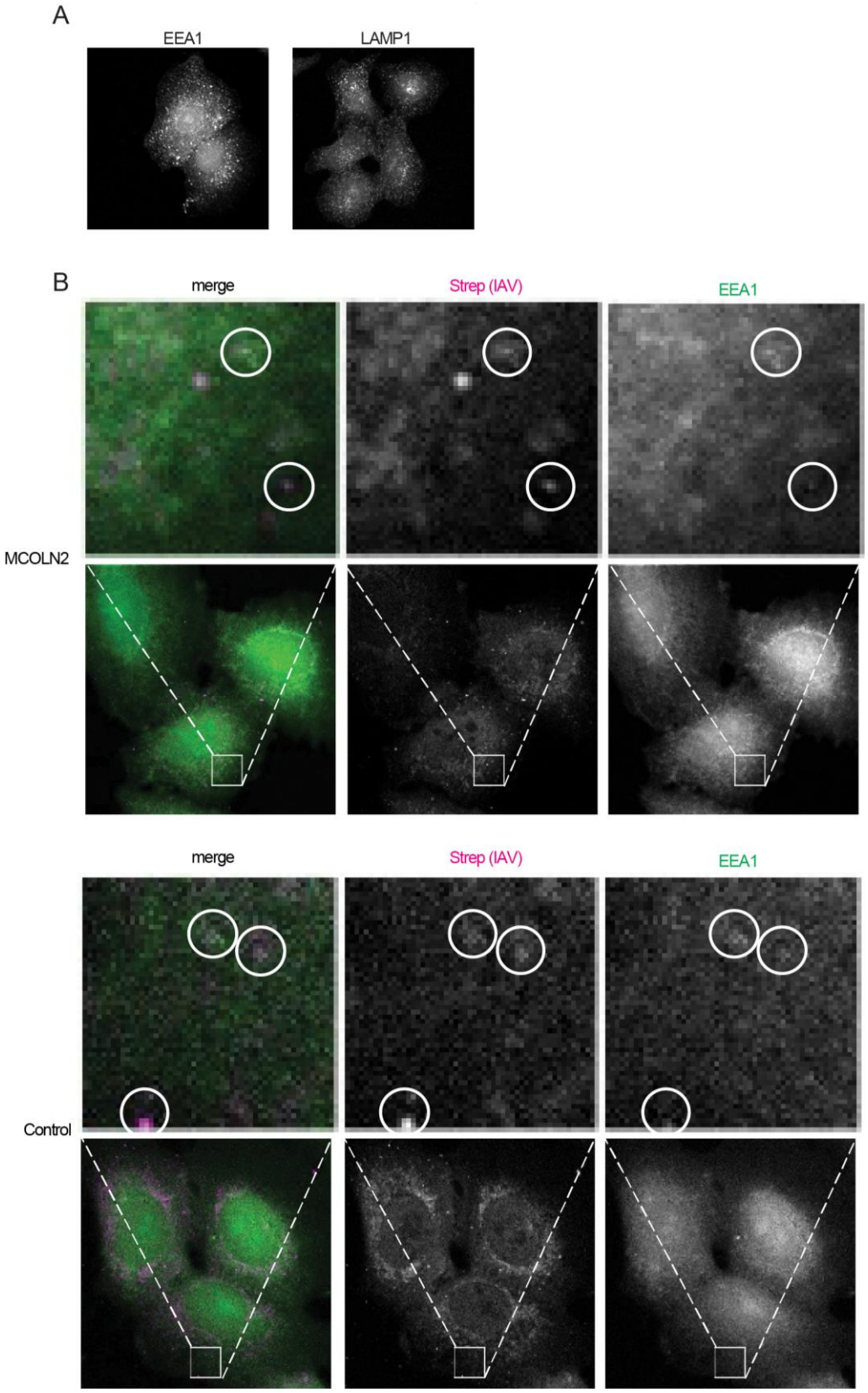
A
EEA1
LAMP1
B
merge
Strep (IAV)
EEA1
MCOLN2
merge
Strep (IAV)
EEA1
Control

Figure 18. Colocalization of IAV with early endosomes is reduced by MCOLN2 expression. (A) A549 cells were fixed with PFA, permeabilized with 0.2% Triton X-100, and stained with anti-EEA1 or anti-LAMP-1 antibodies followed by BV-421 goat anti-rabbit antibody. The cells were imaged by confocal microscopy. (B) Biotinylated IAV was bound to A549 stable cell lines at an MOI of 10 for 1 h at 4°C. The cells were shifted to 37°C for the time points shown and then treated with 15 mM TCEP or PBS. Samples were prepared as described above, stained with anti-EEA1 antibody, and additionally stained with streptavidin-AF488. The cells were imaged by confocal microscopy. White circles in enlarged insets indicate colocalizing puncta.

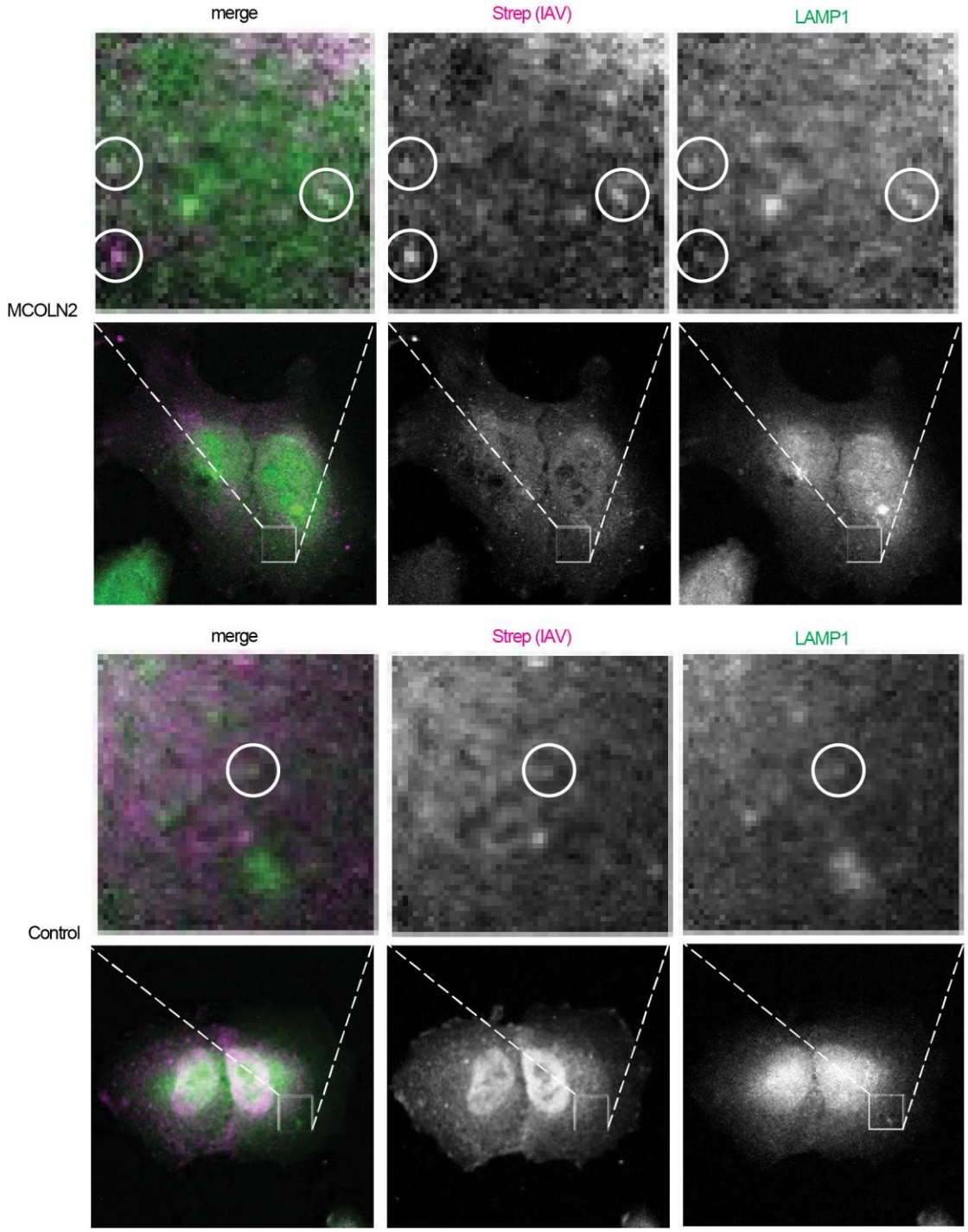
merge
Strep (IAV)
LAMP1
MCOLN2
merge
Strep (IAV)
LAMP1
Control

Figure 19. Colocalization of IAV with late endosomes is increased by MCOLN2 expression. Biotinylated IAV was bound to A549 stable cell lines at an MOI of 10 for 1 h at 4°C. The cells were shifted to 37°C for time points shown and then treated with 15 mM TCEP or PBS. A549 cells were fixed with PFA, permeabilized with 0.2% Triton X-100, and stained with anti-LAMP-1 antibody followed by BV-421 goat anti-rabbit antibody and streptavidin-AF488. Cells were imaged by confocal microscopy. White circles in enlarged insets indicate colocalizing puncta.

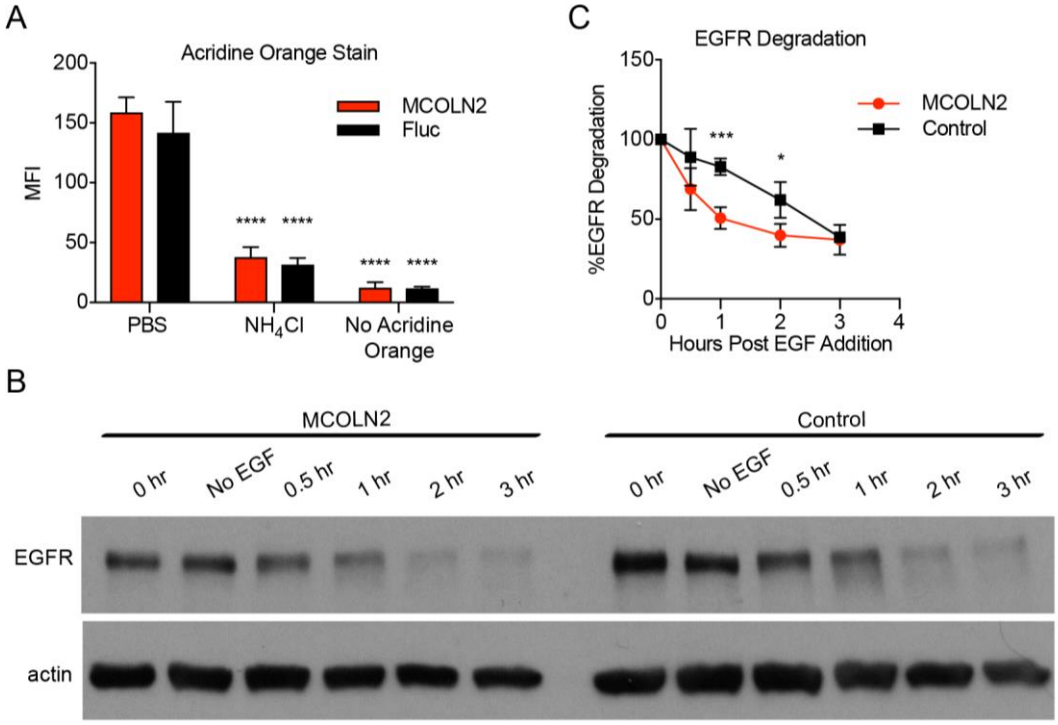

Figure 20. MCOLN2 promotes lysosomal degradation of EGFR. (A) A549 stable cell lines were incubated in media with 200 mM NH_4Cl or without NH_4Cl for 4 h. The cells were subsequently treated with 1 µM acridine orange for 5 min before cell fluorescence was quantitated by flow cytometry. (B and C) Serum-starved A549 stable cell lines were treated with 200 ng/ml EGF or without EGF. At the time points shown, the cells were lysed, and EGFR levels were detected by Western blotting (B) and quantified (C). In panel A, data represent means plus SD (error bars) from three independent experiments performed in technical triplicate. Statistical comparisons were made between treatment conditions and PBS control. In panel C, data represent means ± SD (error bars) from five independent experiments. Values that are significantly different are indicated by asterisks as follows: *, $P \leq 0.1$; ***, $P \leq 0.001$; ****, $P \leq 0.0001$.

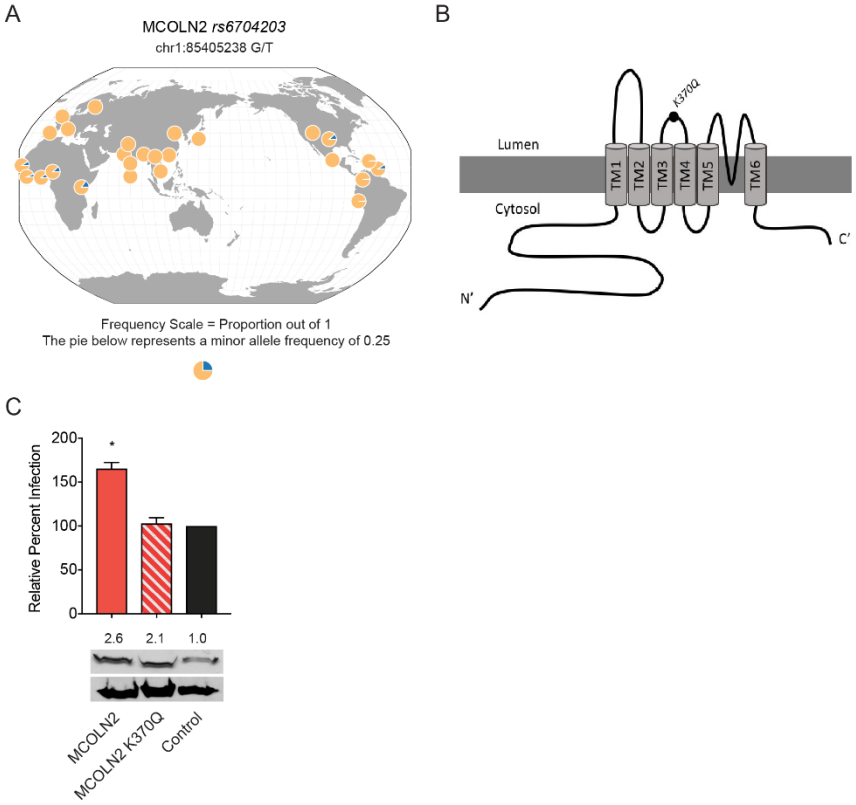

Figure 21. A rare genetic variant of MCOLN2 has a loss of function in viral enhancement. (A) Geographic distribution of *rs6704203*, showing increased frequency of the G allele in African populations. The graphic was generated using GGV browser. (B) Illustration of the location of the K370Q mutation within MCOLN2. Transmembrane domains 1 to 6 (TM1 to TM6) in MCOLN2 are shown. (C, top) A549 cells were infected with IAV (MOI of 0.2) for 8 h. Infection was quantified by staining cells with anti-NP antibody and subsequent flow cytometry-based analysis. (Bottom) MCOLN2 protein expression levels in each cell line were determined by Western blotting. Relative band intensity was quantified by using ImageJ. Values are means plus SD (error bars) from four independent experiments performed in technical triplicate. Values that are significantly different ($P \leq 0.1$) are indicated by an asterisk.

Virus	Enhanced?
Plasma membrane	
coxsackie B virus	no
HIV-1	no
measles virus	no
Newcastle disease virus	no
human parainfluenza virus type 3	no
vaccinia virus	no
Early endosome	
O'nyong nyong virus	no
respiratory syncytial virus	no
*Late endosome / MVB**	
equine arterivirus	yes
influenza A virus	yes
dengue virus	yes
yellow fever virus*	yes

Table 1. Virus entry enhanced by MCOLN2. Viruses were grouped by point of fusion/release into the cell cytoplasm. Viruses were subsequently grouped based on enhancement by MCOLN2, as determined in previous screening studies. * denotes viruses which are released from MVBs.

CHAPTER FOUR
Discussion

DISCUSSION OF CHAPTER TWO

ZIKV is an emerging pathogen of worldwide concern due to the severe neurological disorders associated with infection(123). Understanding the mechanisms underlying ZIKV infection and associated neurological disorders is thus of paramount importance. While at least two lineages of ZIKV exist, only ZIKV strains originating from Asian lineage ZIKV have been associated with significant disease in humans(127-131). Thus, studying the differences between ZIKV lineages may help to uncover important elements of ZIKV pathogenesis. During viral infection, the first challenge that a virus must overcome is gaining access to the host cell cytoplasm. Previous studies suggest that the African lineage of ZIKV is endocytosed via clathrin-mediated endocytosis and fuses with an internal cellular membrane in a Rab5 and pH dependent manner(149, 150, 152, 159). However, previously published studies comparing African and Asian strains identified significant differences in structural protein function and neurovirulence that were associated with lineage-specific mutations in structural genes(134, 139). While it has been suggested that viral attachment to cells is significantly different between ZIKV lineages, I have found that the general process of ZIKV entry is conserved (Figure 10)(139), and mirrors the entry of the flavivirus dengue virus(146, 252). The infection of multiple African and Asian lineage ZIKV strains that I tested was dependent on functional clathrin-mediated endocytosis, endosomal acidification, and Rab-dependent endosomal trafficking. Additionally, I found that all ZIKV strains tested except for MR 766 are sensitive to pH in the range of 6.1-6.3. This suggests that pH-induced fusion peptide exposure occurs

optimally around this pH range. Finally, I showed that ZIKV can fuse at lower frequency with early endosomes but preferentially fuses with MVBs/late endosomes to enter the cytoplasm.

The largest difference I observed between ZIKV strains was in the pH sensitivity of the African lineage ZIKV strains MR 766 and DAKAR 41519 (Figure 1D). While not significant, MR 766 was also inactivated at a higher pH than either Asian lineage strain tested. MR 766 has been passaged over 100 times in tissue culture, and may have adapted distinct entry mechanisms(253). Consistent with this, our data suggests that the cell entry process of MR 766 may not be fully representative of other ZIKV strains. Additional studies are needed to determine if the increased pH sensitivity of MR 766 significantly affects viral fusion.

While the results presented here suggest that ZIKV enters cells via clathrin-mediated endocytosis, it is intriguing to consider the possibility that ZIKV might infect neurons through a different pathway. Indeed, the infection of another neurovirulent flavivirus, Japanese encephalitis virus (JEV), has been found to be dependent on clathrin-mediated endocytosis in Vero and PK15 kidney-derived epithelial cell lines (254, 255). However, in neurons, JEV is endocytosed via caveolar endocytosis or macropinocytosis-like processes(143, 256, 257). While ZIKV entry mechanisms may also be cell-type dependent, a previous study found that infection of the human microglia-derived cell line CHME3 by a single ZIKV strain required clathrin and Rab5 function (149), similar to our findings. Additional studies are needed to delineate and compare the pathways utilized by African and Asian lineage ZIKV to enter neurons.

Together, our findings suggest that while individual lineages of ZIKV may be capable of using distinct processes to attach to cells, entry into cells is a rather inelastic process (139). Our findings further suggest that ZIKV entry is likely not responsible for the observed lineage

specific differences *in vitro* or *in vivo*, as this process is conserved between lineages. This could make ZIKV entry a more favorable target for antiviral therapeutics due to its conserved nature.

DISCUSSION OF CHAPTER THREE

The first challenge a virus must overcome during infection is gaining access to the host cell cytoplasm. To this end, viruses have developed ways of exploiting host factors and existing uptake pathways in order to efficiently enter cells. Significant progress has been made in identifying the mechanisms and cellular factors necessary for viral entry. Viruses often use attachment factors such as heparin sulfate, sialic acid, and gangliosides to bind to the cell surface and subsequently associate with one or more receptors such as dendritic cell-specific intracellular adhesion molecule-3-grabbing non-integrin (DC-SIGN), DAF, CAR, and integrins. This results in either direct penetration of the virion into the cytoplasm or receptor mediated endocytosis which can involve macropinocytosis, phagocytosis, clathrin mediated endocytosis, caveolar endocytosis or other pathways(38). Many endocytosed viruses are quickly delivered to and escape from Rab5-positive early endosomes which can be promoted by acidic endosomal pH as well as endosomal cathepsins and furin-like proteases. However, some viruses such as IAV and flaviviruses need to migrate inward into the cell to reach their preferred replication sites (nuclear for IAV and rough endoplasmic reticulum for flaviviruses). These viruses are thus capable of delaying membrane fusion until after trafficking from early to late endosomes(258). Our study identifies MCOLN2 as a novel endosomal host factor that facilitates viral vesicular trafficking to

ultimately promote productive infection. Specifically, I show that MCOLN2 promotes the efficiency with which certain viruses are transported from early to late endosomal compartments.

TRP superfamily proteins are commonly associated with sensory signaling processes. The TRPML/MCOLN subfamily seems to depart from this paradigm, having reported functions in basic cellular processes including lysosome fusion events, recycling, endocytosis, and autophagy(200-203, 224-226, 232-235). Recently, there is increasing evidence for a role of MCOLNs in immune function and bacterial infection(120, 169, 195, 236, 237). In this study, I found a direct role for MCOLN2 in the context of viral entry, further expanding the functional repertoire of this protein subfamily. An intriguing finding from our study comes from the endocytic trafficking (Figure 17B,C) and membrane fusion (Figure 17E) experiments. These data indicate that while the same amount of virus is endocytosed into MCOLN2 overexpressing cells as compared to control cells, more virus in the MCOLN2 overexpressing cells successfully traffics to the late endosomal compartment, from which it is subsequently released. This finding suggests that a population of IAV is normally lost or diverted in control cells during the entry process, but is better retained in a productive endocytic pathway in MCOLN2 expressing cells. Additional studies are needed to determine the fate of this IAV population in control cells.

Vesicular trafficking is critical for cellular function. However, the methods available to study this complex process are currently limited and the molecular mechanisms underlying vesicular trafficking remain obscure. A major question in the field of vesicular trafficking has been: what factor(s) mediate vesicle fusion and fission events? Specifically, calcium signaling is known to play an important role in certain membrane fusion events(259). Recent evidence suggests calcium may also play an important role in certain membrane fission events as

well(204). However, the channels responsible for Ca^{2+} signaling have remained elusive. The channel regulating lysosomal fusion events was only identified in the last several years(260). MCOLNs are known to be calcium permeable channels localized to endosomal compartments(175, 191). MCOLN1 has been recently found to be involved in lysosomal fission(204). Previous work has shown that MCOLN2 is important for endosomal recycling and the work presented here suggests that MCOLN2 promotes early to late endosomal trafficking of IAV (Figure 17-19)(203, 238). It would thus be interesting to determine if MCOLN2 plays a role in early endosomal fission events.

MCOLN2 has been reported to be induced by LPS and type I IFN(195, 196), hence its inclusion in our prior ISG screens(120, 169). I have also found MCOLN2 to be modestly induced by type I IFN and poly (I:C) treatment (Figure 11A). It is therefore interesting to consider the implications of MCOLN2 upregulation during viral infection *in vivo*, when IFN responses are systemic. In non-immune cells, basal or IFN-induced MCOLN2 expression may lead to enhanced viral uptake in a manner that benefits the virus, for example by viral hijacking. However, in immune cells, which express higher levels of basal MCOLN2(194, 195, 237), increased viral uptake could result in increased PAMP recognition, a stronger immune response, and subsequently improved viral clearance, which benefits the host. This latter model is supported by our finding that MCOLN2 expression results in increased ISG expression after SINV infection (Figure 12B). In a mouse model, *Mcoln2* knockout resulted in impaired chemokine secretion and reduced peripheral macrophage recruitment after bacterial challenge(195, 238). Additionally, a recent study found that MCOLN2 channel activity is important for dendritic cell mediated presentation of antigens from tumor cell-derived

microparticles to $CD8^+$ T cells. Deciphering these models will be important for determining whether MCOLN2-specific agonists or antagonists could be used therapeutically to modulate viral infection.

Lastly, I found that a rare genetic variant of human *MCOLN2* fails to enhance viral infection when ectopically expressed in cell culture. Intriguingly, this allelic variant is found at higher frequencies in African populations when compared to all geographic populations. Additional studies are needed to characterize the nature of the K370Q mutation encoded by *rs6704203*. Moreover, our current data on this variant are only correlative. To determine whether humans with one or two copies of the rare allele have altered susceptibility to viral infection, in depth genetic and clinical studies from multiple individuals or families would be needed.

CONCLUDING REMARKS

Viruses are an important part of the biosphere, infecting organisms from all three domains of life. Viruses play major roles in human disease, impact the survival of economically important livestock and crops, and more broadly have an underappreciated role in the environment(261, 262). As such, it is of great importance that we attempt to understand how viruses infect their hosts and impact the biosphere.

Viruses are obligate, intracellular parasites which commonly rely on an array of host factors for their attachment, entry, replication, and egress from host cells. In turn, hosts have evolved diverse mechanisms to defend against viral infection. Understanding the factors required for viral attachment and entry or for blocking these processes is of special importance since a

virus cannot infect a cell if it cannot gain access to the cell interior. Here, I have identified factors exploited by Zika virus during cell entry and characterized the function of MCOLN2, a host factor expressed in response to IFN-I signaling. Interestingly, while the IFN response is thought of as a form of cell-intrinsic immunity, I found MCOLN2 expression to promote viral entry *in vitro*. This work provides important insight into the processes involved in viral entry which will hopefully assist future work in further defining viral entry and the virus-host interactions involved therein.

APPENDIX A
List of primers used in chapter two

	Forward Primer	Reverse Primer
WT EGFP-Rab5a into pTRIPZ	atacgcgtttagttactacaacactgattcctggttggt	agaccggtcgccaccatggtgagcaagggcgagga
Rab5a BP Cloning	ggggacaagtttgtacaaaaaagcaggcttcaccatggctagtcgaggcg	ggggaccactttgtacaagaaagctggtttagttactacaacactgattcctg
Rab5a S34N Mutagenesis	gttggcaaaaacagcctagtgct	agcactaggctgtttttgccaac
LentiCRISPRv2 sgRab4a #1 Cloning	caccggatgactcaaatcatacaat	aaacattgtatgatttgagtcatcc
LentiCRISPRv2 sgRab4a #2 Cloning	caccgctcaaatcatacaataggag	aaacctcctattgtatgatttgagc
LentiCRISPRv2 sgRab4b #1 Cloning	caccgttcctgcactgccaatcacc	aaacggtgattggcagtgcaggaac
LentiCRISPRv2 sgRab4b #2 Cloning	caccgctccaaccacacaatcggcg	aaaccgccgattgtgtggttggagc
LentiCRISPRv2 sgRab4c #3 Cloning	caccgggatcccgggtggtcaacgt	aaacacgttgaccacccgggatccc
LentiCRISPRv2 sgRab5a #1 Cloning	caccgatttcccgtatttggcccgt	aaacacgggccaaatacgggaaatc
LentiCRISPRv2 sgRab5a #2 Cloning	caccgcgaggcgcaacaagacccaa	aaacttgggtcttgttgcgcctcgc

LentiCRISPRv2 sgRab5a #3 Cloning	caccgatttcaagagagtaccattg	aaaccaatggtactctcttgaaatc
LentiCRISPRv2 sgRab5b #1 Cloning	caccgctttgacaaaacgtaatacc	aaacggtattacgttttgtcaaagc
LentiCRISPRv2 sgRab5b #2 Cloning	caccgtaggcccaatgggcaacccc	aaacggggttgcccattgggcctac
LentiCRISPRv2 sgRab5b #3 Cloning	caccgccagttcaaattggtcctgc	aaacgcaggaccaatttgaactggc
LentiCRISPRv2 sgRab5c #1 Cloning	caccgggaggcgcagcacgacccaa	aaacttgggtcgtgctgcgcctccc
LentiCRISPRv2 sgRab5c #2 Cloning	caccggggacagtttcacgagtacc	aaacggtactcgtgaaactgtcccc
LentiCRISPRv2 sgRab5c #3 Cloning	caccgcaagatctgtcaatttaagc	aaacgcttaaattgacagatcttgc
LentiCRISPRv2 sgRab7a #1 Cloning	caccgcagaaagtcagctcctattg	aaaccaataggagctgactttctgc
LentiCRISPRv2 sgRab7a #2 Cloning	caccggttgctgaaggttatcatcc	aaacggatgataaccttcagcaacc
LentiCRISPRv2 sgRab7a #3 Cloning	caccggttatcatcctgggagattc	aaacgaatctcccaggatgataacc
LentiCRISPRv2 sgRab7b #1 Cloning	caccgctcattatcgtcggagccat	aaacatggctccgacgataatgagc

LentiCRISPRv2 sgRab7b #2 Cloning	caccgtgtgcacaagacgttttatg	aaaccataaaacgtcttgtgcacac
LentiCRISPRv2 sgRab11a #1 Cloning	caccgcatttcgagtaaatcgagac	aaacgtctcgatttactcgaaatgc
LentiCRISPRv2 sgRab11a #2 Cloning	caccgtgttgcaaactctactccaa	aaacttggagtagagtttgcaacac
LentiCRISPRv2 sgRab11a #3 Cloning	caccggtttgcaacaagaagcatcc	aaacggatgcttcttgttgcaaacc
LentiCRISPRv2 sgRab11b #1 Cloning	caccgtgcgggtgaagcgcgacagc	aaacgctgtcgcgcttcacccgcac
LentiCRISPRv2 sgRab11b #2 Cloning	caccggagcaagagcaccatcggcg	aaaccgccgatggtgctcttgctcc
LentiCRISPRv2 sgRab11b #3 Cloning	caccgctcatcggggactcaggcgt	aaacacgcctgagtccccgatgagc

APPENDIX B
List of primers used in chapter three

Name	Forward Primer	Reverse Primer
MCOLN2 BP Cloning	5'-ggggacaagtttgtacaaaaaagcaggcttcaccatggcacatcgtgattctgagatgaa-3'	5'-ggggaccactttgtacaagaaagctgggtttagctaataggtatcaagtgatcatcact-3'
MCOLN2 D463D/KK Mutagenesis	5'-ctggatttgggcaaaggttgcaaacatcttcttaccgttgaccagagaaaacagacac-3'	5'-gtgtctgttttctctggtcaacggtaagaagatgtttgcaacctttgcccaaatccag-3'
MCOLN2 K370Q Mutagenesis	5'-aatggaaatcaaagcaaataatctcacaaactatgatctctgc-3'	5'-gcagagatcatagtttgtgagattatttgctttgatttccatt-3'
sgMCOLN2 #1	5'-caccgaacccagtttccacggaatc-3'	5'-cgattccgtggaaactgggttcaaa-3'
sgMCOLN2 #2	5'-caccgcagctaaaggacattaccct-3'	5'-cagggtaatgtcctttagctgcaaa-3'
sgMCOLN2 #3	5'-caccgtctccaagaagcctccggac-3'	5'-cgtccggaggcttcttggagacaaa-3'
sgControl	5'-caccggttggcatattggcccagac-3'	5'-aaacgtctgggccaatatgccaacc-3'
A/WSN/33 HA – RT-qPCR	5'-taacctgctcgaagacagac-3'	5'-agagccatccggtgatgtta-3'
YFV-17D – RT-qPCR	5'-aatcgagttgctaggcaataaacac-3'	5'-tccctgagctttacgaccaga-3'

BIBLIOGRAPHY

1. Wommack KE, Hill RT, Kessel M, Russek-Cohen E, Colwell RR. 1992. Distribution of viruses in the Chesapeake Bay. Applied and environmental microbiology 58:2965-2970.
2. Hérelle Fld. 1926. The bacteriophage and its behavior. The Williams & Wilkins company, Baltimore, Md.
3. Bertozzi Silva J, Storms Z, Sauvageau D. 2016. Host receptors for bacteriophage adsorption. FEMS Microbiology Letters 363.
4. Heller KJ. 1984. Identification of the phage gene for host receptor specificity by analyzing hybrid phages of T5 and BF23. Virology 139:11-21.
5. Heller K, Braun V. 1982. Polymannose O-antigens of Escherichia coli, the binding sites for the reversible adsorption of bacteriophage T5+ via the L-shaped tail fibers. Journal of virology 41:222-227.
6. Marsh M, Helenius A. 2006. Virus entry: open sesame. Cell 124:729-40.
7. Dalgleish AG, Beverley PC, Clapham PR, Crawford DH, Greaves MF, Weiss RA. 1984. The CD4 (T4) antigen is an essential component of the receptor for the AIDS retrovirus. Nature 312:763-7.
8. Bergelson JM, Cunningham JA, Droguett G, Kurt-Jones EA, Krithivas A, Hong JS, Horwitz MS, Crowell RL, Finberg RW. 1997. Isolation of a common receptor for Coxsackie B viruses and adenoviruses 2 and 5. Science 275:1320-3.
9. Coyne CB, Bergelson JM. 2005. CAR: a virus receptor within the tight junction. Adv Drug Deliv Rev 57:869-82.
10. Weis W, Brown JH, Cusack S, Paulson JC, Skehel JJ, Wiley DC. 1988. Structure of the influenza virus haemagglutinin complexed with its receptor, sialic acid. Nature 333:426-31.
11. Waigmann E, Heinlein M, Blanc S. 2007. Virus Transmission—Getting Out and In, p 1.
12. Buchmann JP, Holmes EC. 2015. Cell Walls and the Convergent Evolution of the Viral Envelope. Microbiology and molecular biology reviews : MMBR 79:403-418.
13. Waigmann E, Curin M, Heinlein M. 2007. Tobacco mosaic virus - A model for macromolecular cell-to-cell spread, vol 7.
14. Wilen CB, Tilton JC, Doms RW. 2012. Molecular mechanisms of HIV entry. Adv Exp Med Biol 726:223-42.
15. Coyne CB, Bergelson JM. 2006. Virus-induced Abl and Fyn kinase signals permit coxsackievirus entry through epithelial tight junctions. Cell 124:119-31.
16. Beveridge TJ, Graham LL. 1991. Surface layers of bacteria. Microbiological reviews 55:684-705.
17. Demchick P, Koch AL. 1996. The permeability of the wall fabric of Escherichia coli and Bacillus subtilis. J Bacteriol 178:768-73.
18. Nikaido H. 2003. Molecular basis of bacterial outer membrane permeability revisited. Microbiol Mol Biol Rev 67:593-656.
19. Labrie SJ, Samson JE, Moineau S. 2010. Bacteriophage resistance mechanisms. Nat Rev Microbiol 8:317-27.

20. Rickgauer JP, Fuller DN, Grimes S, Jardine PJ, Anderson DL, Smith DE. 2008. Portal motor velocity and internal force resisting viral DNA packaging in bacteriophage phi29. Biophysical journal 94:159-167.
21. Smith DE, Tans SJ, Smith SB, Grimes S, Anderson DL, Bustamante C. 2001. The bacteriophage straight phi29 portal motor can package DNA against a large internal force. Nature 413:748-52.
22. Leiman PG, Chipman PR, Kostyuchenko VA, Mesyanzhinov VV, Rossmann MG. 2004. Three-dimensional rearrangement of proteins in the tail of bacteriophage T4 on infection of its host. Cell 118:419-29.
23. Van Etten JL, Meints RH. 1999. Giant viruses infecting algae. Annu Rev Microbiol 53:447-94.
24. Poranen MM, Daugelavicius R, Bamford DH. 2002. Common principles in viral entry. Annu Rev Microbiol 56:521-38.
25. Kao SH, McClain WH. 1980. Baseplate protein of bacteriophage T4 with both structural and lytic functions. J Virol 34:95-103.
26. Hu B, Margolin W, Molineux IJ, Liu J. 2015. Structural remodeling of bacteriophage T4 and host membranes during infection initiation. Proc Natl Acad Sci U S A 112:E4919-28.
27. Bohm J, Lambert O, Frangakis AS, Letellier L, Baumeister W, Rigaud JL. 2001. FhuA-mediated phage genome transfer into liposomes: a cryo-electron tomography study. Curr Biol 11:1168-75.
28. Cumby N, Reimer K, Mengin-Lecreulx D, Davidson AR, Maxwell KL. 2015. The phage tail tape measure protein, an inner membrane protein and a periplasmic chaperone play connected roles in the genome injection process of E. coli phage HK97. Mol Microbiol 96:437-47.
29. Sun L, Young LN, Zhang X, Boudko SP, Fokine A, Zbornik E, Roznowski AP, Molineux IJ, Rossmann MG, Fane BA. 2014. Icosahedral bacteriophage PhiX174 forms a tail for DNA transport during infection. Nature 505:432-5.
30. Hu B, Margolin W, Molineux IJ, Liu J. 2013. The bacteriophage t7 virion undergoes extensive structural remodeling during infection. Science 339:576-9.
31. Xiang Y, Morais MC, Cohen DN, Bowman VD, Anderson DL, Rossmann MG. 2008. Crystal and cryoEM structural studies of a cell wall degrading enzyme in the bacteriophage phi29 tail. Proc Natl Acad Sci U S A 105:9552-7.
32. Xu J, Gui M, Wang D, Xiang Y. 2016. The bacteriophage ϕ29 tail possesses a pore-forming loop for cell membrane penetration. Nature 534:544.
33. Bamford DH, Romantschuk M, Somerharju PJ. 1987. Membrane fusion in prokaryotes: bacteriophage phi 6 membrane fuses with the Pseudomonas syringae outer membrane. Embo j 6:1467-73.
34. Chang A, Dutch RE. 2012. Paramyxovirus fusion and entry: multiple paths to a common end. Viruses 4:613-636.
35. Melikyan GB. 2014. HIV entry: a game of hide-and-fuse? Current opinion in virology 4:1-7.
36. L. Webster R. 1996. Biology of the Filamentous Bacteriophage, p 1-20 doi:10.1016/B978-012402380-2/50003-4.

37. Jovic M, Sharma M, Rahajeng J, Caplan S. 2010. The early endosome: a busy sorting station for proteins at the crossroads. Histology and histopathology 25:99-112.
38. Mercer J, Schelhaas M, Helenius A. 2010. Virus entry by endocytosis. Annu Rev Biochem 79:803-33.
39. Romero-Brey I, Bartenschlager R. 2016. Endoplasmic Reticulum: The Favorite Intracellular Niche for Viral Replication and Assembly. Viruses 8:160.
40. Fay N, Panté N. 2015. Nuclear entry of DNA viruses. 6.
41. Luby-Phelps K. 1994. Physical properties of cytoplasm. Current Opinion in Cell Biology 6:3-9.
42. Kaksonen M, Roux A. 2018. Mechanisms of clathrin-mediated endocytosis. Nature Reviews Molecular Cell Biology 19:313.
43. Edinger TO, Pohl MO, Stertz S. 2014. Entry of influenza A virus: host factors and antiviral targets. J Gen Virol 95:263-77.
44. Acosta EG, Castilla V, Damonte EB. 2008. Functional entry of dengue virus into Aedes albopictus mosquito cells is dependent on clathrin-mediated endocytosis. J Gen Virol 89:474-84.
45. van der Schaar HM, Rust MJ, Chen C, van der Ende-Metselaar H, Wilschut J, Zhuang X, Smit JM. 2008. Dissecting the cell entry pathway of dengue virus by single-particle tracking in living cells. PLoS pathogens 4:e1000244-e1000244.
46. Gastaldelli M, Imelli N, Boucke K, Amstutz B, Meier O, Greber UF. 2008. Infectious adenovirus type 2 transport through early but not late endosomes. Traffic 9:2265-78.
47. Sun X, Yau VK, Briggs BJ, Whittaker GR. 2005. Role of clathrin-mediated endocytosis during vesicular stomatitis virus entry into host cells. Virology 338:53-60.
48. DeTulleo L, Kirchhausen T. 1998. The clathrin endocytic pathway in viral infection. The EMBO journal 17:4585-4593.
49. Rust MJ, Lakadamyali M, Zhang F, Zhuang X. 2004. Assembly of endocytic machinery around individual influenza viruses during viral entry. Nat Struct Mol Biol 11:567-73.
50. Johannsdottir HK, Mancini R, Kartenbeck J, Amato L, Helenius A. 2009. Host cell factors and functions involved in vesicular stomatitis virus entry. J Virol 83:440-53.
51. Ehrlich M, Boll W, Van Oijen A, Hariharan R, Chandran K, Nibert ML, Kirchhausen T. 2004. Endocytosis by random initiation and stabilization of clathrin-coated pits. Cell 118:591-605.
52. Kiss AL, Botos E. 2009. Endocytosis via caveolae: alternative pathway with distinct cellular compartments to avoid lysosomal degradation? Journal of cellular and molecular medicine 13:1228-1237.
53. Anderson HA, Chen Y, Norkin LC. 1996. Bound simian virus 40 translocates to caveolin-enriched membrane domains, and its entry is inhibited by drugs that selectively disrupt caveolae. Mol Biol Cell 7:1825-34.
54. Lim JP, Gleeson PA. 2011. Macropinocytosis: an endocytic pathway for internalising large gulps. 89:836-843.
55. Mercer J, Helenius A. 2008. Vaccinia virus uses macropinocytosis and apoptotic mimicry to enter host cells. Science 320:531-5.

56. de Vries E, Tscherne DM, Wienholts MJ, Cobos-Jimenez V, Scholte F, Garcia-Sastre A, Rottier PJ, de Haan CA. 2011. Dissection of the influenza A virus endocytic routes reveals macropinocytosis as an alternative entry pathway. PLoS Pathog 7:e1001329.
57. Krzyzaniak MA, Zumstein MT, Gerez JA, Picotti P, Helenius A. 2013. Host cell entry of respiratory syncytial virus involves macropinocytosis followed by proteolytic activation of the F protein. PLoS Pathog 9:e1003309.
58. Aleksandrowicz P, Marzi A, Biedenkopf N, Beimforde N, Becker S, Hoenen T, Feldmann H, Schnittler H-J. 2011. Ebola virus enters host cells by macropinocytosis and clathrin-mediated endocytosis. The Journal of infectious diseases 204 Suppl 3:S957-S967.
59. Saeed MF, Kolokoltsov AA, Albrecht T, Davey RA. 2010. Cellular entry of ebola virus involves uptake by a macropinocytosis-like mechanism and subsequent trafficking through early and late endosomes. PLoS Pathog 6:e1001110.
60. Nanbo A, Imai M, Watanabe S, Noda T, Takahashi K, Neumann G, Halfmann P, Kawaoka Y. 2010. Ebolavirus is internalized into host cells via macropinocytosis in a viral glycoprotein-dependent manner. PLoS Pathog 6:e1001121.
61. Meier O, Boucke K, Hammer SV, Keller S, Stidwill RP, Hemmi S, Greber UF. 2002. Adenovirus triggers macropinocytosis and endosomal leakage together with its clathrin-mediated uptake. J Cell Biol 158:1119-31.
62. Cossart P, Helenius A. Endocytosis of viruses and bacteria. Cold Spring Harbor perspectives in biology 6:a016972.
63. Ghigo E, Kartenbeck J, Lien P, Pelkmans L, Capo C, Mege JL, Raoult D. 2008. Ameobal pathogen mimivirus infects macrophages through phagocytosis. PLoS Pathog 4:e1000087.
64. Nonnenmacher M, Weber T. 2011. Adeno-associated virus 2 infection requires endocytosis through the CLIC/GEEC pathway. Cell host & microbe 10:563-576.
65. White JM, Whittaker GR. 2016. Fusion of Enveloped Viruses in Endosomes. Traffic (Copenhagen, Denmark) 17:593-614.
66. Smit JM, Bittman R, Wilschut J. 1999. Low-pH-dependent fusion of Sindbis virus with receptor-free cholesterol- and sphingolipid-containing liposomes. Journal of virology 73:8476-8484.
67. Edinger TO, Pohl MO, Yángüez E, Stertz S. 2015. Cathepsin W Is Required for Escape of Influenza A Virus from Late Endosomes. mBio 6:e00297-e00297.
68. Lu YE, Cassese T, Kielian M. 1999. The cholesterol requirement for sindbis virus entry and exit and characterization of a spike protein region involved in cholesterol dependence. J Virol 73:4272-8.
69. Schornberg K, Matsuyama S, Kabsch K, Delos S, Bouton A, White J. 2006. Role of Endosomal Cathepsins in Entry Mediated by the Ebola Virus Glycoprotein. Journal of Virology 80:4174.
70. Carette JE, Raaben M, Wong AC, Herbert AS, Obernosterer G, Mulherkar N, Kuehne AI, Kranzusch PJ, Griffin AM, Ruthel G, Dal Cin P, Dye JM, Whelan SP, Chandran K, Brummelkamp TR. 2011. Ebola virus entry requires the cholesterol transporter Niemann-Pick C1. Nature 477:340-3.

71. Cote M, Misasi J, Ren T, Bruchez A, Lee K, Filone CM, Hensley L, Li Q, Ory D, Chandran K, Cunningham J. 2011. Small molecule inhibitors reveal Niemann-Pick C1 is essential for Ebola virus infection. Nature 477:344-8.
72. Grant BD, Donaldson JG. 2009. Pathways and mechanisms of endocytic recycling. Nature reviews Molecular cell biology 10:597-608.
73. Scott CC, Vacca F, Gruenberg J. 2014. Endosome maturation, transport and functions. Semin Cell Dev Biol 31:2-10.
74. Hu Y-B, Dammer EB, Ren R-J, Wang G. 2015. The endosomal-lysosomal system: from acidification and cargo sorting to neurodegeneration. Translational neurodegeneration 4:18-18.
75. Huotari J, Helenius A. Endosome maturation. The EMBO journal 30:3481-3500.
76. Guerra F, Bucci C. 2016. Multiple Roles of the Small GTPase Rab7. Cells 5:34.
77. Le Blanc I, Luyet PP, Pons V, Ferguson C, Emans N, Petiot A, Mayran N, Demaurex N, Faure J, Sadoul R, Parton RG, Gruenberg J. 2005. Endosome-to-cytosol transport of viral nucleocapsids. Nat Cell Biol 7:653-64.
78. van der Schaar HM, Rust MJ, Chen C, van der Ende-Metselaar H, Wilschut J, Zhuang X, Smit JM. 2008. Dissecting the Cell Entry Pathway of Dengue Virus by Single-Particle Tracking in Living Cells. PLoS Pathogens 4:e1000244.
79. Potokar M, Korva M, Jorgačevski J, Avšič-Županc T, Zorec R. 2014. Tick-borne encephalitis virus infects rat astrocytes but does not affect their viability. PloS one 9:e86219-e86219.
80. Forzan M, Marsh M, Roy P. 2007. Bluetongue virus entry into cells. Journal of virology 81:4819-4827.
81. Hsiao J-C, Chu L-W, Lo Y-T, Lee S-P, Chen T-J, Huang C-Y, Ping Y-H, Chang W. 2015. Intracellular Transport of Vaccinia Virus in HeLa Cells Requires WASH-VPEF/FAM21-Retromer Complexes and Recycling Molecules Rab11 and Rab22. Journal of virology 89:8365-8382.
82. Zhang W, Kazakov T, Popa A, DiMaio D. 2014. Vesicular trafficking of incoming human papillomavirus 16 to the Golgi apparatus and endoplasmic reticulum requires γ-secretase activity. mBio 5:e01777.
83. Pelkmans L, Kartenbeck J, Helenius A. 2001. Caveolar endocytosis of simian virus 40 reveals a new two-step vesicular-transport pathway to the ER. Nat Cell Biol 3:473-83.
84. Mosso C, Galvan-Mendoza IJ, Ludert JE, del Angel RM. 2008. Endocytic pathway followed by dengue virus to infect the mosquito cell line C6/36 HT. Virology 378:193-9.
85. Bressanelli S, Stiasny K, Allison SL, Stura EA, Duquerroy S, Lescar J, Heinz FX, Rey FA. 2004. Structure of a flavivirus envelope glycoprotein in its low-pH-induced membrane fusion conformation. The EMBO journal 23:728-738.
86. Stiasny K, Bressanelli S, Lepault J, Rey FA, Heinz FX. 2004. Characterization of a Membrane-Associated Trimeric Low-pH-Induced Form of the Class II Viral Fusion Protein E from Tick-Borne Encephalitis Virus and Its Crystallization. Journal of Virology 78:3178.
87. Tosteson MT, Chow M. 1997. Characterization of the ion channels formed by poliovirus in planar lipid membranes. J Virol 71:507-11.

88. Tosteson MT, Wang H, Naumov A, Chow M. 2004. Poliovirus binding to its receptor in lipid bilayers results in particle-specific, temperature-sensitive channels. J Gen Virol 85:1581-9.
89. Fricks CE, Hogle JM. 1990. Cell-induced conformational change in poliovirus: externalization of the amino terminus of VP1 is responsible for liposome binding. J Virol 64:1934-45.
90. Maier O, Galan DL, Wodrich H, Wiethoff CM. 2010. An N-terminal domain of adenovirus protein VI fragments membranes by inducing positive membrane curvature. Virology 402:11-9.
91. Wiethoff CM, Wodrich H, Gerace L, Nemerow GR. 2005. Adenovirus protein VI mediates membrane disruption following capsid disassembly. Journal of virology 79:1992-2000.
92. Fernandez-Garcia MD, Meertens L, Chazal M, Hafirassou ML, Dejarnac O, Zamborlini A, Despres P, Sauvonnet N, Arenzana-Seisdedos F, Jouvenet N, Amara A. 2016. Vaccine and Wild-Type Strains of Yellow Fever Virus Engage Distinct Entry Mechanisms and Differentially Stimulate Antiviral Immune Responses. mBio 7:e01956-15.
93. Hoornweg TE, van Duijl-Richter MKS, Ayala Nuñez NV, Albulescu IC, van Hemert MJ, Smit JM. 2016. Dynamics of Chikungunya Virus Cell Entry Unraveled by Single-Virus Tracking in Living Cells. Journal of Virology 90:4745.
94. Bernard E, Solignat M, Gay B, Chazal N, Higgs S, Devaux C, Briant L. 2010. Endocytosis of chikungunya virus into mammalian cells: role of clathrin and early endosomal compartments. PLoS One 5:e11479.
95. Ooi YS, Stiles KM, Liu CY, Taylor GM, Kielian M. 2013. Genome-wide RNAi screen identifies novel host proteins required for alphavirus entry. PLoS pathogens 9:e1003835-e1003835.
96. Lee RCH, Hapuarachchi HC, Chen KC, Hussain KM, Chen H, Low SL, Ng LC, Lin R, Ng MM-L, Chu JJH. 2013. Mosquito cellular factors and functions in mediating the infectious entry of chikungunya virus. PLoS neglected tropical diseases 7:e2050-e2050.
97. Korte T, Ludwig K, Booy FP, Blumenthal R, Herrmann A. 1999. Conformational Intermediates and Fusion Activity of Influenza Virus Hemagglutinin. Journal of Virology 73:4567.
98. Glomb-Reinmund S, Kielian M. 1998. The Role of Low pH and Disulfide Shuffling in the Entry and Fusion of Semliki Forest Virus and Sindbis Virus. Virology 248:372-381.
99. Smit J. 2002. The role of N-linked glycosylation of Sindbis virus glycoproteins E2 and E1 in viral infectivity and membrane fusion activity. Ph.D. University of Groningen.
100. Cao S, Zhang W. 2013. Characterization of an early-stage fusion intermediate of Sindbis virus using cryoelectron microscopy. Proc Natl Acad Sci U S A 110:13362-7.
101. Takeuchi O, Akira S. 2009. Innate immunity to virus infection. Immunological reviews 227:75-86.
102. Hornung V, Ellegast J, Kim S, Brzozka K, Jung A, Kato H, Poeck H, Akira S, Conzelmann KK, Schlee M, Endres S, Hartmann G. 2006. 5'-Triphosphate RNA is the ligand for RIG-I. Science 314:994-7.
103. Kato H, Takeuchi O, Mikamo-Satoh E, Hirai R, Kawai T, Matsushita K, Hiiragi A, Dermody TS, Fujita T, Akira S. 2008. Length-dependent recognition of double-stranded

ribonucleic acids by retinoic acid-inducible gene-I and melanoma differentiation-associated gene 5. J Exp Med 205:1601-10.
104. Takaoka A, Wang Z, Choi MK, Yanai H, Negishi H, Ban T, Lu Y, Miyagishi M, Kodama T, Honda K, Ohba Y, Taniguchi T. 2007. DAI (DLM-1/ZBP1) is a cytosolic DNA sensor and an activator of innate immune response. Nature 448:501-5.
105. Chen Q, Sun L, Chen ZJ. 2016. Regulation and function of the cGAS–STING pathway of cytosolic DNA sensing. Nature Immunology 17:1142.
106. Unterholzner L, Keating SE, Baran M, Horan KA, Jensen SB, Sharma S, Sirois CM, Jin T, Latz E, Xiao TS, Fitzgerald KA, Paludan SR, Bowie AG. 2010. IFI16 is an innate immune sensor for intracellular DNA. Nat Immunol 11:997-1004.
107. Stark GR, Darnell JE, Jr. 2012. The JAK-STAT pathway at twenty. Immunity 36:503-514.
108. MacMicking JD. 2012. Interferon-inducible effector mechanisms in cell-autonomous immunity. Nature reviews Immunology 12:367-382.
109. Ivashkiv LB, Donlin LT. 2014. Regulation of type I interferon responses. Nature reviews Immunology 14:36-49.
110. Chemudupati M, Kenney AD, Bonifati S, Zani A, McMichael TM, Wu L, Yount JS. 2019. From APOBEC to ZAP: Diverse mechanisms used by cellular restriction factors to inhibit virus infections. Biochimica et Biophysica Acta (BBA) - Molecular Cell Research 1866:382-394.
111. Richardson RB, Ohlson MB, Eitson JL, Kumar A, McDougal MB, Boys IN, Mar KB, De La Cruz-Rivera PC, Douglas C, Konopka G, Xing C, Schoggins JW. 2018. A CRISPR screen identifies IFI6 as an ER-resident interferon effector that blocks flavivirus replication. Nat Microbiol 3:1214-1223.
112. Brass AL, Huang IC, Benita Y, John SP, Krishnan MN, Feeley EM, Ryan BJ, Weyer JL, van der Weyden L, Fikrig E, Adams DJ, Xavier RJ, Farzan M, Elledge SJ. 2009. The IFITM proteins mediate cellular resistance to influenza A H1N1 virus, West Nile virus, and dengue virus. Cell 139:1243-54.
113. Zani A, Yount JS. 2018. Antiviral Protection by IFITM3 In Vivo. Current Clinical Microbiology Reports 5:229-237.
114. Desai TM, Marin M, Chin CR, Savidis G, Brass AL, Melikyan GB. 2014. IFITM3 Restricts Influenza A Virus Entry by Blocking the Formation of Fusion Pores following Virus-Endosome Hemifusion. PLOS Pathogens 10:e1004048.
115. Fu B, Wang L, Li S, Dorf ME. 2017. ZMPSTE24 defends against influenza and other pathogenic viruses. The Journal of Experimental Medicine 214:919.
116. Liu S-Y, Sanchez DJ, Aliyari R, Lu S, Cheng G. 2012. Systematic identification of type I and type II interferon-induced antiviral factors. Proceedings of the National Academy of Sciences of the United States of America 109:4239-4244.
117. Liu SY, Aliyari R, Chikere K, Li G, Marsden MD, Smith JK, Pernet O, Guo H, Nusbaum R, Zack JA, Freiberg AN, Su L, Lee B, Cheng G. 2013. Interferon-inducible cholesterol-25-hydroxylase broadly inhibits viral entry by production of 25-hydroxycholesterol. Immunity 38:92-105.
118. Lipovsky A, Erden A, Kanaya E, Zhang W, Crite M, Bradfield C, MacMicking J, DiMaio D, Schoggins JW, Iwasaki A. 2017. The cellular endosomal protein stannin

inhibits intracellular trafficking of human papillomavirus during virus entry. J Gen Virol 98:2821-2836.
119. Krebs DL, Hilton DJ. 2001. SOCS Proteins: Negative Regulators of Cytokine Signaling. STEM CELLS 19:378-387.
120. Schoggins JW, MacDuff DA, Imanaka N, Gainey MD, Shrestha B, Eitson JL, Mar KB, Richardson RB, Ratushny AV, Litvak V, Dabelic R, Manicassamy B, Aitchison JD, Aderem A, Elliott RM, Garcia-Sastre A, Racaniello V, Snijder EJ, Yokoyama WM, Diamond MS, Virgin HW, Rice CM. 2014. Pan-viral specificity of IFN-induced genes reveals new roles for cGAS in innate immunity. Nature 505:691-5.
121. Mar KB, Rinkenberger NR, Boys IN, Eitson JL, McDougal MB, Richardson RB, Schoggins JW. 2018. LY6E mediates an evolutionarily conserved enhancement of virus infection by targeting a late entry step. Nature Communications 9:3603.
122. Rinkenberger N, Schoggins JW. 2018. Mucolipin-2 Cation Channel Increases Trafficking Efficiency of Endocytosed Viruses. mBio 9:e02314-17.
123. Hills SL, Fischer M, Petersen LR. 2017. Epidemiology of Zika Virus Infection. The Journal of infectious diseases 216:S868-S874.
124. Ventura CV, Ventura LO. 2018. Ophthalmologic Manifestations Associated With Zika Virus Infection. Pediatrics 141:S161-S166.
125. Dick GWA, Kitchen SF, Haddow AJ. 1952. Zika Virus (I). Isolations and serological specificity. Transactions of the Royal Society of Tropical Medicine and Hygiene 46:509-520.
126. Beaver JT, Lelutiu N, Habib R, Skountzou I. 2018. Evolution of Two Major Zika Virus Lineages: Implications for Pathology, Immune Response, and Vaccine Development. Frontiers in immunology 9:1640-1640.
127. Zhu Z, Chan JF, Tee KM, Choi GK, Lau SK, Woo PC, Tse H, Yuen KY. 2016. Comparative genomic analysis of pre-epidemic and epidemic Zika virus strains for virological factors potentially associated with the rapidly expanding epidemic. Emerg Microbes Infect 5:e22.
128. Enfissi A, Codrington J, Roosblad J, Kazanji M, Rousset D. 2016. Zika virus genome from the Americas. Lancet 387:227-8.
129. Lanciotti RS, Lambert AJ, Holodniy M, Saavedra S, Signor LDCC. 2016. Phylogeny of Zika Virus in Western Hemisphere, 2015. Emerging infectious diseases 22:933-935.
130. Haddow AD, Schuh AJ, Yasuda CY, Kasper MR, Heang V, Huy R, Guzman H, Tesh RB, Weaver SC. 2012. Genetic characterization of Zika virus strains: geographic expansion of the Asian lineage. PLoS Negl Trop Dis 6:e1477.
131. Faye O, Freire CCM, Iamarino A, Faye O, de Oliveira JVC, Diallo M, Zanotto PMA, Sall AA. 2014. Molecular evolution of Zika virus during its emergence in the 20(th) century. PLoS neglected tropical diseases 8:e2636-e2636.
132. Wang L, Valderramos SG, Wu A, Ouyang S, Li C, Brasil P, Bonaldo M, Coates T, Nielsen-Saines K, Jiang T, Aliyari R, Cheng G. 2016. From Mosquitos to Humans: Genetic Evolution of Zika Virus. Cell host & microbe 19:561-565.
133. Faria NR, Azevedo RdSdS, Kraemer MUG, Souza R, Cunha MS, Hill SC, Thézé J, Bonsall MB, Bowden TA, Rissanen I, Rocco IM, Nogueira JS, Maeda AY, Vasami FGdS, Macedo FLdL, Suzuki A, Rodrigues SG, Cruz ACR, Nunes BT, Medeiros DBdA,

Rodrigues DSG, Queiroz ALN, da Silva EVP, Henriques DF, da Rosa EST, de Oliveira CS, Martins LC, Vasconcelos HB, Casseb LMN, Simith DdB, Messina JP, Abade L, Lourenço J, Alcantara LCJ, de Lima MM, Giovanetti M, Hay SI, de Oliveira RS, Lemos PdS, de Oliveira LF, de Lima CPS, da Silva SP, de Vasconcelos JM, Franco L, Cardoso JF, Vianez-Júnior JLdSG, Mir D, Bello G, Delatorre E, Khan K, et al. 2016. Zika virus in the Americas: Early epidemiological and genetic findings. Science (New York, NY) 352:345-349.

134. Yuan L, Huang XY, Liu ZY, Zhang F, Zhu XL, Yu JY, Ji X, Xu YP, Li G, Li C, Wang HJ, Deng YQ, Wu M, Cheng ML, Ye Q, Xie DY, Li XF, Wang X, Shi W, Hu B, Shi PY, Xu Z, Qin CF. 2017. A single mutation in the prM protein of Zika virus contributes to fetal microcephaly. Science 358:933-936.
135. Anfasa F, Siegers JY, van der Kroeg M, Mumtaz N, Stalin Raj V, de Vrij FMS, Widagdo W, Gabriel G, Salinas S, Simonin Y, Reusken C, Kushner SA, Koopmans MPG, Haagmans B, Martina BEE, van Riel D. 2017. Phenotypic Differences between Asian and African Lineage Zika Viruses in Human Neural Progenitor Cells. mSphere 2:e00292-17.
136. Simonin Y, Loustalot F, Desmetz C, Foulongne V, Constant O, Fournier-Wirth C, Leon F, Moles JP, Goubaud A, Lemaitre JM, Maquart M, Leparc-Goffart I, Briant L, Nagot N, Van de Perre P, Salinas S. 2016. Zika Virus Strains Potentially Display Different Infectious Profiles in Human Neural Cells. EBioMedicine 12:161-169.
137. Zhang F, Hammack C, Ogden SC, Cheng Y, Lee EM, Wen Z, Qian X, Nguyen HN, Li Y, Yao B, Xu M, Xu T, Chen L, Wang Z, Feng H, Huang WK, Yoon KJ, Shan C, Huang L, Qin Z, Christian KM, Shi PY, Xu M, Xia M, Zheng W, Wu H, Song H, Tang H, Ming GL, Jin P. 2016. Molecular signatures associated with ZIKV exposure in human cortical neural progenitors. Nucleic Acids Res 44:8610-8620.
138. Lazear HM, Govero J, Smith AM, Platt DJ, Fernandez E, Miner JJ, Diamond MS. 2016. A Mouse Model of Zika Virus Pathogenesis. Cell Host Microbe 19:720-30.
139. Bos S, Viranaicken W, Turpin J, El-Kalamouni C, Roche M, Krejbich-Trotot P, Despres P, Gadea G. 2018. The structural proteins of epidemic and historical strains of Zika virus differ in their ability to initiate viral infection in human host cells. Virology 516:265-273.
140. Perera-Lecoin M, Meertens L, Carnec X, Amara A. 2013. Flavivirus entry receptors: an update. Viruses 6:69-88.
141. Chu JJH, Ng ML. 2004. Infectious Entry of West Nile Virus Occurs through a Clathrin-Mediated Endocytic Pathway. Journal of Virology 78:10543.
142. Laureti M, Narayanan D, Rodriguez-Andres J, Fazakerley JK, Kedzierski L. 2018. Flavivirus Receptors: Diversity, Identity, and Cell Entry. Frontiers in immunology 9:2180-2180.
143. Kalia M, Khasa R, Sharma M, Nain M, Vrati S. 2013. Japanese Encephalitis Virus Infects Neuronal Cells through a Clathrin-Independent Endocytic Mechanism. Journal of Virology 87:148.
144. Gollins SW, Porterfield JS. 1984. Flavivirus Infection Enhancement in Macrophages: Radioactive and Biological Studies on the Effect of Antibody on Viral Fate. 65:1261-1272.

145. Boonnak K, Dambach KM, Donofrio GC, Tassaneetrithep B, Marovich MA. 2011. Cell type specificity and host genetic polymorphisms influence antibody-dependent enhancement of dengue virus infection. Journal of virology 85:1671-1683.
146. van der Schaar HM, Rust MJ, Waarts B-L, van der Ende-Metselaar H, Kuhn RJ, Wilschut J, Zhuang X, Smit JM. 2007. Characterization of the Early Events in Dengue Virus Cell Entry by Biochemical Assays and Single-Virus Tracking. Journal of Virology 81:12019.
147. Schalich J, Allison SL, Stiasny K, Mandl CW, Kunz C, Heinz FX. 1996. Recombinant subviral particles from tick-borne encephalitis virus are fusogenic and provide a model system for studying flavivirus envelope glycoprotein functions. Journal of Virology 70:4549.
148. Stiasny K, Heinz FX. 2006. Flavivirus membrane fusion. 87:2755-2766.
149. Meertens L, Labeau A, Dejarnac O, Cipriani S, Sinigaglia L, Bonnet-Madin L, Le Charpentier T, Hafirassou ML, Zamborlini A, Cao-Lormeau VM, Coulpier M, Misse D, Jouvenet N, Tabibiazar R, Gressens P, Schwartz O, Amara A. 2017. Axl Mediates ZIKA Virus Entry in Human Glial Cells and Modulates Innate Immune Responses. Cell Rep 18:324-333.
150. Persaud M, Martinez-Lopez A, Buffone C, Porcelli SA, Diaz-Griffero F. 2018. Infection by Zika viruses requires the transmembrane protein AXL, endocytosis and low pH. Virology 518:301-312.
151. Nowakowski TJ, Pollen AA, Di Lullo E, Sandoval-Espinosa C, Bershteyn M, Kriegstein AR. 2016. Expression Analysis Highlights AXL as a Candidate Zika Virus Entry Receptor in Neural Stem Cells. Cell Stem Cell 18:591-6.
152. Savidis G, McDougall WM, Meraner P, Perreira JM, Portmann JM, Trincucci G, John SP, Aker AM, Renzette N, Robbins DR, Guo Z, Green S, Kowalik TF, Brass AL. 2016. Identification of Zika Virus and Dengue Virus Dependency Factors using Functional Genomics. Cell Rep 16:232-246.
153. Liu S, DeLalio LJ, Isakson BE, Wang TT. 2016. AXL-Mediated Productive Infection of Human Endothelial Cells by Zika Virus. Circ Res 119:1183-1189.
154. Richard AS, Shim BS, Kwon YC, Zhang R, Otsuka Y, Schmitt K, Berri F, Diamond MS, Choe H. 2017. AXL-dependent infection of human fetal endothelial cells distinguishes Zika virus from other pathogenic flaviviruses. Proc Natl Acad Sci U S A 114:2024-2029.
155. Li F, Wang PR, Qu LB, Yi CH, Zhang FC, Tang XP, Zhang LG, Chen L. 2017. AXL is not essential for Zika virus infection in the mouse brain. Emerg Microbes Infect 6:e16.
156. Hastings AK, Yockey LJ, Jagger BW, Hwang J, Uraki R, Gaitsch HF, Parnell LA, Cao B, Mysorekar IU, Rothlin CV, Fikrig E, Diamond MS, Iwasaki A. 2017. TAM Receptors Are Not Required for Zika Virus Infection in Mice. Cell Rep 19:558-568.
157. Wang ZY, Wang Z, Zhen ZD, Feng KH, Guo J, Gao N, Fan DY, Han DS, Wang PG, An J. 2017. Axl is not an indispensable factor for Zika virus infection in mice. J Gen Virol 98:2061-2068.
158. Chen J, Yang YF, Yang Y, Zou P, Chen J, He Y, Shui SL, Cui YR, Bai R, Liang YJ, Hu Y, Jiang B, Lu L, Zhang X, Liu J, Xu J. 2018. AXL promotes Zika virus infection in astrocytes by antagonizing type I interferon signalling. Nat Microbiol 3:302-309.

159. Rawle RJ, Webster ER, Jelen M, Kasson PM, Boxer SG. 2018. pH Dependence of Zika Membrane Fusion Kinetics Reveals an Off-Pathway State. ACS Cent Sci 4:1503-1510.
160. Muller JA, Harms M, Schubert A, Jansen S, Michel D, Mertens T, Schmidt-Chanasit J, Munch J. 2016. Inactivation and Environmental Stability of Zika Virus. Emerg Infect Dis 22:1685-7.
161. Daniels RS, Downie JC, Hay AJ, Knossow M, Skehel JJ, Wang ML, Wiley DC. 1985. Fusion mutants of the influenza virus hemagglutinin glycoprotein. Cell 40:431-439.
162. Stiasny K, Fritz R, Pangerl K, Heinz FX. 2011. Molecular mechanisms of flavivirus membrane fusion. Amino Acids 41:1159-63.
163. Sánchez-San Martín C, Liu CY, Kielian M. 2009. Dealing with low pH: entry and exit of alphaviruses and flaviviruses. Trends in microbiology 17:514-521.
164. Helenius A, Kartenbeck J, Simons K, Fries E. 1980. On the entry of Semliki forest virus into BHK-21 cells. The Journal of cell biology 84:404-420.
165. Allison SL, Schalich J, Stiasny K, Mandl CW, Kunz C, Heinz FX. 1995. Oligomeric rearrangement of tick-borne encephalitis virus envelope proteins induced by an acidic pH. Journal of Virology 69:695.
166. Stauffer S, Feng Y, Nebioglu F, Heilig R, Picotti P, Helenius A. 2014. Stepwise Priming by Acidic pH and a High K⁺ Concentration Is Required for Efficient Uncoating of Influenza A Virus Cores after Penetration. Journal of Virology 88:13029.
167. Hackett BA, Cherry S. 2018. Flavivirus internalization is regulated by a size-dependent endocytic pathway. Proceedings of the National Academy of Sciences 115:4246.
168. Hancock JF, Cadwallader K, Paterson H, Marshall CJ. 1991. A CAAX or a CAAL motif and a second signal are sufficient for plasma membrane targeting of ras proteins. Embo j 10:4033-9.
169. Schoggins JW, Wilson SJ, Panis M, Murphy MY, Jones CT, Bieniasz P, Rice CM. 2011. A diverse range of gene products are effectors of the type I interferon antiviral response. Nature 472:481-5.
170. Schoggins JW, Dorner M, Feulner M, Imanaka N, Murphy MY, Ploss A, Rice CM. 2012. Dengue reporter viruses reveal viral dynamics in interferon receptor-deficient mice and sensitivity to interferon effectors in vitro. Proc Natl Acad Sci U S A 109:14610-5.
171. Cosens DJ, Manning A. 1969. Abnormal Electroretinogram from a Drosophila Mutant. Nature 224:285-287.
172. Pedersen SF, Owsianik G, Nilius B. 2005. TRP channels: An overview. Cell Calcium 38:233-252.
173. Montell C. 2005. The TRP Superfamily of Cation Channels. Science's STKE 2005:re3.
174. Zheng J. 2013. Molecular mechanism of TRP channels. Comprehensive Physiology 3:221-242.
175. Venkatachalam K, Wong C-O, Zhu MX. 2015. The role of TRPMLs in endolysosomal trafficking and function. Cell calcium 58:48-56.
176. Abe K, Puertollano R. 2011. Role of TRP Channels in the Regulation of the Endosomal Pathway. Physiology (Bethesda, Md) 26:14-22.

177. Ong HL, de Souza LB, Ambudkar IS. 2016. Role of TRPC Channels in Store-Operated Calcium Entry. Adv Exp Med Biol 898:87-109.
178. Prakriya M, Lewis RS. 2015. Store-Operated Calcium Channels. Physiological reviews 95:1383-1436.
179. Liu X, Wang W, Singh BB, Lockwich T, Jadlowiec J, O'Connell B, Wellner R, Zhu MX, Ambudkar IS. 2000. Trp1, a candidate protein for the store-operated Ca(2+) influx mechanism in salivary gland cells. J Biol Chem 275:3403-11.
180. Freichel M, Suh SH, Pfeifer A, Schweig U, Trost C, Weißgerber P, Biel M, Philipp S, Freise D, Droogmans G, Hofmann F, Flockerzi V, Nilius B. 2001. Lack of an endothelial store-operated Ca2+ current impairs agonist-dependent vasorelaxation in TRP4−/− mice. Nature Cell Biology 3:121.
181. Stowers L, Holy TE, Meister M, Dulac C, Koentges G. 2002. Loss of Sex Discrimination and Male-Male Aggression in Mice Deficient for TRP2. Science 295:1493.
182. Xu XZ, Sternberg PW. 2003. A C. elegans sperm TRP protein required for sperm-egg interactions during fertilization. Cell 114:285-97.
183. Schlingmann KP, Weber S, Peters M, Niemann Nejsum L, Vitzthum H, Klingel K, Kratz M, Haddad E, Ristoff E, Dinour D, Syrrou M, Nielsen S, Sassen M, Waldegger S, Seyberth HW, Konrad M. 2002. Hypomagnesemia with secondary hypocalcemia is caused by mutations in TRPM6, a new member of the TRPM gene family. Nature Genetics 31:166.
184. Walder RY, Landau D, Meyer P, Shalev H, Tsolia M, Borochowitz Z, Boettger MB, Beck GE, Englehardt RK, Carmi R, Sheffield VC. 2002. Mutation of TRPM6 causes familial hypomagnesemia with secondary hypocalcemia. Nat Genet 31:171-4.
185. Voets T, Nilius B, Hoefs S, van der Kemp AW, Droogmans G, Bindels RJ, Hoenderop JG. 2004. TRPM6 forms the Mg2+ influx channel involved in intestinal and renal Mg2+ absorption. J Biol Chem 279:19-25.
186. Birder LA, Nakamura Y, Kiss S, Nealen ML, Barrick S, Kanai AJ, Wang E, Ruiz G, de Groat WC, Apodaca G, Watkins S, Caterina MJ. 2002. Altered urinary bladder function in mice lacking the vanilloid receptor TRPV1. Nature Neuroscience 5:856.
187. Mizuno A, Matsumoto N, Imai M, Suzuki M. 2003. Impaired osmotic sensation in mice lacking TRPV4. American Journal of Physiology-Cell Physiology 285:C96-C101.
188. Di Palma F, Belyantseva IA, Kim HJ, Vogt TF, Kachar B, Noben-Trauth K. 2002. Mutations in Mcoln3 associated with deafness and pigmentation defects in varitint-waddler (Va) mice. Proc Natl Acad Sci U S A 99:14994-9.
189. Montell C. 2005. The TRP superfamily of cation channels. Sci STKE 2005:re3.
190. Venkatachalam K, Montell C. 2007. TRP Channels. Annual review of biochemistry 76:387-417.
191. Cheng X, Shen D, Samie M, Xu H. 2010. Mucolipins: Intracellular TRPML1-3 channels. FEBS letters 584:2013-2021.
192. Dong XP, Cheng X, Mills E, Delling M, Wang F, Kurz T, Xu H. 2008. The type IV mucolipidosis-associated protein TRPML1 is an endolysosomal iron release channel. Nature 455:992-6.
193. Uhlen M, Fagerberg L, Hallstrom BM, Lindskog C, Oksvold P, Mardinoglu A, Sivertsson A, Kampf C, Sjostedt E, Asplund A, Olsson I, Edlund K, Lundberg E, Navani

S, Szigyarto CA, Odeberg J, Djureinovic D, Takanen JO, Hober S, Alm T, Edqvist PH, Berling H, Tegel H, Mulder J, Rockberg J, Nilsson P, Schwenk JM, Hamsten M, von Feilitzen K, Forsberg M, Persson L, Johansson F, Zwahlen M, von Heijne G, Nielsen J, Ponten F. 2015. Proteomics. Tissue-based map of the human proteome. Science 347:1260419.

194. Samie MA, Grimm C, Evans JA, Curcio-Morelli C, Heller S, Slaugenhaupt SA, Cuajungco MP. 2009. The tissue-specific expression of TRPML2 (MCOLN-2) gene is influenced by the presence of TRPML1. Pflugers Arch 459:79-91.
195. Sun L, Hua Y, Vergarajauregui S, Diab HI, Puertollano R. 2015. Novel role of TRPML2 in the regulation of the innate immune response. Journal of immunology (Baltimore, Md : 1950) 195:4922-4932.
196. Lanford RE, Guerra B, Lee H, Chavez D, Brasky KM, Bigger CB. 2006. Genomic response to interferon-alpha in chimpanzees: implications of rapid downregulation for hepatitis C kinetics. Hepatology 43:961-72.
197. Nagata K, Zheng L, Madathany T, Castiglioni AJ, Bartles JR, García-Añoveros J. 2008. The varitint-waddler (Va) deafness mutation in TRPML3 generates constitutive, inward rectifying currents and causes cell degeneration. Proceedings of the National Academy of Sciences of the United States of America 105:353-358.
198. Xu H, Delling M, Li L, Dong X, Clapham DE. 2007. Activating mutation in a mucolipin transient receptor potential channel leads to melanocyte loss in varitint-waddler mice. Proc Natl Acad Sci U S A 104:18321-6.
199. Venkatachalam K, Hofmann T, Montell C. 2006. Lysosomal localization of TRPML3 depends on TRPML2 and the mucolipidosis-associated protein TRPML1. J Biol Chem 281:17517-27.
200. Pryor PR, Reimann F, Gribble FM, Luzio JP. 2006. Mucolipin-1 is a lysosomal membrane protein required for intracellular lactosylceramide traffic. Traffic 7:1388-98.
201. Martina JA, Lelouvier B, Puertollano R. 2009. The calcium channel mucolipin-3 is a novel regulator of trafficking along the endosomal pathway. Traffic 10:1143-56.
202. Kim HJ, Soyombo AA, Tjon-Kon-Sang S, So I, Muallem S. 2009. The Ca(2+) channel TRPML3 regulates membrane trafficking and autophagy. Traffic 10:1157-67.
203. Karacsonyi C, Miguel AS, Puertollano R. 2007. Mucolipin-2 localizes to the Arf6-associated pathway and regulates recycling of GPI-APs. Traffic 8:1404-14.
204. Cao Q, Yang Y, Zhong XZ, Dong X-P. 2017. The lysosomal Ca(2+) release channel TRPML1 regulates lysosome size by activating calmodulin. The Journal of biological chemistry 292:8424-8435.
205. Dove SK, Dong K, Kobayashi T, Williams FK, Michell RH. 2009. Phosphatidylinositol 3,5-bisphosphate and Fab1p/PIKfyve underPPIn endo-lysosome function. Biochem J 419:1-13.
206. Cabezas A, Pattni K, Stenmark H. 2006. Cloning and subcellular localization of a human phosphatidylinositol 3-phosphate 5-kinase, PIKfyve/Fab1. Gene 371:34-41.
207. Curcio-Morelli C, Zhang P, Venugopal B, Charles FA, Browning MF, Cantiello HF, Slaugenhaupt SA. 2010. Functional multimerization of mucolipin channel proteins. 222:328-335.

208. Zeevi DA, Lev S, Frumkin A, Minke B, Bach G. 2010. Heteromultimeric TRPML channel assemblies play a crucial role in the regulation of cell viability models and starvation-induced autophagy. Journal of cell science 123:3112-3124.
209. Bargal R, Avidan N, Ben-Asher E, Olender Z, Zeigler M, Frumkin A, Raas-Rothschild A, Glusman G, Lancet D, Bach G. 2000. Identification of the gene causing mucolipidosis type IV. Nat Genet 26:118-23.
210. Bassi MT, Manzoni M, Monti E, Pizzo MT, Ballabio A, Borsani G. 2000. Cloning of the gene encoding a novel integral membrane protein, mucolipidin-and identification of the two major founder mutations causing mucolipidosis type IV. Am J Hum Genet 67:1110-20.
211. Altarescu G, Sun M, Moore DF, Smith JA, Wiggs EA, Solomon BI, Patronas NJ, Frei KP, Gupta S, Kaneski CR, Quarrell OW, Slaugenhaupt SA, Goldin E, Schiffmann R. 2002. The neurogenetics of mucolipidosis type IV. Neurology 59:306-13.
212. Amir N, Zlotogora J, Bach G. 1987. Mucolipidosis type IV: clinical spectrum and natural history. Pediatrics 79:953-9.
213. Wakabayashi K, Gustafson AM, Sidransky E, Goldin E. 2011. Mucolipidosis type IV: an update. Molecular genetics and metabolism 104:206-213.
214. Hersh BM, Hartwieg E, Horvitz HR. 2002. The Caenorhabditis elegans mucolipin-like gene cup-5 is essential for viability and regulates lysosomes in multiple cell types. Proc Natl Acad Sci U S A 99:4355-60.
215. Wong C-O, Li R, Montell C, Venkatachalam K. 2012. Drosophila TRPML is required for TORC1 activation. Current biology : CB 22:1616-1621.
216. Venkatachalam K, Long AA, Elsaesser R, Nikolaeva D, Broadie K, Montell C. 2008. Motor deficit in a Drosophila model of mucolipidosis type IV due to defective clearance of apoptotic cells. Cell 135:838-51.
217. Lev S, Zeevi DA, Frumkin A, Offen-Glasner V, Bach G, Minke B. 2010. Constitutive activity of the human TRPML2 channel induces cell degeneration. J Biol Chem 285:2771-82.
218. Kiselyov K, Colletti GA, Terwilliger A, Ketchum K, Lyons CWP, Quinn J, Muallem S. 2011. TRPML: transporters of metals in lysosomes essential for cell survival? Cell calcium 50:288-294.
219. Bach G, Chen C-S, Pagano RE. 1999. Elevated lysosomal pH in Mucolipidosis type IV cells. Clinica Chimica Acta 280:173-179.
220. Soyombo AA, Tjon-Kon-Sang S, Rbaibi Y, Bashllari E, Bisceglia J, Muallem S, Kiselyov K. 2006. TRP-ML1 regulates lysosomal pH and acidic lysosomal lipid hydrolytic activity. J Biol Chem 281:7294-301.
221. Kim HJ, Li Q, Tjon-Kon-Sang S, So I, Kiselyov K, Soyombo AA, Muallem S. 2008. A novel mode of TRPML3 regulation by extracytosolic pH absent in the varitint-waddler phenotype. Embo j 27:1197-205.
222. Li M, Zhang WK, Benvin NM, Zhou X, Su D, Li H, Wang S, Michailidis IE, Tong L, Li X, Yang J. 2017. Structural basis of dual Ca(2+)/pH regulation of the endolysosomal TRPML1 channel. Nature structural & molecular biology 24:205-213.

223. Li X, Saitoh S, Shibata T, Tanimura N, Fukui R, Miyake K. 2015. Mucolipin 1 positively regulates TLR7 responses in dendritic cells by facilitating RNA transportation to lysosomes. Int Immunol 27:83-94.
224. Thompson EG, Schaheen L, Dang H, Fares H. 2007. Lysosomal trafficking functions of mucolipin-1 in murine macrophages. BMC Cell Biol 8:54.
225. Medina Diego L, Fraldi A, Bouche V, Annunziata F, Mansueto G, Spampanato C, Puri C, Pignata A, Martina Jose A, Sardiello M, Palmieri M, Polishchuk R, Puertollano R, Ballabio A. 2011. Transcriptional Activation of Lysosomal Exocytosis Promotes Cellular Clearance. Developmental Cell 21:421-430.
226. LaPlante JM, Sun M, Falardeau J, Dai D, Brown EM, Slaugenhaupt SA, Vassilev PM. 2006. Lysosomal exocytosis is impaired in mucolipidosis type IV. Mol Genet Metab 89:339-48.
227. LaPlante JM, Ye CP, Quinn SJ, Goldin E, Brown EM, Slaugenhaupt SA, Vassilev PM. 2004. Functional links between mucolipin-1 and Ca2+-dependent membrane trafficking in mucolipidosis IV. Biochemical and Biophysical Research Communications 322:1384-1391.
228. Vergarajauregui S, Connelly PS, Daniels MP, Puertollano R. 2008. Autophagic dysfunction in mucolipidosis type IV patients. Human molecular genetics 17:2723-2737.
229. Samie M, Wang X, Zhang X, Goschka A, Li X, Cheng X, Gregg E, Azar M, Zhuo Y, Garrity A, Gao Q, Slaugenhaupt S, Pickel J, Zolov SN, Weisman LS, Lenk GM, Titus S, Bryant-Genevier M, Southall N, Juan M, Ferrer M, Xu H. 2013. A TRP Channel in the Lysosome Regulates Large Particle Phagocytosis via Focal Exocytosis. Developmental cell 26:511-524.
230. De Leo MG, Staiano L, Vicinanza M, Luciani A, Carissimo A, Mutarelli M, Di Campli A, Polishchuk E, Di Tullio G, Morra V, Levtchenko E, Oltrabella F, Starborg T, Santoro M, Di Bernardo D, Devuyst O, Lowe M, Medina DL, Ballabio A, De Matteis MA. 2016. Autophagosome-lysosome fusion triggers a lysosomal response mediated by TLR9 and controlled by OCRL. Nature cell biology 18:839-850.
231. Zhang X, Yu L, Xu H. 2016. Lysosome calcium in ROS regulation of autophagy. Autophagy 12:1954-1955.
232. Zhang X, Cheng X, Yu L, Yang J, Calvo R, Patnaik S, Hu X, Gao Q, Yang M, Lawas M, Delling M, Marugan J, Ferrer M, Xu H. 2016. MCOLN1 is a ROS sensor in lysosomes that regulates autophagy. Nat Commun 7:12109.
233. Medina DL, Di Paola S, Peluso I, Armani A, De Stefani D, Venditti R, Montefusco S, Scotto-Rosato A, Prezioso C, Forrester A, Settembre C, Wang W, Gao Q, Xu H, Sandri M, Rizzuto R, De Matteis MA, Ballabio A. 2015. Lysosomal calcium signalling regulates autophagy through calcineurin and TFEB. Nat Cell Biol 17:288-99.
234. Gray MA, Choy CH, Dayam RM, Ospina-Escobar E, Somerville A, Xiao X, Ferguson SM, Botelho RJ. 2016. Phagocytosis Enhances Lysosomal and Bactericidal Properties by Activating the Transcription Factor TFEB. Curr Biol 26:1955-64.
235. Lelouvier B, Puertollano R. 2011. Mucolipin-3 Regulates Luminal Calcium, Acidification, and Membrane Fusion in the Endosomal Pathway. The Journal of Biological Chemistry 286:9826-9832.

236. Miao Y, Li G, Zhang X, Xu H, Abraham SN. 2015. A TRP Channel Senses Lysosome Neutralization by Pathogens to Trigger Their Expulsion. Cell 161:1306-19.
237. Valadez JA, Cuajungco MP. 2015. PAX5 is the transcriptional activator of mucolipin-2 (MCOLN2) gene. Gene 555:194-202.
238. Plesch E, Chen CC, Butz E, Scotto Rosato A, Krogsaeter EK, Yinan H, Bartel K, Keller M, Robaa D, Teupser D, Holdt LM, Vollmar AM, Sippl W, Puertollano R, Medina D, Biel M, Wahl-Schott C, Bracher F, Grimm C. 2018. Selective agonist of TRPML2 reveals direct role in chemokine release from innate immune cells. Elife 7.
239. Hale BG, Randall RE, Ortin J, Jackson D. 2008. The multifunctional NS1 protein of influenza A viruses. J Gen Virol 89:2359-76.
240. Lelouvier B, Puertollano R. 2011. Mucolipin-3 regulates luminal calcium, acidification, and membrane fusion in the endosomal pathway. J Biol Chem 286:9826-32.
241. Jones CT, Patkar CG, Kuhn RJ. 2005. Construction and applications of yellow fever virus replicons. Virology 331:247-59.
242. Chu VC, Whittaker GR. 2004. Influenza virus entry and infection require host cell N-linked glycoprotein. Proc Natl Acad Sci U S A 101:18153-8.
243. Sieczkarski SB, Whittaker GR. 2003. Differential requirements of Rab5 and Rab7 for endocytosis of influenza and other enveloped viruses. Traffic 4:333-43.
244. Stegmann T, Morselt HW, Scholma J, Wilschut J. 1987. Fusion of influenza virus in an intracellular acidic compartment measured by fluorescence dequenching. Biochim Biophys Acta 904:165-70.
245. Nour AM, Li Y, Wolenski J, Modis Y. 2013. Viral Membrane Fusion and Nucleocapsid Delivery into the Cytoplasm are Distinct Events in Some Flaviviruses. PLoS Pathogens 9:e1003585.
246. Auton A, Brooks LD, Durbin RM, Garrison EP, Kang HM, Korbel JO, Marchini JL, McCarthy S, McVean GA, Abecasis GR. 2015. A global reference for human genetic variation. Nature 526:68-74.
247. Marcus JH, Novembre J. 2017. Visualizing the geography of genetic variants. Bioinformatics 33:594-595.
248. Karczewski KJ, Weisburd B, Thomas B, Solomonson M, Ruderfer DM, Kavanagh D, Hamamsy T, Lek M, Samocha KE, Cummings BB, Birnbaum D, Daly MJ, MacArthur DG. 2017. The ExAC browser: displaying reference data information from over 60 000 exomes. Nucleic Acids Res 45:D840-D845.
249. Balish AL, Katz JM, Klimov AI. 2013. Influenza: propagation, quantification, and storage. Curr Protoc Microbiol Chapter 15:Unit 15G 1.
250. Sanjana NE, Shalem O, Zhang F. 2014. Improved vectors and genome-wide libraries for CRISPR screening. Nat Methods 11:783-4.
251. Sakai T, Ohuchi M, Imai M, Mizuno T, Kawasaki K, Kuroda K, Yamashina S. 2006. Dual Wavelength Imaging Allows Analysis of Membrane Fusion of Influenza Virus inside Cells. Journal of Virology 80:2013-2018.
252. van der Schaar HM, Rust MJ, Chen C, van der Ende-Metselaar H, Wilschut J, Zhuang X, Smit JM. 2008. Dissecting the cell entry pathway of dengue virus by single-particle tracking in living cells. PLoS Pathog 4:e1000244.

253. Helenius A. 2018. Virus Entry: Looking Back and Moving Forward. Journal of Molecular Biology 430:1853-1862.
254. Nawa M, Takasaki T, Yamada K, Kurane I, Akatsuka T. 2003. Interference in Japanese encephalitis virus infection of Vero cells by a cationic amphiphilic drug, chlorpromazine. J Gen Virol 84:1737-41.
255. Yang S, He M, Liu X, Li X, Fan B, Zhao S. 2013. Japanese encephalitis virus infects porcine kidney epithelial PK15 cells via clathrin- and cholesterol-dependent endocytosis. Virol J 10:258.
256. Kalia M, Khasa R, Sharma M, Nain M, Vrati S. 2013. Japanese encephalitis virus infects neuronal cells through a clathrin-independent endocytic mechanism. J Virol 87:148-62.
257. Zhu Y-Z, Xu Q-Q, Wu D-G, Ren H, Zhao P, Lao W-G, Wang Y, Tao Q-Y, Qian X-J, Wei Y-H, Cao M-M, Qi Z-T. 2012. Japanese encephalitis virus enters rat neuroblastoma cells via a pH-dependent, dynamin and caveola-mediated endocytosis pathway. Journal of virology 86:13407-13422.
258. Yamauchi Y, Greber UF. 2016. Principles of Virus Uncoating: Cues and the Snooker Ball. Traffic 17:569-92.
259. Hay JC. 2007. Calcium: a fundamental regulator of intracellular membrane fusion? EMBO reports 8:236-240.
260. Cao Q, Zhong XZ, Zou Y, Murrell-Lagnado R, Zhu MX, Dong X-P. 2015. Calcium release through P2X4 activates calmodulin to promote endolysosomal membrane fusion. The Journal of Cell Biology 209:879.
261. Rohwer F, Prangishvili D, Lindell D. 2009. Roles of viruses in the environment. Environmental Microbiology 11:2771-2774.
262. Williamson KE, Fuhrmann JJ, Wommack KE, Radosevich M. 2017. Viruses in Soil Ecosystems: An Unknown Quantity Within an Unexplored Territory. Annu Rev Virol 4:201-219.